Modelling of the Ballooning Instability in the Near-Earth Magnetotail

LEE ANNE DORMER

Submitted in partial fulfillment of the
requirements for the degree of
Master of Science
in the
Space Physics Research Institute
of the
Department of Physics,
University of Natal

Durban
April, 1995

Acknowledgements

I would like to thank the following people:

Prof. A.D.M. Walker, my supervisor, for his help and encouragement, and for generous financial support.

Terry Holloway, for her help in solving computer related and other problems.

Ken Rice, for helping me with Fortran programming.

Barbara, Denise and Blanche, for always accommodating me.

Kevin Meyer, Richard Mace and Michael Gallias, for all their advice.

The Foundation for Research Development, for financial support.

The University of Natal, Durban, for financial assistance to attend the 39th SAIP conference.

My parents and Kerry, for their patience.

Abstract

In recent years, many alternative models of the substorm process have been proposed to explain different aspects of this magnetospheric phenomenon. Some features in these competing models are compatible while others, such as the nature and location of substorm onset, remain controversial. The objective of this thesis is to assess the viability of the ballooning instability as a mechanism for initiating substorms.

A review of the history and development of magnetospheric substorm research as well as a review of substorm models is presented. In these models, the cross-tail current disruption responsible for the onset of the expansion phase is usually ascribed to the onset of some microinstability. An alternative triggering mechanism is a macroscopic magnetohydrodynamic instability such as the ballooning instability.

To derive a threshold condition for the ballooning instability, a simplified magnetotail geometry with cylindrical symmetry near the equatorial plane is assumed. In such circumstances, the torsion of the magnetic field lines is zero and they can be characterised by their curvature. The hydromagnetic equations with isotropic pressure are linearised to find the dispersion relation. This leads to a threshold condition which depends on the pressure and magnetic field intensity gradients.

In order to obtain realistic numerical results for the threshold condition, a quasi-static, self-consistent, two-dimensional numerical model of the magnetotail during conditions typical of substorm growth phase is used. The model involves solving the Grad-Shafranov equation with appropriate boundary conditions. It provides time-dependent magnetospheric magnetic field configurations that are characterised by the development of a minimum in B_z in the equatorial plane.

Calculations of the detailed configuration of the magnetotail during onset allow an estimate of the instability criterion. In a model which does not allow an increase of pressure with radius, it is found that the magnetotail is not unstable to ballooning.

Part of this work has been presented at a conference, viz.:

Dormer, L.A. and A.D.M. Walker, Investigation of local MHD instabilities in the magnetotail using a two-dimensional magnetospheric convection model. *Poster presented at the 39th annual South African Institute of Physics conference, University of Bophuthatswana, 1994.*

Contents

List of Figures

List of Tables

Chapter 1

Development of Magnetospheric Substorm Research

1.1 Historical Review

The aurora is one of the oldest documented geophysical phenomena. It was only at the turn of the nineteenth century, however, that the magnetic signature of such displays was examined. From his geomagnetic observations at four subpolar stations in the northern hemisphere in 1902–3, Kristian Birkeland deduced the current systems responsible for the geomagnetic disturbance he termed the "elementary polar magnetic storm". This was the first step towards the concept of the magnetospheric substorm.

Sydney Chapman was critical of Birkeland's inclusion of polar positive and negative bays as two distinct classes of elementary magnetic storms. Chapman suggested that, because of their short time scale, they were merely phases of a geomagnetic storm. Subsequently, such disturbances were generally referred to as "auroral bays" or just "bays".

The Chapman-Ferraro theory of geomagnetic storms [*Chapman and Ferraro*, 1931, 1933, 1940] was inferred by considering the effect of the impact of a neutral ionised 'solar stream' on the earth. Central to the theory are two essential mechanisms. The first — the deflection of solar particles by the earth's magnetic field — caused the initial phase of a storm. The second involved the formation of a toroidal current ring to explain the main phase. The theory was, however, unable to explain the motion of the solar gas particles which penetrated the cavity containing the geomagnetic field to form the ring current.

The diffusion of solar particles into the magnetosphere[1] remained a problem. In 1961, two important ideas emerged. *Axford and Hines* [1961] proposed that large scale convection of magnetospheric plasma in the magnetosphere occurred continuously due to a "viscous-like interaction" between the magnetosphere and the solar wind. The interaction mechanism was not specified. Its importance lay in the resulting transfer of momentum across the magnetopause[2] causing general circulation away from the earth at the boundary of the magnetotail, and return flow towards the earth in the centre (figure 1.1). At the same time *Dungey* [1961] recognised the importance of the interaction of the geomagnetic field with the interplanetary magnetic field (IMF) carried by the solar plasma. In the Chapman-Ferraro theory, the magnetosphere is 'closed' in the sense that the earth's magnetic field is enclosed in a cavity formed by the exclusion of the solar plasma. Dungey proposed that southward directed interplanetary magnetic field lines 'reconnect' with the northward directed geomagnetic field lines at the magnetopause boundary. The reconnected field lines are then drawn into the magnetotail by the motion of the solar wind to reconnect at a second neutral point. In this model, the magnetosphere becomes 'open', allowing solar plasma to enter. Figures 1.2 and 1.3 depict the geomagnetic field for closed and open magnetospheric configurations, respectively. The dynamo process of the solar

[1]The term "magnetosphere" was introduced in 1959 by Gold. It refers to the region in which the motion of charged particles is controlled by the earth's magnetic field.

[2]The magnetopause is the boundary between the solar wind and the magnetosphere.

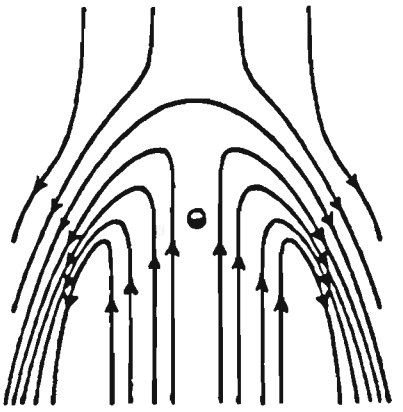

Figure 1.1: Large-scale magnetospheric circulation in the equatorial plane as proposed by *Axford and Hines* [1961]. Effects due to the rotation of the earth are not included in this depiction. From *Hargreaves* [1979].

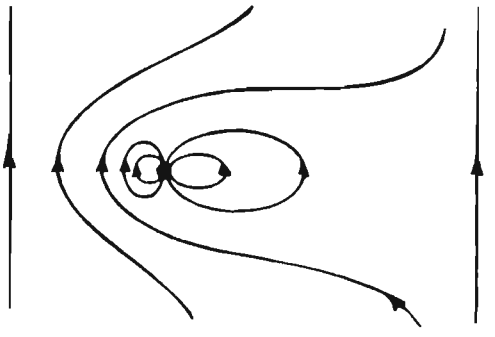

Figure 1.2: Noon-midnight meridian cross-section showing a closed magnetosphere. From *Hargreaves* [1979].

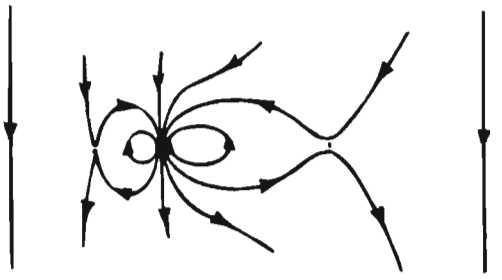

Figure 1.3: The meridian plane showing the reconnection of southward directed interplanetary magnetic field lines with northward directed geomagnetic field lines. This results in an open magnetosphere. From *Hargreaves* [1979].

wind flowing across the reconnected field lines was another important consequence of Dungey's hypothesis. The significance of this to substorm processes, however, was only realised later.

Up until 1958, magnetospheric physics grew on ground-based observations and theoretical research. Some important events in the early development of magnetospheric physics are given in table 1.1. The advent of the era of space exploration was heralded in April of 1958 by the announcement of the discovery of the inner Van Allen radiation belt. The existence of this region of trapped electrically charged particles in the external magnetic field was deduced from data collected by the Explorer I and III satellites. Satellite observations of the magnetosphere made an immense impact on the development of magnetospheric physics by providing the observational evidence by which to test various theoretical suggestions and models. The International Geophysical Year (IGY) in 1957–58, coincident with the first applications of satellite technology, also gave impetus to the field by building up world-wide interest and fostering international cooperation.

Following his work with Ferraro, Chapman continued his study of magnetic storms with Syun-Ichi Akasofu. *Akasofu and Chapman* [1961] resolved the storm's disturbance field, D, into three different parts: DCF, the corpuscular flux component;

Table 1.1: Important events in the development of magnetospheric physics up to 1958. After *Egeland et al.*, 1973.

1621	Gassendi	Aurora borealis described
1716	Halley	Aurora connected with magnetic field
1722	Graham	Transient geomagnetic field variations observed
1741	Celsius	Aurora correlated with magnetic disturbances
1808	Von Humboldt	Magnetic storm concept introduced
1832	Gauss	Magnetic intensity measured
1834	Gauss	First three component magnetograph
1859	Carrington, Hodgson	First solar flare associated with magnetic storm observed
1860	Maxwell	Electromagnetic waves predicted
1908	Birkeland	Observation of magnetic storm and substorm current systems
1930	Chapman, Ferraro	Magnetic cavity and ring current proposed
1957		Sputnik I launched
1958	Van Allen	Discovery of inner radiation belt

DR, the ring current component and DP, the polar component. It was in this paper that the term 'substorm' was first used. Here Birkeland's "polar elementary storm" was referred to as a "DP substorm", produced by currents flowing in the ionosphere. It was also recognised that the development of a DP substorm coincided with the change in the aurora from diffuse to active forms.

Unlike Birkeland, who analysed individual storm and substorm events in detail, *Moos* [1910], Chapman and others concentrated their studies on the average behaviour of storms. It was only much later [*Akasofu and Chapman*, 1963a] that the main phase development of individual storms were examined again. This made significant features that were averaged out by statistical studies more noticeable. It was observed that horizontal component magnetograms for the same storm at high (College, Alaska) and low (Honolulu) latitudes showed a marked difference in the development of magnetic (DP) substorms, now referred to as polar magnetic substorms. Many substorms were observed at the high latitude station which were absent on the Honolulu magnetogram (figure 1.4). The development of these large and intermittent substorms was linked to the increase in auroral activity. The period of a storm was identified as the period when intense substorms occurred frequently [*Akasofu and Chapman*, 1963b].

Chapman [1962] recognised that polar substorms could occur outside of the main phase of a geomagnetic storm. It was Akasofu, however, who correlated these isolated polar substorms to auroral activity. This observation led to the introduction of the "auroral substorm"[3] [*Akasofu*, 1964]. An important point in this paper was the realisation that the auroral displays were of a global nature; that is, the observed features of the aurora were not fixed with respect to the sun while the earth rotated beneath them. This concept was not immediately accepted, however, and had to await the development of auroral imagers in the early 1970's for the global activity to be confirmed by satellite observations [*Akasofu*, 1991].

[3]The term "auroral substorm" was due to Chapman.

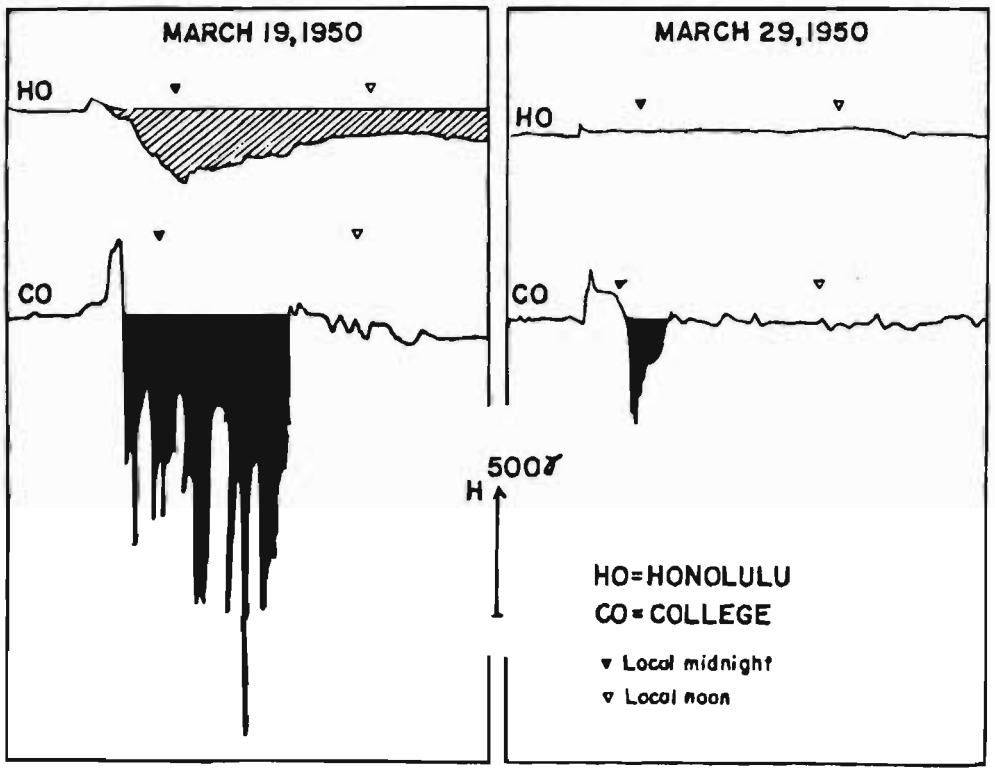

Figure 1.4: The horizontal component magnetograms of geomagnetic storms recorded at Honolulu and College stations. The magnetogram from the high latitude station demonstrates pronounced substorm activity. From *Akasofu and Chapman* [1963].

Satellites also played a role in recognising the involvement of the geomagnetic tail in substorms. The tangential stress at the magnetopause boundary, either due to the friction-like mechanism of *Axford and Hines* [1961] or reconnection [*Dungey*, 1961], was considered responsible for the 'stretching' of the magnetosphere on the anti-sunward side into a tail [*Axford et al.*, 1965]. From the data collected by IMP (Interplanetary Monitor Probe) 1, Axford and co-workers were able to deduce characteristics of the magnetotail such as the neutral sheet "across which the field direction changes from radially outward to radially inward", and the current system associated with the neutral sheet. IMP 4 (Explorer 34) further demonstrated the large-scale changes which the tail undergoes during a substorm. *Fairfield and Ness* [1970] used IMP 4 observations to show that a greater number of magnetic field lines or "lines of force" cross the equatorial plane in the inner tail after a substorm. This supports the picture of the tail relaxing to a more dipolar configuration and suggests that energy is stored in the tail until its release during a substorm. The idea of the tail being a reservoir of energy for substorms was first proposed by *Siscoe and Cummings* [1969]. A few years previous to this, increased substorm activity was correlated with the presence of a southward component in the interplanetary magnetic field. These two concepts led to the question of whether the substorm is a directly driven or unloading process, or something in between [*Akasofu*, 1979a].

The term "magnetospheric substorm" was introduced by Akasofu in 1968 [*Stern*, 1991]. This encompasses a variety of phenomena which occur in association with each other, namely: the auroral substorm, being the only visible manifestation of the magnetospheric substorm; the polar magnetic substorm, which is the magnetic signature; micropulsations; x-rays; ionospheric disturbances and VLF emissions. It is, therefore, within the magnetosphere as a whole that the substorm phenomenon must be examined.

1.2 Defining the magnetospheric substorm

It was over a relatively short period of time that the emphasis of magnetic storm research changed. The geomagnetic storm itself was no longer the focus of attention. Research was now concentrated on the magnetospheric substorm and its associated features.

The rapid growth of substorm research led to various groups using their own definitions of substorm occurrence within different time frames. This problem was compounded by the complex nature of the substorm process. In August 1978, nine magnetospheric physicists met in Victoria, Canada to resolve this issue. The result was a definition of the substorm and its signatures [*Rostoker et al.*, 1980].

The broad nature of the substorm necessitated a broad definition :

> A magnetospheric substorm is a transient process initiated on the night side of the earth in which a significant amount of energy derived from the solar wind-magnetosphere interaction is deposited in the auroral ionosphere and in the magnetosphere.

The physical mechanisms responsible for this process are still in dispute.

Rostoker et al. [1980] recognised that although the probability of substorm occurrence increased with a southward turning of the IMF, substorms could still occur when the IMF was northward or remained southward for an extended period. There were thus dynamical internal and external features of the magnetosphere responsible for the triggering of substorms.

Whereas statistical studies were readily available for magnetic storms, there were no comprehensive studies to indicate an average substorm time scale at this time [*Rostoker et al.*, 1980]. The time scale of the substorm was therefore proposed to

be between one and three hours with parameters such as Pi 2 bursts, electrojet current strength and auroral dynamics used to distinguish between intervals of expansion and recovery. For a substorm with multiple expansions, it was agreed that each discrete expansion be called a "substorm intensification", with the expansion phase of the substorm being onset and all the intensifications up to the time of maximum poleward motion of the disturbed region. The question of whether or not substorms have a growth phase, as suggested by *McPherron* [1970], was not addressed in this paper.

1.3 Magnetospheric substorm signatures

The signatures which follow are those identified and described by *Rostoker et al.* [1980].

The auroral signature as defined by *Rostoker et al.* [1980] is inherently the same as the auroral substorm described by *Akasofu* [1964] with a few qualifications. As has been mentioned, the time scale of the auroral substorm was removed. Another distinction made was that the brightening of an arc followed by the formation of a westward travelling surge could be an onset or an intensification. Data from other sources would then be necessary to distinguish between these possibilities.

As *Akasofu and Chapman* [1963a] observed, the magnetic signature of a substorm is different at auroral and low latitude stations. The H, D and Z magnetogram signatures are dependent on the location of the electrojet currents and substorm-disturbed regions with respect to a particular station. The AE (Auroral Electrojet) index introduced by *Davis and Sigiura* [1966] to gauge substorm activity was felt to be useful for establishing the level of magnetospheric activity, but not accurate enough for studying the temporal development of substorms. Individual magnetograms from as many relevant observatories as possible were recommended for this purpose.

Each substorm intensification has an associated Pi 2 burst [*Rostoker et al.*, 1980]. A Pi 2 is an irregular fluctuation of the geomagnetic field with a period of between 40 and 150 seconds (or larger) [*Jacobs*, 1970]. The initial pulse of a Pi 2 identifies the onset of a substorm or a substorm intensification. A magnetospheric substorm, then, can have several associated Pi 2 bursts, one of which corresponds to the onset of the expansion phase [*Rostoker*, 1968].

In comparison with the other three signatures, observations of the ionospheric electric field behaviour during substorms was in a state of development at this time. Auroral radar facilities such as Stare (the Scandanavian Twin Auroral Radar Experiment), which began operating in 1977, had demonstrated the success and usefulness of such a system in observing ionospheric electric fields. The further establishment of such facilities was therefore encouraged.

1.4 Magnetospheric substorm models

Since the realisation of the importance of the magnetospheric substorm as a fundamental phenomenon in the magnetosphere and ionosphere, many different models of the substorm process have been proposed. These models tend to focus on specific substorm features and neglect others. This means that no model is truly global. Each concentrates on dynamical events in the central plasma sheet or the ionosphere or various other parts of the magnetosphere such as the plasma sheet boundary layer (refer to figure 1.6). Another factor which contributed to the variety of proposals was the problem of how to map satellite observations of specific magnetospheric regions to regions in the auroral ionosphere. Researchers have used different 'mappings' in different models.

Attempts have also been made to describe the sequence of substorm events in a phenomenological way, without close analysis of the physical mechanisms responsible for the effects described. The first of such models was a result of a

coordinated study of two magnetospheric substorms that occurred on 15 August, 1968. Both ground based and satellite observations (from Ogo 4 and 5) were available for these two substorms. These observations were combined to create a phenomenological model [*McPherron et al.*, 1973] which incorporated both new concepts and existing ideas. The following description of the model summarises the key elements.

The substorm was divided into its three phases of growth, expansion and recovery. The growth phase was proposed to be initiated by the southward turning of the interplanetary magnetic field which led to enhanced solar wind erosion of the dayside magnetopause via magnetic merging. Consequent solar wind transport of flux to the magnetotail resulted in an intermediate storing of energy in the tail lobes. Reconnection of the field at a distant neutral point occurred leading to the inward convection of plasma and the development of the near-earth tail current or a partial ring current. Field aligned and ionospheric currents were also established.

The expansion phase of this model included the rapid thinning of a portion of the near-earth plasma sheet. The cross-tail current was then disrupted by some mechanism leading to the formation of the "substorm current wedge", a concept first introduced in this model. Here the electrojet was connected via field aligned currents to the tail current. Collapse of the tail-like field followed with the possible formation of a neutral point in the near-earth tail. Other consequences of the disruption included the energisation and injection of particles close to the earth and the rapid outward expansion of the region of the disrupted tail current. The recovery phase was characterised by the decay of the electrojet currents and the reestablishment of the quiet time auroral displays.

Near-earth neutral line model

The above model is one of the early Near-Earth Neutral Line (NENL) or Near-Earth X-Line models of the magnetospheric substorm. Central to NENL models is the formation of a new near-earth neutral line in the central plasma sheet which is responsible for substorm onset. A similar sequence of plasma sheet activity was proposed by *Hones et al.* [1973]. Here gradual thinning of the plasma sheet occurs during the growth phase. Onset of the expansion phase is a result of merging at approximately $X = -15\,R_E$ and is accompanied by further rapid thinning at distances tailward of $X = -15\,R_E$, but rapid thickening earthward of this location. Recovery in this case was attributed to an overall decrease in cross-tail current intensity between $-10\,R_E$ and $-60\,R_E$. This was modified a few years later [*Hones*, 1979]. Here the neutral line remained at its initial position until recovery when it moved down the tail, inflating closed field lines earthward of it to reform the quiet time plasma sheet. Substorm plasmoid formation, another important component in subsequent NENL models, was introduced in this paper. A plasmoid is a "closed magnetic loop structure" proposed to be a direct consequence of the neutral line formation at the onset of the expansion phase. This "blob of magnetised plasma" is severed from the plasma sheet at onset and carried tailward by the solar wind. Satellite observations have confirmed the existence of such a structure. Later observational evidence indicated that the x-line was formed further from the earth at distances beyond $X = -20\,R_E$ [*Baumjohann*, 1988].

The key elements of the NENL model may be summarised as follows :

1. The substorm growth phase is initiated by the southward turning of the IMF which enhances dayside merging.

2. The increased anti-sunward transport of flux enlarges the tail and increases the tail lobe field strength.

3. This results in the 'stretching' of the field in the near-earth tail as well as

plasma sheet thinning in this region.

4. Onset of the expansion phase occurs when an x-type neutral line forms. The location of this neutral line remains controversial. Earlier models place it at ~ -10 to $-20\,R_E$. Revised models place it at a radial distance greater than $20\,R_E$.

5. This causes the formation of a plasmoid which travels down the tail.

6. Earthward of the neutral line, the magnetic field becomes more dipolar with the earthward flow of energised plasma.

7. The neutral line remains at its original location until recovery, when it propagates tailward.

8. This results in the thickening of the plasma sheet.

The above process is represented pictorially in figure 1.5.

The success of the NENL model lies in its ability to account for all three phases of the substorm. It is mainly for this reason that it has become the most widely accepted model of the substorm process. It is, however, not without deficiencies. Although it is an advanced morphological model, most of the physics behind the NENL model is not yet well understood. For example, the NENL model does not explain the time-dependent nature of the plasma sheet thinning process. *Kan* [1990] has criticised magnetohydrodynamic (MHD) treatments of the NENL model for their use of dissipative MHD in the collisionless plasma sheet.

The main point of contention in the NENL model is the location of the neutral line. The host of evidence [*Lui*, 1991b] for substorm initiation occurring close to the earth ($|X| \leq 15\,R_E$) and the lack of neutral line signatures in this region make the position of the x-line a critical problem in this model. Another criticism levelled at the NENL model is how it relates to the directly driven component

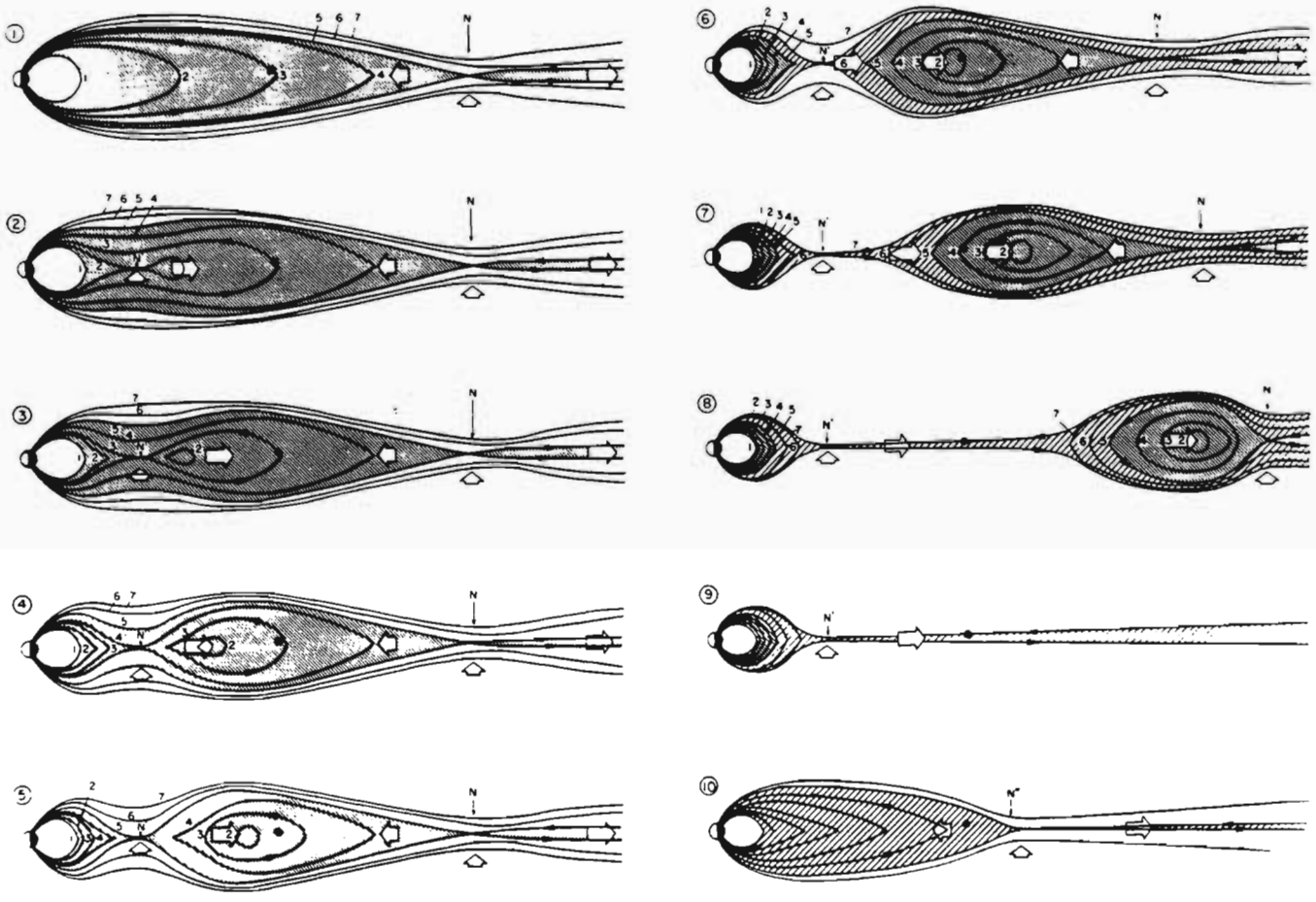

Figure 1.5: Schematic representation of the near-earth neutral line model of magnetospheric substorms. The magnetic field lines 1, 2, 3, 4 and 5 are closed; 6 and 7 are lobe field lines. The letter N indicates a neutral line. Broad white arrows indicate plasma flow. From *Hones* [1984].

of substorm activity [*Rostoker*, 1991]. Evidence of this lies in the examination of magnetotail plasma and field behaviour while ionospheric signatures are ignored.

Wave-induced precipitation model

An early model which did not require a neutral line was proposed by *Parks et al.* [1972]. This may be described as a "wave-induced precipitation model" [*Lui*, 1991a]. Here the earthward transport of previously isotropic plasma sheet plasma results in an anisotropic temperature distribution with the perpendicular temperature component being higher than the parallel temperature component. This results in the excitation of electrostatic waves, which in turn promotes whistler wave growth and thus enhances particle precipitation. The immediate consequence of this is the restoration of the near-earth field to a more dipolar configuration and the acceleration of particles in this region by the betatron effect. This enhances temperature and pitch angle anisotropy to provide a self-sustaining process. This feedback loop is destroyed when the source (the plasma sheet) can no longer supply the required electron flux.

This model, though, accounts for only a few of the observed auroral, ionospheric and magnetospheric features of the substorm, a problem common to many alternative substorm scenarios.

Boundary layer model

The boundary layer (BL) model suggested by *Rostoker and Eastman* [1987] has a growth phase similar to that of the NENL model. In the BL model it is emphasised that the growth phase is due to an intensification of processes directly driven by the solar wind-magnetosphere interaction; that is, it represents part of the directly driven component of substorm activity. Plasma circulation in the

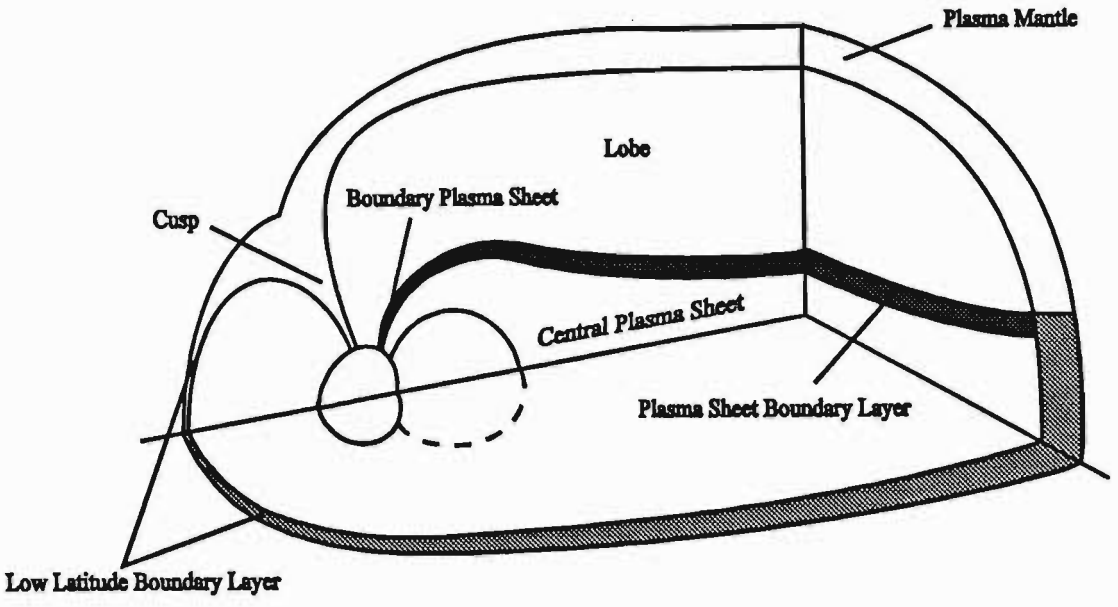

Figure 1.6: Simplified representation of the different regions in the magnetotail. In the boundary layer model, the boundary plasma sheet is assumed to map to the plasma sheet boundary layer. After *Burch*, [1989].

central plasma sheet (CPS) and low latitude boundary layer (LLBL) is increased during the growth phase.

The enhanced energy flow into the magnetosphere during the growth phase leads to a burst of reconnection in the far tail around $\sim -100\,R_E$ at onset. This reconnection results in strong earthward convective flows in the central plasma sheet and field aligned flow in the plasma sheet boundary layer (PSBL). The plasma sheet boundary layer is a region approximately $2\,R_E$ thick between the CPS and the tail lobes [*Baumjohann*, 1988]. The different magnetotail regions are depicted in figure 1.6. Vital to the BL model is the proposed mapping of the boundary plasma sheet (BPS) region in the topside ionosphere to the PSBL in the magnetotail. This mapping correlates the brightening of a pre-existing auroral arc to the increased earthward ion flow in the PSBL in the expansive phase.

Anti-sunward convective flow in the low latitude boundary layer adjacent to the central plasma sheet results in a velocity shear zone between these two plasma

regimes. When the earthward flow in the CPS is enhanced, the velocity shear is increased. This leads to the growth of the Kelvin-Helmholtz instability at the CPS/LLBL interface. A direct consequence of this is the generation of spatially localised field aligned currents. This is seen as the establishment of the substorm current wedge, the evening edge of which corresponds to the westward travelling surge in the ionosphere [*Lui*, 1991b]. Multiple surges are the result of the wave-like forms generated by the instability at the CPS/LLBL boundary (figure 1.7). *Rostoker and Eastman* [1987] suggest that the satellite observations used to support the concept of neutral line formation may be interpreted in terms of the motion of the plasma sheet boundary layer over the satellite.

A question that needs to be addressed is whether earthward flows in the CPS are strong enough to permit the growth of the Kelvin-Helmholtz instability on time scales of surge evolution [*Rostoker*, 1991]. The boundary layer model also neglects middle and distant tail effects after onset. Even so it must be recognised that the plasma sheet boundary layer is probably not a distinct regime in these regions [*Nishida et al.*, 1988]. It has also been pointed out [*Kan*, 1990] that later mappings are in contrast to that used by *Rostoker and Eastman* [1987].

Thermal catastrophe model

The thermal catastrophe (TC) model proposed by *Smith et al.* [1986] and *Goertz and Smith* [1989] ascribes onset to a discontinuous increase in temperature in the plasma sheet boundary layer. The PSBL has been recognised as the principal region of particle heating and a source, by convective transport, of hot plasma in the central plasma sheet. In the TC model, ions in the PSBL are heated by the resonant absorption of Alfvén waves. These Alfvén waves are generated by the Kelvin-Helmholtz instability at the magnetopause, which has been well documented (e. g. *Walker* [1981] and references therein). During the growth phase, the heating of the PSBL evolves through a succession of quasi-static, or equilibrium,

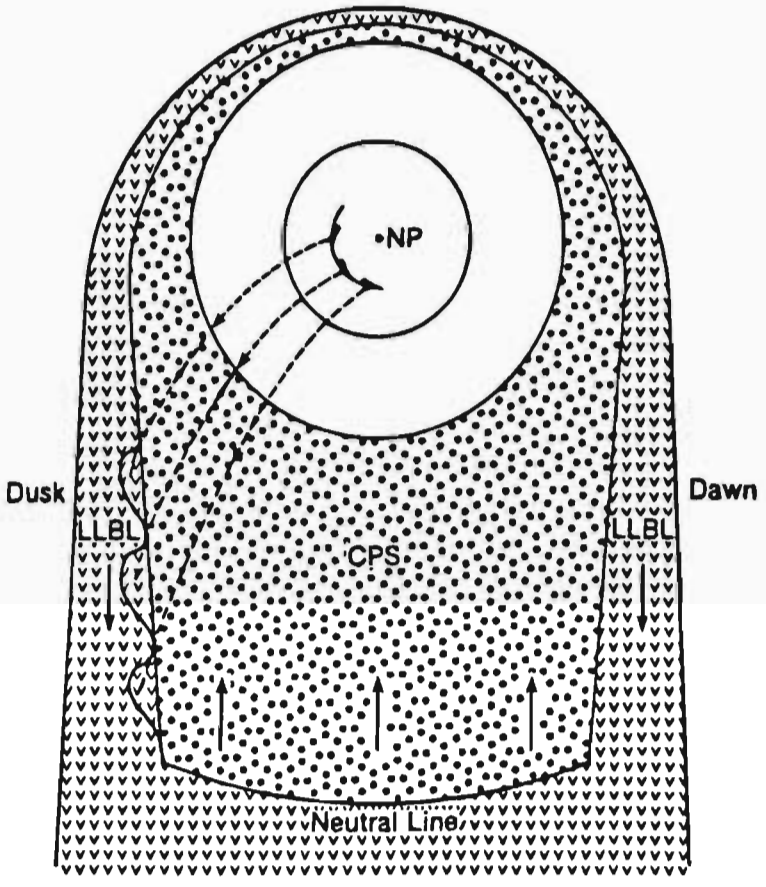

Figure 1.7: In the boundary layer model, the growth of the Kelvin-Helmholtz instability at the interface between the low latitude boundary layer (LLBL) and the central plasma sheet (CPS) leads to multiple surges in the auroral ionosphere. From *Rostoker* [1991].

states. These states are described by an equation of state for the PSBL whose solution is parameterised by a quantity which depends on the incident power of Alfvén waves, the local density and the convection velocity toward the CPS. In *Goertz and Smith* [1989], the treatment was generalised further to include the effects of finite B_z, the magnetic field perpendicular to the resonance layer. In this later version of the model, the control variables are the lobe magnetic field and the incident power flux.

Onset occurs at some critical point when the PSBL becomes effectively opaque to the incident Alfvén waves. In the early model [*Smith et al.*, 1986] this corresponded to some critical combination of the appropriate parameters. In the later treatment [*Goertz and Smith*, 1989] opacity (for a physically reasonable range of incident power flux) was achieved at some critical value of the lobe field. At this critical point, the heating in the PSBL becomes too rapid for the excess to be convected toward the CPS and the temperature increases discontinuously.

The thermal catastrophe model [*Goertz and Smith*, 1989] is a one dimensional model and is therefore unable to explain two and three dimensional features such as the westward travelling surge and the substorm current wedge . The model explains the heating of plasma sheet ions, but neglects the other main features of the substorm.

Magnetosphere-ionosphere coupling model

The basic elements of the magnetosphere-ionosphere coupling (MIC) model of the magnetospheric substorm were first suggested by *Coroniti and Kennel* [1973]. The pivotal concept in the MIC model is that the onset of the expansive phase may be triggered by the ionosphere. In the transient response MIC model [*Kan et al.*, 1988] southward turning of the IMF results in enhanced magnetospheric convection. This enhancement is responsible for the generation of Alfvén waves

which bounce back and forth between the ionosphere and magnetosphere until ionospheric convection has been elevated to match the increase in magnetospheric convection [*Kan*, 1990]. The time delay of the ionospheric response (approximately 30 minutes) corresponds to the growth phase of the substorm. The establishment of intense upward field aligned currents follows, the most intense of these being located near the poleward boundary of diffuse aurora at onset. The criteria for onset include a polar cap potential drop of greater than 70 kV and an overlap of the convection reversal region with the poleward gradient of the diffuse auroral conductance in the ionosphere in the midnight sector [*Kan et al.*, 1988]. Recovery begins when either of these two conditions are violated.

Kan [1993] has suggested that the localised dipolarisation in the near-earth plasma sheet may be a direct consequence of the intense upward field aligned current which propagates by Alfvén waves toward the plasma sheet. When the wave front reaches the plasma sheet, the cross-tail current is disrupted and the substorm current wedge formed.

The magnetosphere-ionosphere coupling model has very little to say about the magnetotail signatures of the substorm. It specifies the condition and evolution of the substorm current system while ignoring temporal and spatial changes in the tail [*Lui*, 1991b]. Some of these problems may be overcome by combining salient features of the NENL and MIC models [*Kan*, 1993].

Current disruption model

The current disruption model [*Chao et al.*, 1977; *Lui*, 1979] was introduced when observational evidence was found to be inconsistent with the formation of a large scale neutral line within a tailward distance of 20 R_E. The expected tailward flows and changes in magnetic field configuration were seldom found. Plasma sheet thinning, however, was observed to be initiated in the near-earth mag-

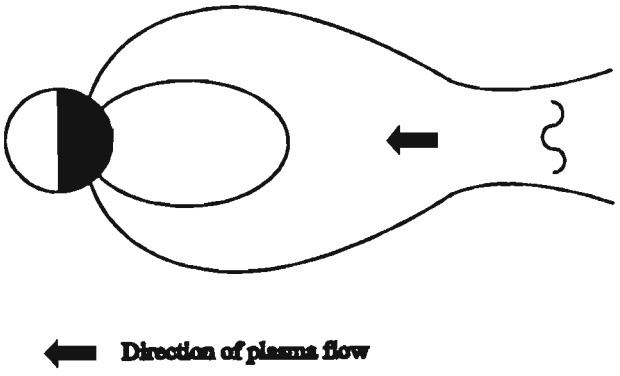

Figure 1.8: The launching of a rarefraction wave down the tail as envisioned by the current disruption model. After *Lui* [1991b].

netotail at onset, and then travel rapidly tailward. In the current disruption model, thinning is achieved when a change in the cross-tail current launches a fast mode magnetohydrodynamic rarefraction wave in the anti-sunward direction. The propagation of this wave is associated with the earthward drainage of plasma (figure 1.8) rather than the tailward loss of plasma suggested by the neutral line model. The disruption or diversion of the cross-tail current can account for the reconfiguration of the magnetic field in the near-earth tail at onset as well as particle injection and energisation by convection surges [*Lui*, 1991b].

Ballooning instability model

The ballooning instability model [*Roux et al.*, 1991a; *Roux et al.*, 1991b] examines the boundary between the dipole-like and tail-like field lines in the near-earth tail at the end of the growth phase. In the equatorial plane, the gradient of the magnetic field and that of the ion pressure are directed earthward in the dipole-like region. In the tail-like region, these gradients become tailward. The boundary between these two regions is unstable and a polarisation electric field develops. Drifting ions carry the disturbance westward, with charges accumulating at the edges of the perturbation. These charges generate field aligned currents which

are mapped down to the ionosphere as the westward travelling surge.

Again, criticism of both the current disruption model and the ballooning instability model is centered on their description of limited aspects of substorm dynamics.

1.5 Synthesising a global model

It is obvious that the fundamental problem with the above models is that they concentrate on a few features of the substorm while neglecting others. This is mainly the result of attempting to explain substorm phenomena in a specific region. Despite their differences, certain aspects of the various models may be synthesised to give a model with an improved compatibility with observations.

With this in mind, *Lyons and Nishida* [1988] combined the near-earth neutral line and boundary layer models, while *Kan* [1993] has combined features of the magnetosphere-ionosphere coupling and NENL models. Both of these give a more global picture of the substorm process. It would be wrong to discard any of the mechanisms suggested in the alternative models, however, as each is not without merit. *Lui* [1991a, 1991b] has attempted to synthesise a global model that draws on the strengths of these various proposals.

The most controversial aspect of the models that have been discussed is the location of the onset of the expansion phase. As has been mentioned, there is much direct and indirect evidence supporting substorm initiation in the near-earth region. This position is thus adopted by *Lui* [1991a, 1991b] in his synthesis model as the location for onset. *Lui* [1991a, 199b] divides the magnetotail into the near-earth ($-5\,R_E \geq X \geq -15\,R_E$), mid-tail ($-15\,R_E \geq X \geq -80\,R_E$), and far-tail ($X \leq -80\,R_E$) regions.

Synthesis model

Growth Phase: This follows the sequence of events proposed by the NENL model. Southward turning of the IMF results in a reconfiguration of the magnetosphere. The dayside magnetopause moves toward the earth as magnetic flux is transported to the tail by the solar wind. The inner edge of the cross-tail current moves earthward. The cross-section of the tail increases. In the ionosphere this is apparent as the equatorward motion of the polar cap boundary. The cross-tail current in the near-earth region at ~ -6 to $-15\,R_E$ increases resulting in the thinning of the plasma sheet and the magnetic field becoming more stressed, or tail-like. No significant thinning is apparent in the mid-tail.

Expansion Phase: Onset of the expansion phase occurs when the intense cross-tail current in the near-earth region is disrupted. This may be due to various mechanisms such as sudden heating of the plasma sheet, ion or electron tearing, the cross-field current instability or the ballooning (interchange) instability. A portion of the cross-tail current is diverted to the ionosphere. If conditions in the ionosphere are not suitable for the imposed current, the current diversion is prevented leading to pseudo-breakup with no subsequent poleward expansion of the aurora. If conditions are favourable, a substorm current wedge is formed. Dipolarisation of the magnetic field in the disturbance region produces an earthward convection surge. The partial evacuation of plasma at this site results in a rarefraction wave which propagates tailward. Current disruption may occur at more than one location at different times during the expansive phase. Each disturbance which results in successful current diversion gives rise to a convection surge and corresponding rarefraction wave. These are evident as substorm intensifications. The rarefraction waves lead to plasma sheet thinning in the mid-tail and transient earthward plasma flows. The initial disruption may set up a perturbation at the boundary of the dipole-like and tail-like field in the near-earth region which propagates as a surface wave as described in the ballooning instability model. This

mechanism, as well as the cross-field current and Kelvin-Helmholtz instabilities, can give rise to the local time widening of the disturbance region. On reaching the far tail, the rarefraction wave could set up a region of strong velocity shear at the low latitude boundary layer giving rise to the Kelvin-Helmholtz instability and resulting in multiple surge forms or vortices.

Recovery Phase: After the passage of the rarefraction waves, the plasma sheet is thin, with a small B_z component and may be unstable to the tearing instability. Reconnection could occur at a downstream distance of 20 to 80 R_E resulting in one or more x-lines. This allows for plasmoid formation and the subsequent thickening of the plasma sheet earthward of these locations. When the plasma sheet becomes thick enough to limit this reconnection process, substorm activity subsides.

The development of the substorm in the synthesis model is represented schematically in figure 1.9.

This model avoids the questionable formation of a near-earth neutral line by invoking a two stage process of current disruption and subsequent reconnection at a later stage further downstream. Pseudo-breakups are accounted for as are multiple intensifications. It does not, however, explain the evolution of substorms which occur during intervals of northward IMF or as a result of solar wind pressure pulses. It has also been observed that a substorm does not necessarily have to be preceded by a growth phase.

1.6 A magnetohydrodynamic model

A recently proposed magnetohydrodynamic model of substorms [*Walker and Samson*, 1994] provides an alternative physical framework for the substorm process. The model depends on the natural modes of oscillation of the magneto-

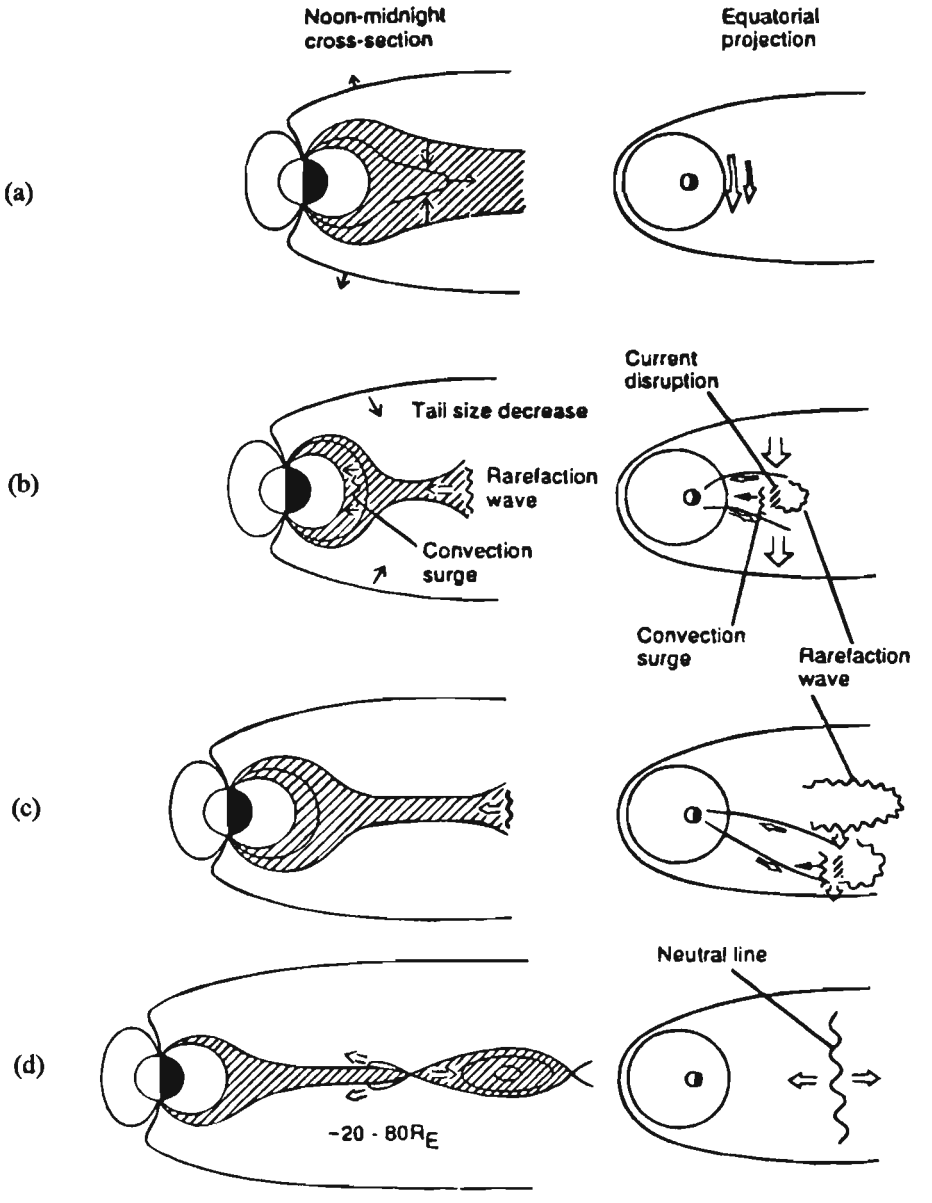

Figure 1.9: The synthesis model proposed by *Lui* [1991a, 1991b]. The left panel shows substorm development in the meridian plane. The right panel depicts the corresponding equatorial view. The substorm phases depicted are (a) Growth (b) Onset (c) Expansion (d) Late Expansion/Recovery. From *Lui* [1991].

sphere and the excitation of magnetohydrodynamic waves. The attribution of certain phases of substorm development to magnetohydrodynamic wave activity has only been demonstrated in a few models, such as the thermal catastrophe and the boundary layer models. *Walker and Samson* [1994] emphasise the importance of magnetohydrodynamic waves and oscillations in understanding the dynamics of processes within the magnetosphere. Central to the model are the physical mechanisms of cavity oscillations and toroidal resonances.

1.6.1 Cavity modes and field line resonances

Ground based observations have demonstrated that quasi-monochromatic, long-period ULF pulsations display certain characteristic features [*Samson et al.*, 1971]. These include a latitudinal dependence of both peak amplitude with frequency and the sense of polarisation. The fact that these pulsations are quasi-monochromatic suggests that they originate from toroidal, or field line, resonances of the magnetic field in the earth's magnetosphere [*Samson et al.*, 1971] as described below.

In a cold uniform plasma two magnetohydrodynamic waves—the fast and shear Alfvén waves—can exist [*Walker et al.*, 1992]. Associated with each of these waves is a natural magnetohydrodynamic mode of oscillation. The poloidal or compressional mode corresponds to the fast Alfvén wave. The plasma displacement and magnetic field perturbation in this case lie in the magnetic meridian. The outer boundary for this mode is the magnetopause, with the ionosphere forming further boundaries at the ends of the magnetic field lines. The radially inward gradient of Alfvén speed in the nightside magnetosphere results in an inner boundary. This provides a turning point where the compressional mode may be reflected. This radial mode of oscillation is known as a cavity mode.

The toroidal mode corresponds to the shear Alfvén wave. Here the plasma dis-

placement and magnetic field perturbation are perpendicular to the meridian plane. Each magnetic shell may be defined by the radial distance at which it cuts the equatorial plane. This is termed the 'L value'. A magnetic shell of a particular L value will oscillate toroidally (perpendicular to the meridian plane) with a specific frequency. It is these transverse (or azimuthal) oscillations which are referred to as field line resonances.

If the magnetosphere were cylindrically symmetrical with a perfectly conducting ionosphere, the poloidal and toroidal modes would be separated [*Walker et al.*, 1992]. In the real magnetosphere, however, these two modes are coupled. Early theories of field line resonances [*Southwood*, 1974; *Chen and Hasegawa*, 1974] concentrated on weak coupling between these modes. Here it was suggested that the fast Alfvén waves (probably generated by the Kelvin-Helmholtz instability at the magnetopause) provided the energy source for field line resonance via this coupling. Although this successfully accounts for the characteristics reported by *Samson et al.* [1971], it does not explain why field line resonances are observed to occur at discrete frequencies. The Kelvin-Helmholtz instability in the LLBL and pressure pulses at the magnetopause, both proposed as sources of field line resonances, have very broad spectra [*Samson et al.*, 1991]. *Kivelson and Southwood* [1985] suggested that the shortcoming in these models lay in the weak coupling restriction. They predicted that the observed discrete frequencies were the resonant fast mode frequencies of the cavity formed by the magnetopause and the turning point due to the gradient in Alfvén velocity. This was confirmed [*Allan et al.*, 1986; *Kivelson and Southwood*, 1986] by demonstrating that a compressional perturbation at the magnetopause sets up compressional resonances which in turn drive field line resonances where the field line eigenfrequencies match the cavity resonance eigenfrequencies.

1.6.2 The linear mini-substorm

Walker and Samson [1994] have described the basic set of processes for their picture of substorm development in terms of a "mini-substorm". In this scenario, a disturbance of the cross-tail current results in the radiation of a magnetohydrodynamic wave. The instability causing the perturbation may be magnetohydrodynamic, such as the ballooning mode, although the nature of the instability is not crucial to the model. The part of the magnetohydrodynamic wave which propagates earthward encounters a cavity whose boundary is proposed to take the form of a density step. This cavity is excited into oscillation at its discrete natural frequencies. These in turn excite toroidal resonances with the appropriate frequencies. Energy leaks via evanescent barrier penetration from the poloidal to the toroidal modes as well as through the cavity boundary, where it takes the form of a wave travelling up the tail. Strong magnetic shear across the L-shell on which the toroidal resonance is located leads to the establishment of strong field aligned currents. These may be intense enough to lead to precipitation so that auroral arcs develop which oscillate at the resonant frequency.

The cross-tail current disturbance is not necessarily located outside of the natural magnetospheric cavity. If located within the cavity, the described development still applies. The cavity excitation mechanism is also not absolute. A disturbance in the solar wind, such as a pressure pulse, is another possibility. Again, the excitation and behaviour of the field line resonances remains unchanged.

The above processes are linear and constitute the linear mini-substorm.

1.6.3 Substorm development

In the magnetohydrodynamic model, the growth phase (where it occurs) develops in the conventional way. Enhanced merging at the dayside magnetopause leads to

subsequent plasma sheet thinning, with an increased near-earth cross-tail current. Disturbances in this current result in mini-substorm activity. If the disturbance is large enough, the process becomes non-linear.

In this case, the perturbation of the cross-tail current leads to the formation of the substorm current wedge. The field in the isotropic magnetosonic wave which is radiated causes the background field to become more dipolar. The tailward propagating portion of the wave increases in amplitude and steepens into a shock front. This is a non-linear effect. Behind the shock, conditions are such that reconnection may occur. Neutral line formation leads to the observed particle acceleration in the plasma sheet.

The earthward propagating wavefront encounters the natural magnetospheric cavity, with cavity and toroidal modes being excited as in the linear mini-substorm. The toroidal oscillations are, however, now more extreme than before. Strong shocks form above the ionosphere with the typical inverted-V structure. In the equatorial plane, the resonance may be driven to non-linearity by the Kelvin-Helmholtz instability. This results in the formation of a vortex structure which maps down to the ionosphere as an auroral surge. This surge structure may move polewards when lower frequency resonances are excited. Alternatively, the dipolarisation of the field could result in the same resonance mapping to higher latitudes.

As has been mentioned, the initiation mechanism may vary. For the case of an external disturbance on the magnetopause, the substorm is proposed to develop in a similar way.

The model depends crucially on the natural magnetospheric cavity which has been described. Although direct evidence for the invoked density step in the tail is not available, pulsation observations [*Ruohoniemi et al.*, 1991; *Samson et al.*, 1991; *Walker et al.*, 1992] require that such a cavity or "equivalent resonator"

[*Walker and Samson*, 1994] exist.

1.6.4 Onset of the expansion phase

One of the areas of greatest controversy in substorm research is the identification of the nature and location of the mechanisms responsible for the onset of the expansive phase. Much attention has been given to microinstabilities as possible triggering mechanisms. *Axford* [1984] pointed out that it is necessary to establish why a previously stable configuration should change rapidly into an unstable one. In order to do this, the overall stress balance needs to be examined. This implies that macroscopic instabilities in configuration space are also important to the stability of a system such as the magnetotail.

In this vein, *Walker and Samson* [1994] have suggested the ballooning instability as a possible magnetohydrodynamic onset triggering mechanism. The purpose of the following chapters is to establish whether this is viable.

This study is similar to recent investigations by *Lee and Wolf* [1992] and *Ohtani and Tamao* [1993]. *Lee and Wolf* [1992] have used the energy principle to test the stability of flux tubes against ballooning in the limit $k_\perp = k_y \rightarrow \infty$. *Ohtani and Tamao* [1993] used an eigenmode analysis for the same limit. In both of these investigations it was concluded that the magnetotail is stable against ballooning.

Chapter 2 details the normal mode analysis and derivation of the ballooning instability condition in the limit $k_\parallel \approx 0$.

Chapter 2

The Ballooning Instability

2.1 Introduction

Under average conditions in the near-earth plasma sheet, the magnetic field and plasma pressure gradients transverse to the magnetic field are directed earthwards, so that the gradient of the total pressure is in this direction. Here the plasma is held in equilibrium by the Maxwell stress acting along the line of force. This 'tension' is a result of the curvature of the field. A situation such as this may be unstable to the interchange, or ballooning instability. If a perturbation causes the plasma or field to be displaced tailwards, the field will tend to 'balloon' in this direction.

The purpose of this chapter is to derive an instability threshold condition for the ballooning mode in the region near the equatorial plane. With the help of a suitably realistic model of the magnetotail during growth phase conditions to give numerical results, this condition may then be used to predict whether the ballooning instability contributes to the triggering of magnetospheric substorms.

The normal mode stability analysis and derivation in this chapter are due to

Walker [1994].

2.2 The model

2.2.1 Simplifications

The geometry of the magnetic field in the geomagnetic tail is complicated, with both torsion and curvature required to define it. In order to simplify the analysis, the elements essential to the instability need to be extracted.

The region of interest is the equatorial plane. Here cylindrical symmetry is assumed, which allows any azimuthal dependence to be treated separately. As a result the magnetic field lines have no torsion and lie in the meridian plane. Symmetry is also assumed about the equatorial plane. The quantities of interest are the magnetic field intensity and plasma pressure. These may be characterised by their gradients in the meridian plane. Near the equator these are approximately perpendicular to the magnetic field.

2.2.2 Geometrical considerations

For any curve it is possible to define three orthogonal unit vectors, $\hat{\boldsymbol{\mu}}$, $\hat{\boldsymbol{\nu}}$ and $\hat{\boldsymbol{\varphi}}$ where $\hat{\boldsymbol{\mu}}$ is tangent to the curve, $\hat{\boldsymbol{\nu}}$ points away from the centre of curvature in the osculating plane and $\hat{\boldsymbol{\varphi}} = \hat{\boldsymbol{\mu}} \times \hat{\boldsymbol{\nu}}$. Figure 2.1 shows the three unit vectors in relation to a magnetic field line.

These vectors obey Frenet's formulae [*Rutherford*, 1957]

$$\frac{d\hat{\boldsymbol{\mu}}}{ds} = -\kappa\hat{\boldsymbol{\nu}}, \quad \frac{d\hat{\boldsymbol{\nu}}}{ds} = -\tau\hat{\boldsymbol{\varphi}} + \kappa\hat{\boldsymbol{\mu}}, \quad \frac{d\hat{\boldsymbol{\varphi}}}{ds} = -\tau\hat{\boldsymbol{\nu}} \tag{2.1}$$

Here s is the arc distance measured along the curve, κ is the curvature and τ is

the torsion. In order to make the initial analysis as coordinate-free as possible, a local set of Cartesian coordinates $(x_\mu, x_\nu, x_\varphi)$ at a point on a magnetic field line is used. These coordinates are shown in figure 2.2.

2.2.3 Basic equations

In the model it is assumed that pressure is isotropic. The magnetohydrodynamic equations are then:

the momentum equation,

$$\rho \frac{D\mathbf{v}}{Dt} = -\nabla \left(P + \frac{B^2}{2\mu_0} \right) + \frac{(\mathbf{B}.\nabla)\mathbf{B}}{\mu_0} \tag{2.2}$$

the continuity equation,

$$\frac{\partial \rho}{\partial t} + \nabla.(\rho \mathbf{v}) = 0 \tag{2.3}$$

the adiabatic law,

$$\frac{D}{Dt}\left(\frac{P}{\rho^\gamma} \right) = 0 \tag{2.4}$$

Faraday's law,

$$\nabla \times \mathbf{E} = -\frac{\partial \mathbf{B}}{\partial t} \tag{2.5}$$

Ampére's law,

$$\nabla \times \mathbf{B} = \mu_0 \mathbf{J} \tag{2.6}$$

and Ohm's law (with infinite conductivity),

$$\mathbf{E} + \mathbf{v} \times \mathbf{B} = 0, \; E_\parallel = 0 \tag{2.7}$$

In the above, the operator

$$\frac{D}{Dt} \equiv \frac{\partial}{\partial t} + \mathbf{v}.\nabla$$

is the convective derivative with respect to time. These equations will be linearised to derive the appropriate dispersion relation.

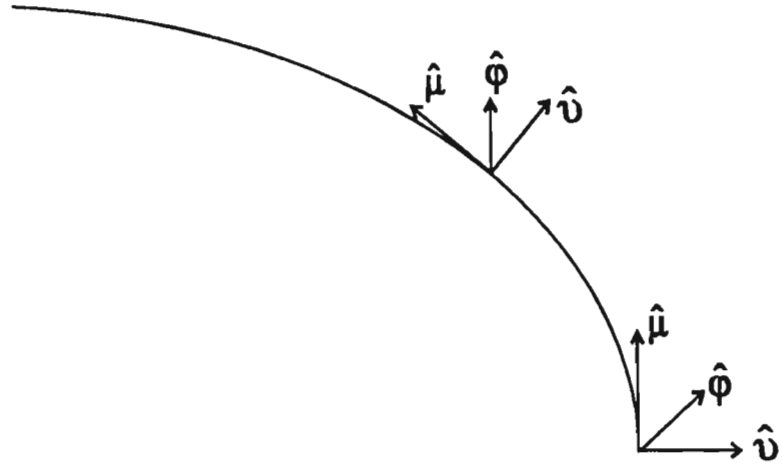

Figure 2.1: The tangent, normal and binormal unit vectors at two points on a magnetic field line in the meridian plane.

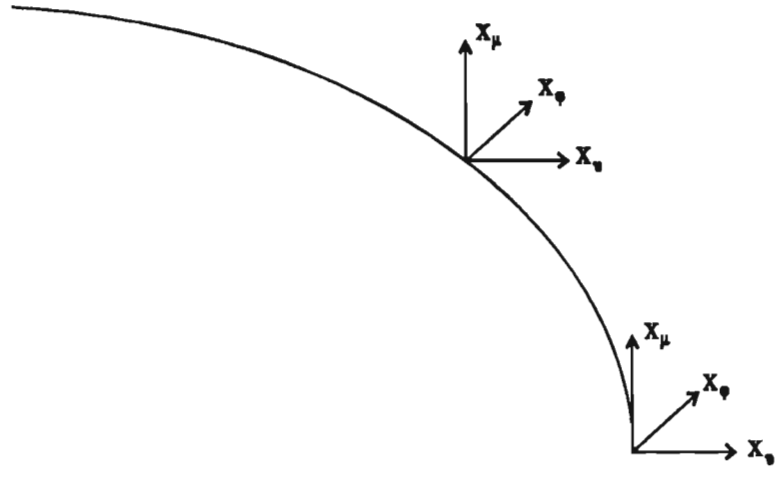

Figure 2.2: The local set of Cartesian coordinates $(x_\mu, x_\nu, x_\varphi)$ at two points on a magnetic field line. At the equator, the Cartesian coordinates are in the direction of $(\hat{\mu}, \hat{\nu}, \hat{\varphi})$.

2.2.4 Geometrical results

It is useful to establish certain conditions which are a result of the geometry that has been adopted. In local Cartesian coordinates, the most general form of the tensor $\nabla \mathbf{B}$ is

$$\nabla \mathbf{B} = \begin{pmatrix} \frac{\partial B_\mu}{\partial x_\mu} & \frac{\partial B_\nu}{\partial x_\mu} & \frac{\partial B_\varphi}{\partial x_\mu} \\ \frac{\partial B_\mu}{\partial x_\nu} & \frac{\partial B_\nu}{\partial x_\nu} & \frac{\partial B_\varphi}{\partial x_\nu} \\ \frac{\partial B_\mu}{\partial x_\varphi} & \frac{\partial B_\nu}{\partial x_\varphi} & \frac{\partial B_\varphi}{\partial x_\varphi} \end{pmatrix} \tag{2.8}$$

The components of this tensor may be expressed in terms of inverse length scales for magnetic field variation κ_μ, κ_ν and κ_φ such that

$$\kappa_\mu = \frac{1}{B}\frac{\partial B_\mu}{\partial x_\mu}, \quad \kappa_\nu = \frac{1}{B}\frac{\partial B_\mu}{\partial x_\nu}, \quad \kappa_\varphi = \frac{1}{B}\frac{\partial B_\varphi}{\partial x_\varphi} \tag{2.9}$$

Using the geometry of the magnetic field demonstrated in figure 2.3 and noting that $\kappa = 1/R$ (where R is the radius of curvature) gives the result

$$\frac{\partial B_\nu}{\partial x_\mu} = -\kappa B \tag{2.10}$$

The assumption of azimuthal symmetry implies that

$$\frac{\partial B_\varphi}{\partial x_\mu} = \frac{\partial B_\varphi}{\partial x_\nu} = 0 \tag{2.11}$$

The cross-tail current is assumed to flow completely in the $\hat{\varphi}$ direction (which is approximately the case near the equatorial plane). By Ampére's law, then, $\nabla \times \mathbf{B}$ has no components in the meridian plane. Since

$$\nabla \times \mathbf{B} = \left[\frac{\partial B_\varphi}{\partial x_\nu} - \frac{\partial B_\nu}{\partial x_\varphi}\right]\hat{\mu} + \left[\frac{\partial B_\mu}{\partial x_\varphi} - \frac{\partial B_\varphi}{\partial x_\mu}\right]\hat{\nu} + \left[\frac{\partial B_\nu}{\partial x_\mu} - \frac{\partial B_\mu}{\partial x_\nu}\right]\hat{\varphi} \tag{2.12}$$

equation 2.11 implies that

$$\frac{\partial B_\mu}{\partial x_\varphi} = \frac{\partial B_\nu}{\partial x_\varphi} = 0 \tag{2.13}$$

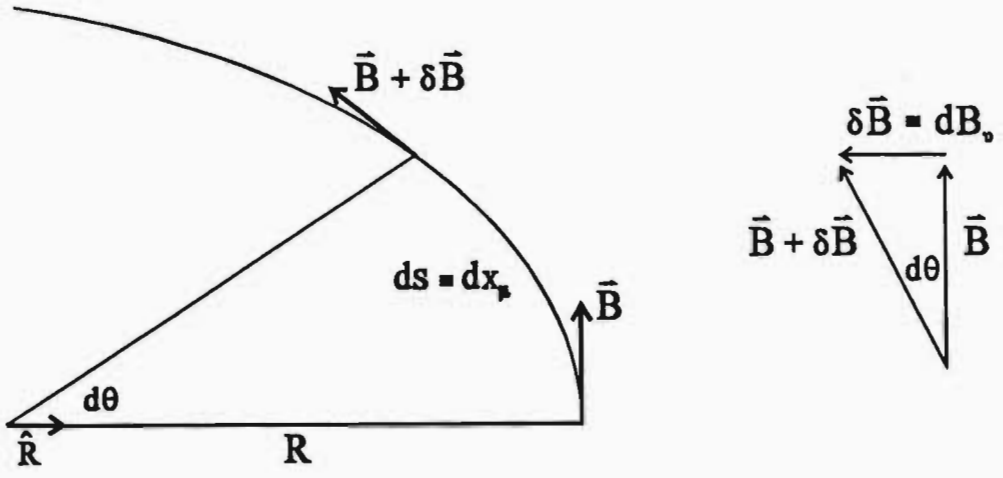

Figure 2.3: The geometry of a magnetic field line in the meridian plane.

Now $\nabla.\mathbf{B} = 0$. Explicitly,

$$\frac{\partial B_\mu}{\partial x_\mu} + \frac{\partial B_\nu}{\partial x_\nu} + \frac{\partial B_\varphi}{\partial x_\varphi} = 0 \tag{2.14}$$

so that, using the expressions in 2.9,

$$\frac{\partial B_\nu}{\partial x_\nu} = -B\kappa_\mu - B\kappa_\varphi = -B(\kappa_\mu + \kappa_\varphi) \tag{2.15}$$

The expression for $\nabla\mathbf{B}$ in equation 2.8 now becomes

$$\nabla\mathbf{B} = B \begin{pmatrix} \kappa_\mu & -\kappa & 0 \\ \kappa_\nu & -(\kappa_\mu + \kappa_\varphi) & 0 \\ 0 & 0 & \kappa_\varphi \end{pmatrix} \tag{2.16}$$

The unit vectors $\hat{\mu}$, $\hat{\nu}$ and $\hat{\varphi}$ may be written as $(1,0,0)$, $(0,1,0)$ and $(0,0,1)$ in this coordinate frame. This is useful in deriving the gradient tensors of these vectors.

Near the equatorial plane, the zero order magnetic field is $\mathbf{B} = \hat{\mu}B$. Thus

$$\begin{aligned} \nabla\mathbf{B} &= \nabla(\hat{\mu}B) \\ &= (\nabla\hat{\mu})B + (\nabla B)\hat{\mu} \end{aligned}$$

so that

$$\nabla\hat{\mu} = \frac{\nabla\mathbf{B} - (\nabla B)\hat{\mu}}{B} \tag{2.17}$$

From equation 2.16 then,

$$\nabla\hat{\boldsymbol{\mu}} = \begin{pmatrix} 0 & -\kappa & 0 \\ 0 & -(\kappa_\mu + \kappa_\varphi) & 0 \\ 0 & 0 & \kappa_\varphi \end{pmatrix} \tag{2.18}$$

From the above,

$$\hat{\boldsymbol{\nu}}.\nabla\hat{\boldsymbol{\mu}} = -\hat{\boldsymbol{\nu}}(\kappa_\mu + \kappa_\varphi) \tag{2.19}$$

and

$$\hat{\boldsymbol{\varphi}}.\nabla\hat{\boldsymbol{\mu}} = \hat{\boldsymbol{\varphi}}\kappa_\varphi \tag{2.20}$$

Using the fact that the torsion is zero, Frenet's formulae in 2.1 become

$$\hat{\boldsymbol{\mu}}.\nabla\hat{\boldsymbol{\mu}} \equiv \frac{d\hat{\boldsymbol{\mu}}}{ds} = -\hat{\boldsymbol{\nu}}\kappa \tag{2.21}$$

and

$$\hat{\boldsymbol{\mu}}.\nabla\hat{\boldsymbol{\nu}} \equiv \frac{d\hat{\boldsymbol{\nu}}}{ds} = \hat{\boldsymbol{\mu}}\kappa \tag{2.22}$$

Now

$$\begin{aligned} \nabla.\mathbf{B} &= \nabla.(\hat{\boldsymbol{\mu}}B) \\ &= (\nabla.\hat{\boldsymbol{\mu}})B + \hat{\boldsymbol{\mu}}.(\nabla B) \\ &= 0 \end{aligned}$$

Since $\mathbf{B} = \hat{\boldsymbol{\mu}}B$, $B = \hat{\boldsymbol{\mu}}^t\mathbf{B}$ and the above becomes

$$(\nabla.\hat{\boldsymbol{\mu}})B + \hat{\boldsymbol{\mu}}.(\nabla\hat{\boldsymbol{\mu}}^t\mathbf{B}) = 0$$

Thus

$$\begin{aligned} \nabla.\hat{\boldsymbol{\mu}} &= -\frac{1}{B}\hat{\boldsymbol{\mu}}.(\nabla B_\mu) \\ &= -\frac{1}{B}(1,0,0).\left(\frac{\partial B_\mu}{\partial x_\mu}, \frac{\partial B_\mu}{\partial x_\nu}, \frac{\partial B_\mu}{\partial x_\varphi}\right) \\ &= -\frac{1}{B}(1,0,0).(B\kappa_\mu, B\kappa_\nu, 0) \\ &= -\kappa_\mu \end{aligned} \tag{2.23}$$

Using the appropriate vector identity,

$$\nabla \times \mathbf{B} = (\nabla \times \hat{\boldsymbol{\mu}})B + \nabla B \times \hat{\boldsymbol{\mu}}$$

Equations 2.9 to 2.13 give

$$\nabla \times \mathbf{B} = (0, 0, -B(\kappa + \kappa_\nu))$$

Now

$$\nabla B \times \hat{\boldsymbol{\mu}} = (0, 0, -B\kappa_\nu)$$

so

$$\begin{aligned} \nabla \times \hat{\boldsymbol{\mu}} &= \frac{1}{B}(\nabla \times \mathbf{B} - \nabla B \times \hat{\boldsymbol{\mu}}) \\ &= \frac{1}{B}(0, 0, -B\kappa) \end{aligned}$$

and therefore

$$\nabla \times \hat{\boldsymbol{\mu}} = -\hat{\boldsymbol{\varphi}}\kappa \tag{2.24}$$

From the geometry, $\hat{\boldsymbol{\nu}}.\nabla\hat{\boldsymbol{\nu}}$ is normal to $\hat{\boldsymbol{\nu}}.\nabla\hat{\boldsymbol{\mu}}$ so that, from equation 2.19

$$\hat{\boldsymbol{\nu}}.\nabla\hat{\boldsymbol{\nu}} = \hat{\boldsymbol{\mu}}(\kappa_\mu + \kappa_\varphi)$$

Also

$$\hat{\boldsymbol{\mu}}.\nabla\hat{\boldsymbol{\varphi}} = \hat{\boldsymbol{\nu}}.\nabla\hat{\boldsymbol{\varphi}} = 0$$

while

$$\hat{\boldsymbol{\varphi}}.\nabla\hat{\boldsymbol{\varphi}} = -\hat{\boldsymbol{\nu}}\kappa_s$$

where $\kappa_s^{-1} \equiv R_s$ is the perpendicular distance to the axis of symmetry. This gives

$$\hat{\boldsymbol{\varphi}}.\nabla\hat{\boldsymbol{\nu}} = \hat{\boldsymbol{\varphi}}\kappa_s$$

Collecting all these results, the tensors $\nabla\hat{\boldsymbol{\nu}}$ and $\nabla\hat{\boldsymbol{\varphi}}$ can therefore be written

$$\nabla\hat{\boldsymbol{\nu}} = \begin{pmatrix} \kappa & 0 & 0 \\ \kappa_\mu + \kappa_\varphi & 0 & 0 \\ 0 & 0 & \kappa_s \end{pmatrix}, \quad \nabla\hat{\boldsymbol{\varphi}} = \begin{pmatrix} 0 & 0 & 0 \\ 0 & 0 & 0 \\ 0 & -\kappa_s & 0 \end{pmatrix} \tag{2.25}$$

In the neighbourhood of the equatorial plane $R_\mu \to \infty$ and $R_\varphi \to \infty$, where R_μ and R_φ are defined in a similar way to R_s. The gradient tensors may then be simplified further:

$$\nabla \mathbf{B} = B \begin{pmatrix} 0 & -\kappa & 0 \\ \kappa_\nu & 0 & 0 \\ 0 & 0 & 0 \end{pmatrix} \tag{2.26}$$

and

$$\nabla \hat{\boldsymbol{\mu}} = \begin{pmatrix} 0 & -\kappa & 0 \\ 0 & 0 & 0 \\ 0 & 0 & 0 \end{pmatrix}, \quad \nabla \hat{\boldsymbol{\nu}} = \begin{pmatrix} \kappa & 0 & 0 \\ 0 & 0 & 0 \\ 0 & 0 & \kappa_s \end{pmatrix}, \quad \nabla \hat{\boldsymbol{\varphi}} = \begin{pmatrix} 0 & 0 & 0 \\ 0 & 0 & 0 \\ 0 & -\kappa_s & 0 \end{pmatrix} \tag{2.27}$$

2.2.5 Zero order momentum balance

Since the zero order velocity is zero, the zero order momentum equation is

$$\nabla \left(P + \frac{B^2}{2\mu_0} \right) = \frac{(\mathbf{B}.\nabla)\mathbf{B}}{\mu_0} \tag{2.28}$$

Using equation 2.26

$$\begin{aligned} \frac{(\mathbf{B}.\nabla)\mathbf{B}}{\mu_0} &= \frac{B}{\mu_0}(B,0,0) \begin{pmatrix} 0 & -\kappa & 0 \\ \kappa_\nu & 0 & 0 \\ 0 & 0 & 0 \end{pmatrix} \\ &= \left(\frac{B}{\mu_0}\right)(-\hat{\boldsymbol{\nu}}\kappa B) \\ &= -\hat{\boldsymbol{\nu}}\kappa \frac{B^2}{\mu_0} \end{aligned}$$

Equation 2.28 may then be written as

$$\nabla_\perp \left(P + \frac{B^2}{2\mu_0} \right) = -\hat{\boldsymbol{\nu}}\kappa \frac{B^2}{\mu_0} \tag{2.29}$$

and

$$\nabla_\parallel \left(P + \frac{B^2}{2\mu_0} \right) = 0 \tag{2.30}$$

where $\nabla_\perp$ and $\nabla_\parallel$ denote the gradients perpendicular and parallel to the field, respectively. In the above, $\nabla_\perp = \nabla_\nu$, since the assumption of cylindrical symmetry

allows no variation with x_φ . Since $B^2/2\mu_0$ is the magnetic pressure transverse to the field line, equation 2.30 becomes

$$\nabla_{\|} P = 0 \tag{2.31}$$

This implies that the pressure is constant along a field line. From equation 2.29 the sum of the kinetic and magnetic pressure is constant perpendicular to the field.

By expanding 2.29,

$$\nabla_{\perp}(P) + \nabla_{\perp}\left(\frac{B^2}{2\mu_0}\right) = -\hat{\nu}\kappa\frac{B^2}{\mu_0} \tag{2.32}$$

Using the expression for κ_ν in 2.9, the second term on the left of 2.32 may be written as

$$\begin{aligned}\nabla_\nu\left(\frac{B^2}{2\mu_0}\right) &= \frac{2B}{2\mu_0}\frac{\partial B_\nu}{\partial x_\nu} \\ &= \frac{B}{\mu_0}(B\kappa_\nu) \\ &= \kappa_\nu\frac{B^2}{\mu_0}\end{aligned}$$

Substitution of the above result into 2.32 gives

$$\nabla_\nu P = -\frac{B^2}{\mu_0}(\kappa + \kappa_\nu) \tag{2.33}$$

An inverse scale length for the pressure gradient may be defined as

$$\kappa_p = \frac{1}{P}\frac{\partial P}{\partial x_\nu} \tag{2.34}$$

Now

$$\nabla_\nu P = \frac{\partial P}{\partial x_\nu}$$

therefore, combining 2.33 and 2.34,

$$\kappa_p P = -\frac{B^2}{\mu_0}\kappa - \frac{B^2}{\mu_0}\kappa_\nu \tag{2.35}$$

Rearranging the above gives

$$\begin{aligned} \kappa_\nu &= -\kappa - \frac{P}{B^2/\mu_0}\kappa_p \\ &= -(\kappa + \frac{1}{2}\beta\kappa_p) \end{aligned} \tag{2.36}$$

where β is the plasma pressure to magnetic pressure ratio.

2.3 Linearisation of the MHD equations

It is assumed that the perturbation imposed has a time behaviour of the form $exp(-i\omega t)$. In order to linearise the magnetohydrodynamic equations, it is necessary to express the variables concerned in terms of the sum of zero and first order perturbation components. First order terms are then retained to examine the linear response of the perturbed system.

The zero order variables that will be used are the pressure, P, the density, ρ_0, and the magnetic field, $\mathbf{B}$. Near the equatorial plane the ambient magnetic field has a B_μ component only. The zero order electric field and velocity are zero. The corresponding first order pressure, density and magnetic field are p, ρ and $\mathbf{b}$ respectively. $\mathbf{E}$ and $\mathbf{v}$ represent the perturbation electric field and velocity.

As an initial step, then, the momentum equation is expressed as:

$$(\rho_0+\rho)\frac{\partial \mathbf{v}}{\partial t} + (\rho_0+\rho)\mathbf{v}.\nabla\mathbf{v} = -\nabla\left[(P+p) + \frac{(\mathbf{B}+\mathbf{b})^2}{2\mu_0}\right] + \frac{((\mathbf{B}+\mathbf{b}).\nabla)(\mathbf{B}+\mathbf{b})}{\mu_0}$$

Expanding this expression further gives

$$\begin{aligned} \rho_0\frac{\partial \mathbf{v}}{\partial t} + \rho\frac{\partial \mathbf{v}}{\partial t} + \rho_0\mathbf{v}.\nabla\mathbf{v} + \rho\mathbf{v}.\nabla\mathbf{v} &= -\nabla(P+p) - \nabla\left[\frac{1}{2\mu_0}(B^2 + 2\mathbf{B}.\mathbf{b} + b^2)\right] \\ &\quad + \frac{1}{\mu_0}[(\mathbf{B}.\nabla)(\mathbf{B}+\mathbf{b})] + \frac{1}{\mu_0}[(\mathbf{b}.\nabla)(\mathbf{B}+\mathbf{b})] \end{aligned}$$

or

$$\rho_0\frac{\partial \mathbf{v}}{\partial t} + \rho\frac{\partial \mathbf{v}}{\partial t} + \rho_0\mathbf{v}.\nabla\mathbf{v} + \rho\mathbf{v}.\nabla\mathbf{v} = -\nabla(P+p) - \nabla\left[\frac{1}{2\mu_0}(B^2 + 2\mathbf{B}.\mathbf{b} + b^2)\right] +$$

$$\frac{1}{\mu_0}[(\mathbf{B}.\nabla)\mathbf{B} + (\mathbf{B}.\nabla)\mathbf{b} + (\mathbf{b}.\nabla)\mathbf{B} + (\mathbf{b}.\nabla)\mathbf{b}]$$

To first order,

$$\rho_0 \frac{\partial \mathbf{v}}{\partial t} = -\nabla p - \nabla\left[\frac{1}{2\mu_0}(2\mathbf{B}.\mathbf{b})\right] + \frac{1}{\mu_0}[(\mathbf{B}.\nabla)\mathbf{b} + (\mathbf{b}.\nabla)\mathbf{B}]$$

Time variation of the form $exp(-i\omega t)$ implies that the partial derivative with respect to time, $\partial/\partial t \equiv -i\omega$. The above equation may therefore be expressed as

$$-i\omega\rho_0\mathbf{v} = -\nabla\left(p + \frac{\mathbf{B}.\mathbf{b}}{\mu_0}\right) + \frac{1}{\mu_0}[(\mathbf{B}.\nabla)\mathbf{b} + (\mathbf{b}.\nabla)\mathbf{B}] \tag{2.37}$$

This is the linearised momentum equation.

When the adiabatic law is expanded in terms of zero and first order terms, the following results are obtained:

$$\begin{aligned}
\left(\frac{\partial}{\partial t} + \mathbf{v}.\nabla\right)\left[\frac{P+p}{(\rho_0+\rho)^\gamma}\right] &= \left(\frac{\partial}{\partial t} + \mathbf{v}.\nabla\right)\left[(P+p)\frac{1}{\rho_0^\gamma}\frac{1}{\left(1+\frac{\rho}{\rho_0}\right)^\gamma}\right] \\
&\simeq \left(\frac{\partial}{\partial t} + \mathbf{v}.\nabla\right)\left[(P+p)\frac{1}{\rho_0^\gamma}\left(1-\frac{\gamma\rho}{\rho_0}\right)\right] \\
&= \left(\frac{\partial}{\partial t} + \mathbf{v}.\nabla\right)\left[\frac{P}{\rho_0^\gamma}\left(1+\frac{p}{P}-\frac{\gamma\rho}{\rho_0}-\frac{p}{P}\frac{\gamma\rho}{\rho_0}\right)\right] \\
&= 0
\end{aligned}$$

In the above the first order approximation $(1+x)^\alpha \simeq 1 + \alpha x$ has been used. Excluding zero and second order terms gives

$$\frac{\partial}{\partial t}\left[\frac{P}{\rho_0^\gamma}\left(\frac{p}{P} - \frac{\gamma\rho}{\rho_0}\right)\right] + \mathbf{v}.\nabla\left(\frac{P}{\rho_0^\gamma}\right) = 0$$

Expanding the above yields

$$\frac{1}{\rho_0^\gamma}\frac{\partial p}{\partial t} - \frac{\gamma P}{\rho_0^{\gamma+1}}\frac{\partial \rho}{\partial t} + \frac{1}{\rho_0^\gamma}\mathbf{v}.\nabla P - \frac{\gamma P}{\rho_0^{\gamma+1}}\mathbf{v}.\nabla\rho_0 = 0$$

Multiplication by ρ_0^γ reduces this expression to

$$\frac{\partial p}{\partial t} - \frac{\gamma P}{\rho_0}\frac{\partial \rho}{\partial t} + \mathbf{v}.\nabla P - \frac{\gamma P}{\rho_0}\mathbf{v}.\nabla\rho_0 = 0$$

Since the sound speed, $V_S = \sqrt{\gamma P/\rho_0}$, this takes the form

$$-i\omega p + i\omega V_S^2\rho + \mathbf{v}.\nabla P - V_S^2\mathbf{v}.\nabla\rho_0 = 0 \tag{2.38}$$

The continuity equation, expressed in terms of zero and perturbation terms becomes

$$\frac{\partial}{\partial t}(\rho_0 + \rho) + \nabla.[(\rho_0 + \rho)\mathbf{v}] = 0$$

The first order continuity equation is then

$$\frac{\partial \rho}{\partial t} + \nabla.(\rho_0 \mathbf{v}) = 0$$

or

$$-i\omega\rho + \nabla.(\rho_0 \mathbf{v}) = 0 \tag{2.39}$$

By inspection, the linearised forms of Faraday's law, Ampére's law and Ohm's law are

$$\nabla \times \mathbf{E} = i\omega \mathbf{b}, \tag{2.40}$$

$$\nabla \times \mathbf{b} = \mu_0 \mathbf{j} \tag{2.41}$$

and

$$\mathbf{E} + \mathbf{v} \times \mathbf{B} = 0 \tag{2.42}$$

Eliminating ρ

It is convenient to express the gradients of the ambient magnetic field and pressure in terms of the curvature, κ, and the inverse scale length, κ_p. This may be done using the results 2.26 and 2.33. Using the latter in equation 2.38 gives

$$-i\omega p + i\omega V_S^2 \rho - \mathbf{v}.\frac{B^2}{\mu_0}(\kappa + \kappa_\nu)\hat{\boldsymbol{\nu}} - V_S^2 \mathbf{v}.\nabla\rho_0 = 0$$

If equation 2.39 is multiplied by V_S^2 and added to the above, the result is

$$-i\omega p - \frac{B^2}{\mu_0}(\kappa + \kappa_\nu)\hat{\boldsymbol{\nu}}.\mathbf{v} + \rho_0 V_S^2 \nabla.\mathbf{v} = 0$$

Using the definition of the Alfvén speed,

$$V_A = \frac{B}{\sqrt{\mu_0 \rho_0}}$$

this may be written as

$$-i\omega p = -\rho_0 V_S^2 \nabla.\mathbf{v} + \rho_0 V_A^2 (\kappa + \kappa_\nu)\hat{\boldsymbol{\nu}}.\mathbf{v} \tag{2.43}$$

Eliminating E

Substituting for $\mathbf{E}$ from equation 2.42 into equation 2.40 gives

$$\nabla \times (\mathbf{v} \times \mathbf{B}) = -i\omega\mathbf{b}$$

Now

$$\nabla \times (\mathbf{X} \times \mathbf{Y}) = (\mathbf{Y}.\nabla)\mathbf{X} - \mathbf{Y}(\nabla.\mathbf{X}) - (\mathbf{X}.\nabla)\mathbf{Y} + \mathbf{X}(\nabla.\mathbf{Y})$$

so that

$$\begin{aligned} -i\omega\mathbf{b} &= (\mathbf{B}.\nabla)\mathbf{v} - \mathbf{B}(\nabla.\mathbf{v}) - (\mathbf{v}.\nabla)\mathbf{B} + \mathbf{v}(\nabla.\mathbf{B}) \\ &= (\mathbf{B}.\nabla)\mathbf{v} - \mathbf{B}(\nabla.\mathbf{v}) - (\mathbf{v}.\nabla)\mathbf{B} \end{aligned} \tag{2.44}$$

From expression 2.26,

$$(\mathbf{v}.\nabla)\mathbf{B} = \hat{\boldsymbol{\mu}}\kappa_\nu B\hat{\boldsymbol{\nu}}.\mathbf{v} - \hat{\boldsymbol{\nu}}\kappa B\hat{\boldsymbol{\mu}}.\mathbf{v}$$

Equation 2.44 now becomes

$$i\omega\mathbf{b} = \mathbf{B}(\nabla.\mathbf{v}) - (\mathbf{B}.\nabla)\mathbf{v} + \hat{\boldsymbol{\mu}}\kappa_\nu B\hat{\boldsymbol{\nu}}.\mathbf{v} - \hat{\boldsymbol{\nu}}\kappa B\hat{\boldsymbol{\mu}}.\mathbf{v} \tag{2.45}$$

Substituting for $(\mathbf{b}.\nabla)\mathbf{B}$ in a similar way, the linearised momentum equation, 2.37, may be written as

$$-i\omega\rho_0\mathbf{v} = -\nabla\left(p + \frac{\mathbf{B}.\mathbf{b}}{\mu_0}\right) + \frac{1}{\mu_0}[(\mathbf{B}.\nabla)\mathbf{b} + \hat{\boldsymbol{\mu}}\kappa_\nu B\hat{\boldsymbol{\nu}}.\mathbf{b} - \hat{\boldsymbol{\nu}}\kappa B\hat{\boldsymbol{\mu}}.\mathbf{b}] \tag{2.46}$$

Any vector in the coordinate system that has been adopted may be expressed as

$$\mathbf{a} = \hat{\boldsymbol{\mu}}a_\mu + \hat{\boldsymbol{\nu}}a_\nu + \hat{\boldsymbol{\varphi}}a_\varphi$$

Using 2.26

$$(\mathbf{a}.\nabla)\mathbf{B} = \hat{\boldsymbol{\mu}}B\kappa_\nu a_\nu - \hat{\boldsymbol{\nu}}B\kappa a_\mu \tag{2.47}$$

Also

$$\begin{aligned} (\mathbf{B}.\nabla)\mathbf{a} &= (\mathbf{B}.\nabla)a_\mu\hat{\boldsymbol{\mu}} + (\mathbf{B}.\nabla)a_\nu\hat{\boldsymbol{\nu}} + (\mathbf{B}.\nabla)a_\varphi\hat{\boldsymbol{\varphi}} \\ &= \hat{\boldsymbol{\mu}}(\mathbf{B}.\nabla)a_\mu + a_\mu(\mathbf{B}.\nabla)\hat{\boldsymbol{\mu}} + \hat{\boldsymbol{\nu}}(\mathbf{B}.\nabla)a_\nu + a_\nu(\mathbf{B}.\nabla)\hat{\boldsymbol{\nu}} + \\ &\quad \hat{\boldsymbol{\varphi}}(\mathbf{B}.\nabla)a_\varphi + a_\varphi(\mathbf{B}.\nabla)\hat{\boldsymbol{\varphi}} \end{aligned}$$

The gradients of the unit vectors are given by equation 2.27. Using these and the fact that $\mathbf{B} = (B, 0, 0)$ the above becomes

$$\begin{aligned}(\mathbf{B}.\nabla)\mathbf{a} &= \hat{\boldsymbol{\mu}}(\mathbf{B}.\nabla)a_\mu + \hat{\boldsymbol{\nu}}(\mathbf{B}.\nabla)a_\nu + \hat{\boldsymbol{\varphi}}(\mathbf{B}.\nabla)a_\varphi - \\ & a_\mu B\kappa\hat{\boldsymbol{\nu}} + a_\nu B\kappa\hat{\boldsymbol{\mu}} \end{aligned} \tag{2.48}$$

Expressions 2.47 and 2.48 allow 2.46 and 2.45 to be expanded:

$$\begin{aligned}-i\omega\rho_0\mathbf{v} &= -\nabla_\parallel p - \nabla_\parallel\left(\frac{\mathbf{B}.\mathbf{b}}{\mu_0}\right) - \nabla_\perp\left(p + \frac{\mathbf{B}.\mathbf{b}}{\mu_0}\right) + \frac{1}{\mu_0}[\hat{\boldsymbol{\mu}}(\mathbf{B}.\nabla)b_\mu + \\ & \hat{\boldsymbol{\nu}}(\mathbf{B}.\nabla)b_\nu + \hat{\boldsymbol{\varphi}}(\mathbf{B}.\nabla)b_\varphi + \hat{\boldsymbol{\mu}}\kappa B b_\nu - \hat{\boldsymbol{\nu}}\kappa B b_\mu + \hat{\boldsymbol{\mu}}\kappa_\nu B b_\nu - \hat{\boldsymbol{\nu}}\kappa B b_\mu] \end{aligned} \tag{2.49}$$

Now

$$\begin{aligned}\nabla_\parallel\left(\frac{\mathbf{B}.\mathbf{b}}{\mu_0}\right) &= \frac{1}{\mu_0}\hat{\boldsymbol{\mu}}\frac{\partial}{\partial x_\mu}(Bb_\mu) \\ &= \frac{1}{\mu_0}\mathbf{B}\frac{\partial b_\mu}{\partial x_\mu}\end{aligned}$$

since $R_\mu \to \infty$ near the equatorial plane. Also,

$$\begin{aligned}\frac{1}{\mu_0}\hat{\boldsymbol{\mu}}(\mathbf{B}.\nabla)b_\mu &= \frac{1}{\mu_0}\hat{\boldsymbol{\mu}}\mathbf{B}\left(\frac{\partial b_\mu}{\partial x_\mu}, \frac{\partial b_\mu}{\partial x_\nu}, \frac{\partial b_\mu}{\partial x_\varphi}\right) \\ &= \frac{1}{\mu_0}\mathbf{B}\frac{\partial b_\mu}{\partial x_\mu}\end{aligned}$$

Therefore equation 2.49 reduces to

$$-i\omega\rho_0\mathbf{v} = -\nabla_\parallel p - \nabla_\perp\tau + \frac{1}{\mu_0}[\hat{\boldsymbol{\nu}}(\mathbf{B}.\nabla)b_\nu + \hat{\boldsymbol{\varphi}}(\mathbf{B}.\nabla)b_\varphi + \mathbf{B}(\kappa + \kappa_\nu)b_\nu - 2\hat{\boldsymbol{\nu}}\kappa B b_\mu] \tag{2.50}$$

where the total pressure

$$\tau = p + \frac{\mathbf{B}.\mathbf{b}}{\mu_0}$$

Using 2.47 and 2.48 in 2.45,

$$\begin{aligned}i\omega\mathbf{b} &= \mathbf{B}(\nabla.\mathbf{v}) - \hat{\boldsymbol{\mu}}(\mathbf{B}.\nabla)v_\mu - \hat{\boldsymbol{\nu}}(\mathbf{B}.\nabla)v_\nu - \hat{\boldsymbol{\varphi}}(\mathbf{B}.\nabla)v_\varphi - \hat{\boldsymbol{\mu}}\kappa B v_\nu + \\ & \hat{\boldsymbol{\nu}}\kappa B v_\mu + \hat{\boldsymbol{\mu}}\kappa_\nu B v_\nu - \hat{\boldsymbol{\nu}}\kappa B v_\mu \end{aligned} \tag{2.51}$$

Now

$$\begin{aligned}\hat{\mu}(\mathbf{B}.\nabla)v_\mu &= \hat{\mu}\mathbf{B}\left(\frac{\partial v_\mu}{\partial x_\mu}, \frac{\partial v_\mu}{\partial x_\nu}, \frac{\partial v_\mu}{\partial x_\varphi}\right) \\ &= \hat{\mu}B\frac{\partial v_\mu}{\partial x_\mu}\end{aligned}$$

and

$$\mathbf{B}(\nabla.\mathbf{v}) = \hat{\mu}B\left(\frac{\partial v_\mu}{\partial x_\mu} + \frac{\partial v_\nu}{\partial x_\nu} + \frac{\partial v_\varphi}{\partial x_\varphi}\right)$$

so that

$$\mathbf{B}(\nabla.\mathbf{v}) - \hat{\mu}(\mathbf{B}.\nabla)v_\mu = \mathbf{B}(\nabla_\perp.\mathbf{v}_\perp)$$

Equation 2.51 may then be written as

$$i\omega\mathbf{b} = \mathbf{B}(\nabla_\perp.\mathbf{v}_\perp) - \hat{\nu}(\mathbf{B}.\nabla)v_\nu - \hat{\varphi}(\mathbf{B}.\nabla)v_\varphi + \hat{\mu}(\kappa_\nu - \kappa)Bv_\nu \qquad (2.52)$$

Equations 2.43, 2.50 and 2.52 are the linearised equations which will be used to derive the dispersion relation.

2.4 Separation of variables

The assumption of azimuthal symmetry implies that conditions in the $\hat{\varphi}$ direction (perpendicular to the meridian plane) are homogeneous. The azimuthal behaviour of the perturbation may then be expressed as $exp\ ik_\varphi x_\varphi$, so that $\partial/\partial x_\varphi \equiv ik_\varphi$. In the meridian plane conditions are inhomogeneous. It is, however, useful to assume that these conditions vary slowly in the $\hat{\mu}$ direction, so that homogeneity holds on length scales of the order of a wavelength. In this case, the eikonal function

$$exp\ i\int^{x_\mu} k_\mu\, dx_\mu$$

may be used to describe variation along the field. This means that $\partial/\partial x_\mu \equiv ik_\mu$. When these results are used it is possible to eliminate all variables except τ and v_ν from the appropriate equations.

Expanding 2.43 in terms of the above gives

$$i\omega p = \rho_0 V_S^2 \left(ik_\mu v_\mu + \frac{\partial v_\nu}{\partial x_\nu} + ik_\varphi v_\varphi \right) - \rho_0 V_A^2 (\kappa + \kappa_\nu) v_\nu \tag{2.53}$$

Similarly, 2.52 and 2.50 become

$$\begin{aligned} i\omega(b_\mu \hat{\mu} + b_\nu \hat{\nu} + b_\varphi \hat{\varphi}) \;=\; & B_\mu \hat{\mu} \left(\frac{\partial v_\nu}{\partial x_\nu} + ik_\varphi v_\varphi \right) - \hat{\nu}(ik_\mu B_\mu) v_\nu - \\ & \hat{\varphi}(ik_\mu B_\mu) v_\varphi + \hat{\mu}(\kappa_\nu - \kappa) B v_\nu \end{aligned} \tag{2.54}$$

and

$$\begin{aligned} -i\omega\rho_0(v_\mu \hat{\mu} + v_\nu \hat{\nu} + v_\varphi \hat{\varphi}) \;=\; & -ik_\mu p \hat{\mu} - \frac{\partial \tau}{\partial x_\nu} \hat{\nu} - ik_\varphi \tau \hat{\varphi} + \frac{1}{\mu_0} (ik_\mu B_\mu b_\nu \hat{\nu} + \\ & ik_\mu B_\mu b_\varphi \hat{\varphi} + B_\mu(\kappa + \kappa_\nu) b_\nu \hat{\mu} - 2\kappa B b_\mu \hat{\nu}) \end{aligned} \tag{2.55}$$

Equations 2.54 and 2.55 may be expressed in terms of their component equations.

From equation 2.54 :

$$i\omega b_\mu = B \left(\frac{dv_\nu}{dx_\nu} + ik_\varphi v_\varphi \right) + (\kappa_\nu - \kappa) B v_\nu \tag{2.56}$$

$$b_\nu = -\frac{k_\mu}{\omega} B v_\nu \tag{2.57}$$

and

$$b_\varphi = -\frac{k_\mu}{\omega} B v_\varphi \tag{2.58}$$

From equation 2.55:

$$v_\mu = \frac{k_\mu}{\omega\rho_0} p + \frac{iB}{\omega\mu_0\rho_0} (\kappa + \kappa_\nu) b_\nu$$

Substituting for b_ν from 2.57 and using the definition for V_A gives the result

$$v_\mu = \frac{k_\mu}{\omega\rho_0} p + \frac{ik_\mu}{\omega^2} (\kappa + \kappa_\nu) V_A^2 v_\nu \tag{2.59}$$

The $\hat{\nu}$ component of 2.55 is

$$v_\nu = -\frac{i}{\omega\rho_0} \frac{d\tau}{dx_\nu} - \frac{k_\mu}{\omega\mu_0\rho_0} B b_\nu - \frac{i}{\omega\mu_0\rho_0} 2\kappa B b_\mu$$

In terms of V_A,

$$v_\nu = -\frac{k_\mu V_A^2}{\omega B} b_\nu - \frac{2i\kappa V_A^2}{\omega B} b_\mu - \frac{i}{\omega\rho_0} \frac{d\tau}{dx_\nu} \tag{2.60}$$

The $\hat{\varphi}$ component of 2.55 may be written as

$$v_\varphi = \frac{k_\varphi}{\omega\rho_0}\tau - \frac{k_\mu V_A^2}{\omega B}b_\varphi \tag{2.61}$$

The variable b_φ is eliminated using 2.58 and 2.61:

$$v_\varphi = \frac{k_\varphi}{\omega\rho_0}\tau + \frac{k_\mu^2 V_A^2}{\omega^2}v_\varphi$$

so that

$$v_\varphi\left[\frac{\omega^2 - k_\mu^2 V_A^2}{\omega^2}\right] = \frac{k_\varphi}{\omega\rho_0}\tau$$

and

$$v_\varphi = \frac{\omega k_\varphi}{\omega^2 - k_\mu^2 V_A^2}\frac{\tau}{\rho_0} \tag{2.62}$$

Substituting for v_μ from 2.59 and v_φ from 2.62, 2.53 becomes

$$\begin{aligned} i\omega p &= \rho_0 V_S^2\left[\frac{ik_\mu^2}{\omega\rho_0}p + \frac{k_\mu^2}{\omega^2}(\kappa+\kappa_\nu)V_A^2 v_\nu\right] + \rho_0 V_S^2\left[\frac{dv_\nu}{dx_\nu} + \frac{i\omega k_\varphi^2}{(\omega^2 - k_\mu^2 V_A^2)}\frac{\tau}{\rho_0}\right] \\ &\quad -\rho_0 V_A^2(\kappa+\kappa_\nu)v_\nu \end{aligned}$$

Now

$$\left[i\omega - \rho_0 V_S^2\frac{ik_\mu^2}{\omega\rho_0}\right]p = -\frac{1}{i\omega}\left(\omega^2 - k_\mu^2 V_S^2\right)p$$

thus

$$\begin{aligned} \left(\omega^2 - k_\mu^2 V_S^2\right)p &= -\frac{i\rho_0 k_\mu^2 V_S^2 V_A^2}{\omega}(\kappa+\kappa_\nu)v_\nu - i\omega\rho_0 V_S^2\frac{dv_\nu}{dx_\nu} + \frac{\omega^2 k_\varphi^2}{\omega^2 - k_\mu^2 V_A^2}V_S^2\tau + \\ &\quad i\omega\rho_0 V_A^2(\kappa+\kappa_\nu)v_\nu \\ &= \frac{i\rho_0 V_A^2}{\omega}(\kappa+\kappa_\nu)\left(\omega^2 - k_\mu^2 V_S^2\right)v_\nu + \frac{\omega^2}{\omega^2 - k_\mu^2 V_A^2}k_\varphi^2 V_S^2\tau - \\ &\quad i\omega\rho_0 V_S^2\frac{dv_\nu}{dx_\nu} \end{aligned} \tag{2.63}$$

With v_φ given by 2.62, 2.56 becomes

$$i\omega b_\mu = B\frac{dv_\nu}{dx_\nu} + \frac{i\omega k_\varphi^2 B}{\omega^2 - k_\mu^2 V_A^2}\frac{\tau}{\rho_0} + (\kappa_\nu - \kappa)Bv_\nu$$

Multiplying the above by

$$\frac{1}{i\omega}\frac{B}{\mu_0}(\omega^2 - k_\mu^2 V_S^2)$$

gives

$$\begin{aligned}(\omega^2 - k_\mu^2 V_S^2)\frac{Bb_\mu}{\mu_0} &= -\frac{i}{\omega}\rho_0 V_A^2(\omega^2 - k_\mu^2 V_S^2)\frac{dv_\nu}{dx_\nu} + \frac{k_\varphi^2 V_A^2(\omega^2 - k_\mu^2 V_S^2)}{\omega^2 - k_\mu^2 V_A^2}\tau \\ &\quad -\frac{i}{\omega}\rho_0 V_A^2(\omega^2 - k_\mu^2 V_S^2)(\kappa_\nu - \kappa)v_\nu \end{aligned} \tag{2.64}$$

Adding 2.63 and 2.64 then gives

$$\begin{aligned}(\omega^2 - k_\mu^2 V_S^2)\tau &= \frac{i\rho_0 V_A^2}{\omega}(\omega^2 - k_\mu^2 V_S^2)(\kappa + \kappa_\nu - \kappa_\nu + \kappa)v_\nu + \frac{k_\varphi^2}{\omega^2 - k_\mu^2 V_A^2}(\omega^2 V_S^2 \\ &\quad +\omega^2 V_A^2 - k_\mu^2 V_S^2 V_A^2)\tau - \frac{i\rho_0}{\omega}(\omega^2 V_S^2 + \omega^2 V_A^2 - k_\mu^2 V_S^2 V_A^2)\frac{dv_\nu}{dx_\nu}\end{aligned}$$

Rearranging the above and using the definition for the hybrid characteristic speed, $V = \sqrt{V_A^2 + V_S^2}$, results in the expression

$$\begin{aligned}(\omega^2 V^2 - k_\mu^2 V_A^2 V_S^2)\frac{dv_\nu}{dx_\nu} = -\frac{i\omega k_\varphi^2}{\rho_0(\omega^2 - k_\mu^2 V_A^2)}\Big[\omega^2 V^2 - k_\mu^2 V_S^2 V_A^2 - \\ \frac{(\omega^2 - k_\mu^2 V_S^2)(\omega^2 - k_\mu^2 V_A^2)}{k_\varphi^2}\Big]\tau + 2V_A^2\kappa(\omega^2 - k_\mu^2 V_S^2)v_\nu\end{aligned} \tag{2.65}$$

The bracketed portion multiplying τ in 2.65 may be rewritten as:

$$\begin{aligned}&\frac{1}{k_\varphi^2}[k_\varphi^2\omega^2 V^2 - k_\mu^2 k_\varphi^2 V_S^2 V_A^2 - \omega^4 + \omega^2 k_\mu^2 V_S^2 + \omega^2 k_\mu^2 V_A^2 - k_\mu^4 V_A^2 V_S^2] \\ &= -\frac{1}{k_\varphi^2}[\omega^4 - \omega^2 V^2(k_\mu^2 + k_\varphi^2) + (k_\mu^2 + k_\varphi^2)k_\mu^2 V_A^2 V_S^2] \\ &= -\frac{1}{k_\varphi^2}[\omega^4 - (k_\mu^2 + k_\varphi^2)(\omega^2 V^2 - k_\mu^2 V_A^2 V_S^2)] \\ &= -\frac{\mathcal{G}}{k_\varphi^2\mathcal{H}}\end{aligned} \tag{2.66}$$

where

$$\mathcal{G} = \omega^4\mathcal{H} - (k_\mu^2 + k_\varphi^2) \tag{2.67}$$

and

$$\mathcal{H} = \frac{1}{\omega^2 V^2 - k_\mu^2 V_S^2 V_A^2} \tag{2.68}$$

Therefore 2.65 may be expressed as

$$\frac{1}{\mathcal{H}}\frac{dv_\nu}{dx_\nu} = \frac{i\omega}{\rho_0(\omega^2 - k_\mu^2 V_A^2)}\frac{\mathcal{G}}{\mathcal{H}}\tau + 2\kappa V_A^2(\omega^2 - k_\mu^2 V_S^2)v_\nu$$

so that

$$\frac{dv_\nu}{dx_\nu} = \frac{i\omega\mathcal{G}}{\rho_0(\omega^2 - k_\mu^2 V_A^2)}\tau + 2\kappa V_A^2(\omega^2 - k_\mu^2 V_S^2)\mathcal{H}v_\nu \tag{2.69}$$

This equation is only dependent on τ and v_ν.

Now, from 2.56,

$$\frac{b_\mu}{B} = -\frac{i}{\omega}\frac{dv_\nu}{dx_\nu} + \frac{k_\varphi v_\varphi}{\omega} - \frac{i}{\omega}(\kappa_\nu - \kappa)v_\nu$$

Substituting for κ_ν from 2.36, v_φ from 2.62 and dv_ν/dx_ν from 2.69, this becomes

$$\begin{aligned}\frac{b_\mu}{B} &= \frac{\mathcal{G}}{\rho_0(\omega^2 - k_\mu^2 V_A^2)}\tau - \frac{2i}{\omega}\kappa V_A^2(\omega^2 - k_\mu^2 V_S^2)\mathcal{H}v_\nu + \frac{k_\varphi^2}{\rho_0(\omega^2 - k_\mu^2 V_A^2)}\tau + \\ &\quad \frac{i}{\omega}(2\kappa + \frac{1}{2}\beta\kappa_p)v_\nu \\ &= (\mathcal{G} + k_\varphi^2)\frac{\tau}{\rho_0(\omega^2 - k_\mu^2 V_A^2)} - \frac{2i\kappa}{\omega}[\mathcal{H}V_A^2(\omega^2 - k_\mu^2 V_S^2) - 1]v_\nu + \frac{1}{2}\frac{i\beta\kappa_p}{\omega}v_\nu\end{aligned}$$

Now

$$\begin{aligned}(\mathcal{G} + k_\varphi^2) &= \frac{\omega^4}{\omega^2(V_A^2 + V_S^2) - k_\mu^2 V_A^2 V_S^2} - k_\mu^2 \\ &= \frac{\omega^4 - \omega^2 k_\mu^2(V_A^2 + V_S^2) + k_\mu^4 V_A^2 V_S^2}{\omega^2(V_A^2 + V_S^2) - k_\mu^2 V_A^2 V_S^2} \\ &= \mathcal{H}(\omega^2 - k_\mu^2 V_S^2)(\omega^2 - k_\mu^2 V_A^2)\end{aligned}$$

Therefore

$$\begin{aligned}\frac{b_\mu}{B} &= \mathcal{H}(\omega^2 - k_\mu^2 V_S^2)\frac{\tau}{\rho_0} - \frac{2i\kappa}{\omega}(\omega^2 V_A^2 - k_\mu^2 V_A^2 V_S^2 - \omega^2 V^2 + k_\mu^2 V_A^2 V_S^2)\mathcal{H}v_\nu \\ &\quad + \frac{1}{2}\frac{i\beta\kappa_p}{\omega}v_\nu \\ &= \mathcal{H}(\omega^2 - k_\mu^2 V_S^2)\frac{\tau}{\rho_0} + 2i\kappa\omega V_S^2\mathcal{H}v_\nu + \frac{1}{2}\frac{i\beta\kappa_p}{\omega}v_\nu\end{aligned} \tag{2.70}$$

From equation 2.60

$$\frac{1}{\rho_0}\frac{d\tau}{dx_\nu} = i\omega v_\nu + \frac{ik_\mu V_A^2}{B}b_\nu - \frac{2\kappa V_A^2}{B}b_\mu$$

Using the expression for b_ν from 2.57 and equation 2.70 gives

$$\begin{aligned}\frac{1}{\rho_0}\frac{d\tau}{dx_\nu} &= i\omega v_\nu - \frac{ik_\mu^2 V_A^2}{\omega}v_\nu - 2\kappa V_A^2\left[\mathcal{H}(\omega^2 - k_\mu^2 V_S^2)\frac{\tau}{\rho_0}\right] - \\ &\quad 2i\kappa V_A^2(2\kappa\omega V_S^2\mathcal{H} + \frac{1}{2}\frac{\beta\kappa_p}{\omega})v_\nu \\ &= \frac{i}{\omega}(\omega^2 - k_\mu^2 V_A^2)v_\nu - 2i\kappa V_A^2(2\kappa\omega V_S^2\mathcal{H} + \frac{1}{2}\frac{\beta\kappa_p}{\omega})v_\nu - \\ &\quad 2\kappa V_A^2\left[\mathcal{H}(\omega^2 - k_\mu^2 V_S^2)\frac{\tau}{\rho_0}\right] \qquad (2.71)\end{aligned}$$

As *Walker* [1994] has noted, equations 2.69 and 2.71 are similar to those that would be derived in a model with straight field lines. Here, however, correction terms allowing for the finite field line curvature are evident.

2.5 Dispersion relation

A further assumption of slow variation in the inhomogeneous meridian plane is now made for the $\hat{\nu}$ direction. As for x_μ, x_ν dependent variation may be expressed in terms of an eikonal function :

$$exp\, i\int^{x_\nu} k_\nu\, dx_\nu$$

so that $d/dx_\nu \equiv ik_\nu$.

The above may used in 2.69 and 2.71 to obtain two homogeneous simultaneous equations in the variables τ and v_ν. These may be expressed in matrix form as:

$$\begin{pmatrix} \frac{i}{\omega}(\omega^2 - k_\mu^2 V_A^2) - \frac{2i\kappa V_A^2}{\omega}\mathcal{K} & -ik_\nu - 2\kappa V_A^2(\omega^2 - k_\mu^2 V_S^2)\mathcal{H} \\ -ik_\nu + 2\kappa V_A^2(\omega^2 - k_\mu^2 V_S^2)\mathcal{H} & \frac{i\omega\mathcal{G}}{\omega^2 - k_\mu^2 V_A^2} \end{pmatrix}\begin{pmatrix} v_\nu \\ \frac{\tau}{\rho_0} \end{pmatrix} = 0 \qquad (2.72)$$

where

$$\mathcal{K} = \left[\frac{1}{2}\beta\kappa_p + 2\kappa\omega^2 V_S^2\mathcal{H}\right] \qquad (2.73)$$

In order for these equations to have a solution, the determinant of the coefficient matrix in 2.72 must be zero:

$$\begin{vmatrix} \frac{i}{\omega}(\omega^2 - k_\mu^2 V_A^2) - \frac{2i\kappa V_A^2}{\omega}\mathcal{K} & -ik_\nu - 2\kappa V_A^2(\omega^2 - k_\mu^2 V_S^2)\mathcal{H} \\ -ik_\nu + 2\kappa V_A^2(\omega^2 - k_\mu^2 V_S^2)\mathcal{H} & \frac{i\omega\mathcal{G}}{\omega^2 - k_\mu^2 V_A^2} \end{vmatrix} = 0 \qquad (2.74)$$

When the scale of variation along the magnetic field is large, $k_\mu \approx 0$. For this special case, the determinant equation reduces to

$$\frac{i\mathcal{G}}{\omega}\left[i\omega - \frac{2i\kappa V_A^2}{\omega}\mathcal{K}\right] - (-ik_\nu - 2\kappa V_A^2\omega^2\mathcal{H})(-ik_\nu + 2\kappa V_A^2\omega^2\mathcal{H}) = 0 \qquad (2.75)$$

Here

$$\mathcal{H} = \frac{1}{\omega^2 V^2}, \quad \mathcal{G} = \frac{\omega^2}{V^2} - k_\varphi^2 \qquad (2.76)$$

so that

$$\mathcal{K} = \frac{1}{2}\beta\kappa_p + \frac{2\kappa V_S^2}{V^2} \qquad (2.77)$$

Expanding equation 2.75:

$$\begin{aligned} 0 &= -\mathcal{G} + \frac{2\kappa V_A^2}{\omega^2}\mathcal{G}\mathcal{K} + k_\nu^2 + 4\kappa^2 V_A^4\omega^4\mathcal{H}^2 \\ &= k_\varphi^2 - \frac{\omega^2}{V^2} + \frac{2\kappa V_A^2}{\omega^2}\left[\frac{\omega^2}{V^2} - k_\varphi^2\right]\mathcal{K} + k_\nu^2 + \frac{4\kappa^2 V_A^4}{V^4} \\ &= k_\varphi^2 + k_\nu^2 - \frac{\omega^2}{V^2} + \frac{4\kappa^2 V_A^4}{V^4} + \frac{2\kappa V_A^2}{V^2}\left[\frac{1}{2}\beta\kappa_p + \frac{2\kappa V_S^2}{V^2}\right] - \\ &\quad \frac{2\kappa V_A^2 k_\varphi^2}{\omega^2}\left[\frac{1}{2}\beta\kappa_p + \frac{2\kappa V_S^2}{V^2}\right] \\ &= k_\varphi^2 + k_\nu^2 - \frac{\omega^2}{V^2} + \frac{4\kappa^2 V_A^4}{V^4} + \frac{\beta\kappa\kappa_p V_A^2}{V^2} + \frac{4\kappa^2 V_A^2 V_S^2}{V^4} - \frac{\beta\kappa\kappa_p V_A^2 k_\varphi^2}{\omega^2} - \\ &\quad \frac{4\kappa^2 V_A^2 V_S^2 k_\varphi^2}{\omega^2 V^2} \end{aligned}$$

Multiplying this by $\omega^2 V^2$ gives

$$\begin{aligned} 0 &= k_\varphi^2 V^2\omega^2 + k_\nu^2 V^2\omega^2 - \omega^4 + \frac{4\kappa^2 V_A^4}{V^2}\omega^2 + \beta\kappa\kappa_p V_A^2\omega^2 + \frac{4\kappa^2 V_A^2 V_S^2}{V^2}\omega^2 - \\ &\quad \beta\kappa\kappa_p V_A^2 V^2 k_\varphi^2 - 4\kappa^2 V_A^2 V_S^2 k_\varphi^2 \end{aligned}$$

This may be expressed as a quadratic in ω^2:

$$\omega^4 - \omega^2\left[(k_\varphi^2 + k_\nu^2)V^2 + \frac{4\kappa^2 V_A^4}{V^2} + \frac{4\kappa^2 V_A^2 V_S^2}{V^2} + \beta\kappa\kappa_p V_A^2\right] + k_\varphi^2\kappa V_A^2\left[4\kappa V_S^2 + \beta\kappa_p V^2\right] = 0$$

From 2.36

$$\kappa_p = \frac{2}{\beta}(-\kappa - \kappa_\nu)$$

Using the above equation, and expanding the hybrid characteristic speed in terms of the Alfvén and sound speeds yields the result

$$\omega^4 - \omega^2\left[4\kappa^2 V_A^2 + 2\kappa(-\kappa - \kappa_\nu)V_A^2 + (k_\varphi^2 + k_\nu^2)V^2\right] + k_\varphi^2 \kappa V_A^2\left[4\kappa V_S^2 + 2(-\kappa - \kappa_\nu)(V_A^2 + V_S^2)\right] = 0$$

Rearranging this expression gives,

$$\omega^4 - \omega^2\left[2(\kappa - \kappa_\nu)\kappa V_A^2 + (k_\varphi^2 + k_\nu^2)V^2)\right] + k_\varphi^2 V_A^2 \kappa\left[2\kappa V_S^2 - 2\kappa V_A^2 - 2\kappa_\nu V_A^2 - 2\kappa_\nu V_S^2\right] = 0$$

thus

$$\omega^4 - \omega^2\left[2(\kappa - \kappa_\nu)\kappa V_A^2 + (k_\varphi^2 + k_\nu^2)V^2\right] + 2k_\varphi^2 V_A^2 \kappa\left[\kappa(V_S^2 - V_A^2) - \kappa_\nu(V_S^2 + V_A^2)\right] = 0 \quad (2.78)$$

2.6 Threshold for Instability

In a normal mode stability analysis, the development of the perturbation that has been applied to the system must be examined. If the disturbance grows with time, the system is considered unstable. It has been assumed that the time behaviour of the perturbation is of the form $exp(-i\omega t)$. In general, ω is complex:

$$\omega = \alpha + i\delta$$

so that

$$e^{-i\omega t} = e^{-i\alpha t}e^{\delta t}$$

If the imaginary part of ω is positive, the wave grows exponentially and instability results.

If the discriminant of equation 2.78 is negative, ω^2 has a positive imaginary root and so does ω. This implies instability. If the discriminant is positive,

$$\kappa(V_S^2 - V_A^2) - \kappa_\nu(V_S^2 + V_A^2) < 0 \tag{2.79}$$

or, in terms of the ambient pressure and magnetic field,

$$\kappa\left(\gamma P - \frac{B^2}{\mu_0}\right) - \kappa_\nu\left(\gamma P + \frac{B^2}{\mu_0}\right) < 0 \tag{2.80}$$

In this case, the quadratic equation 2.78 will have a negative root so that ω has a positive imaginary root.

In the magnetotail, the curvature of the field lines, κ, is positive. During the growth phase, the curvature in the near-earth tail increases as the field here adopts a more stressed configuration. The magnetic field in the equatorial plane, B_z, usually increases with decreasing radial distance from the earth. This implies that κ_ν is negative. As the tail becomes more tail-like in the near-earth region, B_z may decrease. In this case, κ_ν may be positive. If κ_ν is greater than κ, this can lead to instability for suitable values of the plasma pressure and magnetic field.

2.7 Numerical results

To obtain numerical results for the instability condition, a realistic self-consistent model of the magnetotail during growth phase conditions is needed. This may be used to investigate the curvature, pressure and magnetic field in the region of interest. The various scale lengths may also be deduced from the variations of these quantities with radial distance from the earth.

Chapter 3

Quasi-static Convection Model

3.1 Introduction

The earth's magnetospheric magnetic field has been modelled with varying degrees of accuracy since 1960. The lowest order approximations are the vacuum models which hold within 5 to 7 R_E from the earth [*Voigt*, 1986]. In this region the ambient magnetic field is due to the dipole field (the dominant component) and the field generated by the Chapman-Ferraro currents at the magnetopause. The magnetic field which results from magnetospheric currents is considered as a perturbation component. The next level of magnetic field models is the group of quasi-static equilibrium models. The model used in this investigation is of this type. These models are self-consistent — the magnetospheric magnetic field, plasma flow and currents determine each other through the set of MHD equations for hydrostatic equilibrium. Alternatively, observationally based models describe the magnetic field configuration for average measurements and do not enforce momentum balance and flux conservation [*Walker and Southwood*, 1982]. Full magnetohydrodynamic codes describe the whole magnetosphere and represent the highest order of modelling.

3.2 The Model

The model which is used has been developed by *Erickson* [1984, 1992], and is similar to models presented by *Schindler and Birn* [1982] and *Birn and Schindler* [1983]. *Erickson* [1984, 1992] has computed self-consistent, static-equilibrium solutions for two-dimensional magnetospheric magnetic field configurations by the adiabatic earthward convection of plasma sheet flux tubes. This requires solving the Grad-Shafranov equation for specified initial and boundary conditions in two dimensions.

3.2.1 Model Assumptions

The magnetosphere up to approximately 60 R_E from the earth in the tailward direction may be modelled by the equations describing hydromagnetic equilibrium [*Voigt*, 1986]. Here quasi-static magnetohydrodynamic processes may be considered within the "slow-flow" approximation. This implies that the time-scale of solar wind driven plasma convection is large compared with the typical Alfvén wave travel time and that plasma velocities are small compared with the typical Alfvén speed [*Schindler and Birn*, 1982; *Voigt and Wolf*, 1988]. As a result the inertial term

$$\rho \frac{D\mathbf{v}}{Dt} = \rho \left(\frac{\partial}{\partial t} + \mathbf{v}.\nabla \right) \mathbf{v}$$

in the MHD momentum equation (refer to equation 2.2) may be neglected [*Hau et al.*, 1989]. In addition, pressure isotropy is assumed, therefore

$$\mathbf{J} \times \mathbf{B} = \nabla P \tag{3.1}$$

This approximation thus excludes boundary layer regions in which rapid plasma streaming velocities are found. In Ampére's law (equation 2.6), the displacement current is ignored:

$$\nabla \times \mathbf{B} = \mu_0 \mathbf{J} \tag{3.2}$$

The other basic equations necessary for a complete description of ideal, one-fluid MHD (refer to equations 2.3 to 2.7) are Ohm's law for infinite conductivity,

$$\mathbf{E} + \mathbf{v} \times \mathbf{B} = 0, \tag{3.3}$$

the continuity equation,

$$\frac{\partial \rho}{\partial t} + \nabla.(\rho \mathbf{v}) = 0 \tag{3.4}$$

Faraday's law,

$$\nabla \times \mathbf{E} = -\frac{\partial \mathbf{B}}{\partial t} \tag{3.5}$$

and the divergence condition

$$\nabla.\mathbf{B} = 0 \tag{3.6}$$

In quasi-static MHD, this set of equations is completed by the adiabatic law which places a thermodynamic constraint on the pressure [*Voigt and Wolf*, 1988]

$$\frac{D}{Dt}\left(\frac{P}{\rho^{\gamma}}\right) = 0 \tag{3.7}$$

Convection is also assumed to be lossless.

3.2.2 Results From the Two-Dimensional Approach

The two-dimensional approach allows the essential physical mechanisms of interest to be examined while simplifying the computational analysis. The plane in consideration is the x-z plane which contains the earth's dipole (figure 3.1). This represents the magnetospheric noon-midnight meridian. All **y** dependence is ignored and $\partial/\partial y = 0$ is assumed. The magnetic field in this case has no B_y component. The remaining components may be expressed in terms of the magnetic vector potential, **A**. In the specified coordinates **A** becomes $\mathrm{A}(x, z)\,\hat{\mathbf{y}}$. Since $\mathbf{B} = \nabla \times \mathbf{A}$,

$$B_x = -\frac{\partial A}{\partial z}, \quad B_z = \frac{\partial A}{\partial x} \tag{3.8}$$

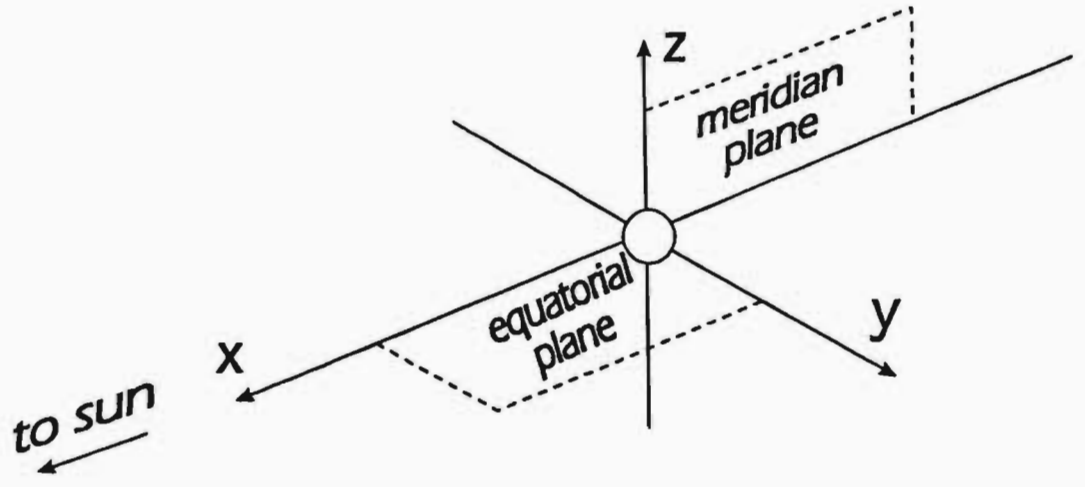

Figure 3.1: The magnetospheric coordinate system showing the equatorial $(x-y)$ and meridian $(x-z)$ planes.

Now

$$\begin{aligned} \nabla A &= \frac{\partial A}{\partial x}\hat{\mathbf{x}} + \frac{\partial A}{\partial z}\hat{\mathbf{z}} \\ &= B_z\hat{\mathbf{x}} - B_x\hat{\mathbf{z}} \end{aligned}$$

therefore

$$\mathbf{B}.\nabla A = B_x B_z - B_z B_x = 0$$

This implies that A is constant along a magnetic field line. Also

$$\begin{aligned} \nabla \times \mathbf{B} &= \nabla \times \nabla \times \mathbf{A} \\ &= \nabla(\nabla.\mathbf{A}) - \nabla^2\mathbf{A} \end{aligned}$$

But

$$\nabla.\mathbf{A} = 0$$

thus

$$\nabla \times \mathbf{B} = -\nabla^2\mathbf{A}$$

From Ampére's law, then,

$$\nabla^2 A = -\mu_0 J \tag{3.9}$$

where the current density, J, is in the $\hat{\mathbf{y}}$ direction and consists of both dipole current and plasma current components.

The momentum equation 3.1 implies that

$$\begin{aligned} \mathbf{B}.\nabla P &= \mathbf{B}.(\mathbf{J} \times \mathbf{B}) \\ &= 0 \end{aligned}$$

since **B** is perpendicular to **J** × **B**. The plasma pressure, P, is therefore also constant along magnetic field lines. Using the definition of the vector potential and the momentum equation again

$$\mathbf{J} \times (\nabla \times \mathbf{A}) = \nabla P$$

Writing components gives

$$\begin{aligned} \nabla P &= J\hat{\mathbf{y}} \times \left(-\frac{\partial A}{\partial z}\hat{\mathbf{x}} + \frac{\partial A}{\partial x}\hat{\mathbf{z}} \right) \\ &= J\left(\frac{\partial A}{\partial x}\hat{\mathbf{x}} + \frac{\partial A}{\partial z}\hat{\mathbf{z}} \right) \\ &= J\,\nabla A \end{aligned}$$

Since ∇A and ∇P are parallel (perpendicular to **B** in the x-z plane)

$$J = \frac{dP}{dA} \tag{3.10}$$

$P = P(A)$, $J = J(A)$ and A are then all constant along field lines.

Combining equation 3.9 and 3.10 gives the Grad-Shafranov equation in two dimensions

$$\nabla^2 A = -\mu_0 \frac{dP}{dA} \tag{3.11}$$

The current density may be decomposed into its plasma current and dipole contributions as

$$\nabla^2 A = -\mu_0 \frac{dP}{dA} - \mu_0 m_d \frac{\partial}{\partial x}\delta(x)\delta(z) \tag{3.12}$$

The dipole term is obtained [*Voigt and Wolf*, 1988] by considering the earth's dipole moment to be in the negative $\hat{\mathbf{z}}$ direction

$$\mathbf{M} = -m_d \delta(x)\delta(z)\,\hat{\mathbf{z}}$$

with magnitude m_d. The dipole magnetisation current is then

$$\mathbf{J}_d = \nabla \times \mathbf{M}$$

so that

$$J_d = m_d \frac{\partial}{\partial x} \delta(x)\delta(z)$$

in the $\hat{\mathbf{y}}$ direction.

The assumption of ideal MHD (infinite conductivity) implies that the magnetic field and plasma move together — the magnetic field is said to be "frozen-into" the plasma [*Cowling*, 1976]. As magnetic field lines are surfaces of constant A, it is possible to follow the motion of the plasma as it convects by observation of the motion of a field line of a particular A-value.

For lossless convection, the total number of particles in a flux tube is constant in time. Now

$$\rho = \frac{M}{V}$$

where M is the total mass and

$$V = \int \frac{ds}{B} \tag{3.13}$$

is the volume of a flux tube of unit magnetic flux. The integral is a line integral which extends over the arc length of the field line from the southern to the northern ionosphere. Substituting this definition of ρ in 3.7

$$\frac{D}{Dt}\left[P\left(\frac{V}{M}\right)^{\gamma}\right] = 0$$

For constant M

$$\frac{D}{Dt}\left(PV^{\gamma}\right) = 0$$

Since A is constant for a particular field line and the field lines move with the plasma, the adiabatic condition above may also be expressed as

$$PV^{\gamma}(A) = \text{constant in time} \tag{3.14}$$

Also, from Faraday's law,

$$E_y = -\frac{\partial A}{\partial t} \tag{3.15}$$

which is the convection electric field due to motion of the solar wind at the magnetopause.

3.3 Numerical Method

The vector potential may be written in terms of plasma current and dipole terms

$$A = A_p + A_d$$

Equation 3.12 may then be expressed as two separate equations

$$\nabla^2 A_p = -\mu_0 \frac{dP}{dA} \tag{3.16}$$

and

$$\nabla^2 A_d = -\mu_0 m_d \frac{\partial}{\partial x}\delta(x)\delta(z) \tag{3.17}$$

The latter has a singularity at $(x, z) = (0, 0)$, while everywhere else

$$\nabla^2 A_d = 0$$

A solution to equation 3.17 (for all points except the origin) is then

$$A_d = \mu_0 m_d \frac{x}{x^2 + z^2} \tag{3.18}$$

Equation 3.12 is a non-linear partial differential equation which, for the general case, needs to be solved numerically. Separation of this equation into 3.16 and 3.17 allows for greater accuracy and a decrease in the computational time required as the dipole part of the solution may be calculated analytically from 3.18. The plasma current part of equation 3.12 requires numerical solution for specified boundary conditions.

3.3.1 Boundary Conditions

The boundary conditions for the solution of equation 3.16 may take the form of either Dirichlet or Neumann conditions. Dirichlet conditions are those for which only values of the function are specified at the boundary, while Neumann conditions require the specification of the normal gradient. A Cauchy boundary condition specifies both the value and normal gradient. The solution to equation 3.16 is required within a closed region. For closed boundaries, however, Cauchy conditions over specify the solution of an elliptic equation such as this [*Morse and Feshbach*, 1953]. Thus for a unique, stable solution, only the values of A and P, or their gradients, may be set at the boundaries.

For numerical simplicity, a rectangular computational region is used. This is bounded by the magnetopause, the equatorial plane and a vertical far-tail boundary.

The Magnetopause Boundary

The magnetopause, assumed rectangular, forms the vertical left ($x = 10.8$ R_E) and horizontal top ($z = 18$ R_E) boundaries. This boundary is treated as a field line, with the (constant) value of the vector potential denoted A_{mp} and a constant pressure, P_{mp}.

Initial conditions: To obtain an initial self-consistent magnetic field configuration typical of the quiet magnetotail, A_{mp} is set to zero. The pressure at the magnetopause, P_{mp}, is also set to zero in the initial configuration for simplicity. The choice of pressure on this boundary has no effect on the development of the near-earth tail, which is the area of interest.

The Equatorial Boundary

At the equatorial plane ($z = 0$) the pressure variation with radial distance, $P(x_e)$, is specified[1]. Symmetry in the magnetic field is also imposed. This implies that the horizontal component of the field, B_x, which is the gradient in A in the normal direction, is zero. In keeping with the restriction to either Dirichlet or Neumann conditions, the modelling region is extended one grid point below the equatorial plane with the value of A here being specified by the value of A one grid point above the equatorial plane. The field is thus symmetrical about $z = 0$.

Initial conditions: The pressure at the equatorial plane is initially assumed to decline exponentially down the tail as in the Fuchs-Voigt model [*Fuchs and Voigt*, 1979]. This requires that

$$\frac{dP}{dA} = \frac{1}{\mu_0} k^2 A$$

where k is the Fuchs-Voigt constant referred to in section 3.3.3. Within the plasmasphere ($0 \geq x \geq -4.5$ R_E), pressure is assumed constant. Initially A is positive on the tailward side of the polar cusp and negative on the day-side. For simplicity, pressure is also assumed constant for negative values of the total vector potential, as pressure variation on the day-side has a minimal effect on the evolution of the magnetotail.

The Far-Tail Boundary

At the tail boundary, $x = -60.3$ R_E. This grid point lies closest to the -60 R_E point. Here the asymptotic approximation

$$\frac{\partial^2 A}{\partial z^2} >> \frac{\partial^2 A}{\partial x^2}$$

[1]The subscript "e" denotes the value of a variable at the equatorial plane.

holds as the dipole field in this region of the tail is weak. One dimensional force balance then requires that

$$\frac{\partial^2 A}{\partial z^2} = -\mu_0 \frac{dP(A)}{dA} \tag{3.19}$$

If P is given as a function of A, the above may be solved analytically for $A(z)$.

Initial conditions: A simple parabolic model for which $P(A) \propto A^2$ is used at the tail boundary. Specifically,

$$\frac{dP}{dA} = \frac{1}{\mu_0} k^2 A \tag{3.20}$$

Initially, $k = 1.54$, and the tail boundary values correspond to Fuchs-Voigt model values (refer to section 3.3.3).

3.3.2 Gauss-Seidel Method

Solutions to equation 3.16 for the above boundary conditions are calculated for a rectangular region of extent 10.8 $R_E \geq x \geq -60.3$ R_E and 0 $R_E \leq z \leq 18$ R_E. The grid size, Δ, is uniform in both the x and z directions and corresponds to a distance of 0.9 R_E. This gives a modelling grid of 80×21 and results in the far-tail equatorial boundary having a non-integer value (-60.3 R_E). The grid size may be decreased as desired. In the model, z and x grid points are represented by the modelling coordinates I and J respectively. Each grid spacing corresponds to a unit increment in I or J.

The numerical method used to solve this boundary value problem is the Gauss-Seidel method. This uses the finite difference form of the partial differential equation 3.16.

Finite Difference Equation

The left hand side of equation 3.16 involves the operator

$$\nabla^2 = \frac{\partial^2}{\partial x^2} + \frac{\partial^2}{\partial z^2}$$

At any interior point on the modelling grid

$$\begin{aligned} \frac{\partial A^2}{\partial x^2} &= \frac{\partial}{\partial x}\left(\frac{\partial A}{\partial x}\right) \\ &\simeq \frac{1}{\Delta}\left[\frac{A_{j+1,i} - A_{j,i}}{\Delta} - \frac{A_{j,i} - A_{j-1,i}}{\Delta}\right] \\ &= \frac{A_{j+1,i} - 2A_{j,i} + A_{j-1,i}}{\Delta^2} \end{aligned}$$

A similar expression may be obtained for $\partial^2 A/\partial z^2$ so that the finite difference representation of 3.16 is

$$\frac{A_{j+1,i} - 2A_{j,i} + A_{j-1,i}}{\Delta^2} + \frac{A_{j,i+1} - 2A_{j,i} + A_{j,i-1}}{\Delta^2} = \sigma_{j,i}$$

where σ is the "source" term on the right hand side of equation 3.16. This may be written as

$$A_{j+1,i} + A_{j-1,i} + A_{j,i+1} + A_{j,i-1} - 4A_{j,i} = \Delta^2 \sigma_{j,i}$$

or

$$A_{j,i} = \frac{1}{4}\left(A_{j+1,i} + A_{j-1,i} + A_{j,i+1} + A_{j,i-1} - \Delta^2 \sigma_{j,i}\right) \tag{3.21}$$

This equation holds for all interior grid points [*Press et al.*, 1989].

The Gauss-Seidel method is an iterative procedure that uses updated values of A on the right hand side of 3.21 as soon as they are available. Let n represent the current value (and current iteration), and $n+1$ the updated value. Equation 3.21 becomes

$$A^{n+1}_{j,i} = \frac{1}{4}\left(A^{n}_{j+1,i} + A^{n+1}_{j-1,i} + A^{n}_{j,i+1} + A^{n+1}_{j,i-1} - \Delta^2 \sigma_{j,i}\right) \tag{3.22}$$

For each iteration, the values of the current density (σ in the above equation) are obtained from the values of the total vector potential from the previous iteration.

This procedure is continued until the maximum change in the function $A(x, z)$ at each grid point is less than an amount, ϵ, for successive iterations. The speed of convergence will depend on the extent of the modelling region, the size of the grid spacing and the magnitude of ϵ.

3.3.3 Equilibrium Solutions

The solution of the Grad-Shafranov equation for given boundary conditions by the method described in the previous section provides quasi-static equilibrium configurations for the magnetospheric magnetic field. For the numerical procedure to be efficient, reasonable values of the vector potential and the current density are needed at each point as an initial approximation. The first solution, for time $t = 0$, corresponds to an average "quiet" magnetic field configuration. Initial estimations of the required variables for this solution are made using the Fuchs-Voigt model [*Fuchs and Voigt*, 1979]. Subsequent configurations, each valid at a later time than the one before, use the previous solution as a starting point.

Fuchs-Voigt Model

The Fuchs-Voigt model [*Fuchs and Voigt*, 1979] considers a special case of the Grad-Shafranov equation for which an analytical solution is possible. The pressure in this model varies parabolically with vector potential. This dependence is a reasonable approximation to observation.

For a rectangular magnetopause geometry, the Fuchs-Voigt analytical solution for $A(x, z)$ is

$$A = -\frac{m}{2} \sum_{n=0}^{\infty} \left[e^{-|\lambda_n x|} \text{sign}(x) + e^{-|\lambda_n (x+2b)|} \text{sign}(x + 2b) \right] . \cos(\alpha_n z) \qquad (3.23)$$

In the above, m is a modified magnetic dipole moment and b is the position of the sub-solar point. For $A = 0$ at the magnetopause, $\alpha = \pi/2$. The variable λ is

specified by the choice of k through the relation

$$k^2 = \alpha^2 - \lambda^2$$

Here k ranges from zero to $\pi/2$. For $k = 0$, the field lines described by contours of constant A correspond to a dipole field in a vacuum. Increasing k effectively increases the plasma population of the magnetosphere and the magnetic field configuration becomes more tail-like.

To initialise the modelling grid, a Fuchs-Voigt model with k = 1.54 is used. This value is used as it gives magnetic field and plasma pressure variations comparable to those found in an average quiet magnetosphere. The Fuchs-Voigt dipole solution is then subtracted to give initial values for A_p, the plasma current vector potential.

Magnetic Dipole Moment

The magnitude of the magnetic dipole moment, m_d, in equation 3.12 is not the same as that of the modified magnetic dipole moment in equation 3.23. The Fuchs-Voigt 'dipole solution' includes effects due to Chapman-Ferraro currents on the magnetopause, while the analytical dipole solution 3.18 does not. For consistency, the two values may be linked by specifying the value of the magnetic field at a point on the equatorial plane for an average quiet magnetosphere.

Alternatively, since the Fuchs-Voigt model is only used as an initial guess for the values of A_p on the modelling grid, m_d may be chosen to reflect the desired value of the dipole magnetic field at any point on the equatorial plane, with m being fixed at a value which gives realistic variations of the equatorial magnetic field and plasma pressure.

Initial Configuration

An initial self-consistent magnetospheric magnetic field configuration is thus obtained by

1. Generating the analytical dipole vector potential from 3.18.
2. Generating an initial approximation for A_p from the Fuchs-Voigt models.
3. Generating boundary conditions. At the tail boundary, this involves calculating $A(z)$ and thus A_p.
4. Generating values of dP/dA given $P(x_e)$.
5. Using Gauss-Seidel iteration to find a self-consistent solution for $A(x, z)$.

The algorithms used in each step are discussed in Appendix A.

The initial approximation thus converges to a self-consistent solution for the specified boundary conditions. The magnetic field corresponding to this solution may be visualised by tracing contours of constant vector potential, A.

3.4 Adiabatic convection

To achieve time-dependent convection, the boundary conditions are altered to effect the presence of an electric field on the magnetopause. This simulates the substorm growth phase scenario in which enhanced reconnection at the day-side magnetopause results in an increase of flux in the tail. Imposition of a thermodynamic constraint in the form of the adiabatic law forces any new equilibrium solution corresponding to the changed boundary conditions to have the same $PV^{\gamma}(A)$ as the initial ($t = 0$) configuration, as required by equation 3.14. This

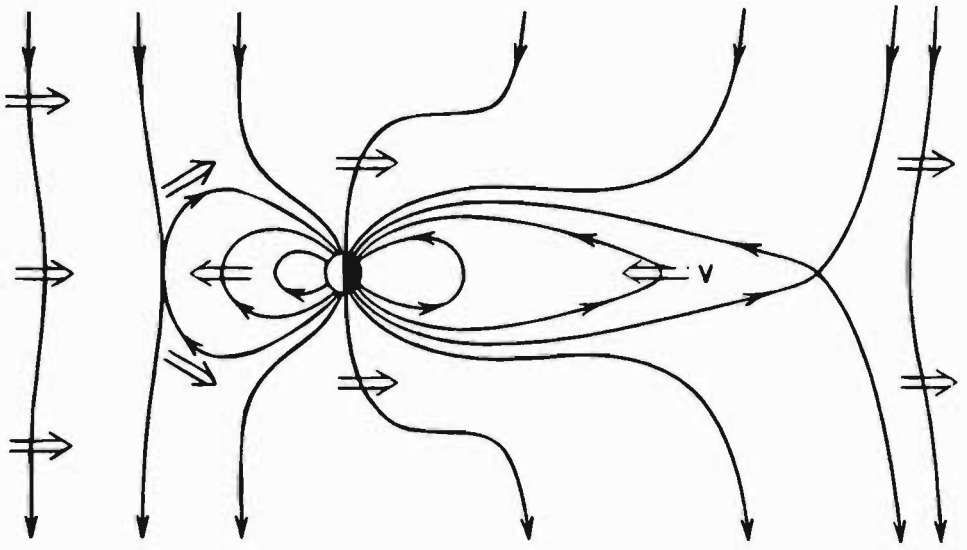

Figure 3.2: Reconnection and magnetospheric convection in the meridian plane. From *Lyons and Williams* [1984].

results in sequences of quasi-static equilibrium solutions in which plasma sheet flux tubes convect earthward in time.

3.4.1 Magnetospheric Shielding

The motion of the solar wind across open magnetic field lines gives rise to an electric field at the polar caps from the dawn-side to the dusk-side. Consequently, a dawn-to-dusk electric field is also present across the region of closed magnetic field lines. This electric field, called the convection electric field, drives the large scale plasma flow depicted in figure 3.2, with anti-sunward flow across the poles and sunward flow in the equatorial plane [*Lyons and Williams*, 1984].

As plasma convects toward the earth in the equatorial plane, it encounters increasing magnetic field strengths and gains energy. Gradient and curvature drift forces, which are charge dependent, now become important. The paths of the electrons and ions thus separate and travel in different directions around the

inner magnetosphere at the Alfvén layer [*Schield et al.*, 1969]. This partially shields the inner magnetosphere from the convection electric field and earthward adiabatic drift [*Lyons and Williams*, 1984].

In the two-dimensional model which has been used, this tendency of plasma to drift azimuthally around the earth is accounted for by not allowing plasma sheet flux tubes to convect earthward of the Alfvén layer. The position of the Alfvén layer is termed the 'shielding distance'. In two dimensions, this shielding results in the plasma pressure at this position increasing as more flux tubes reach the shielding distance [*Voigt and Wolf*, 1988].

The build-up of pressure is prevented by holding the pressure at the shielding distance constant. The plasma pressure of a convecting flux tube may not exceed the maximum set by this value. As a consequence, the position of the Alfvén layer in the model moves tailward as convection proceeds. Even though observation indicates that the Alfvén layer moves earthward as activity increases [*Schield et al.*, 1969], in contrast to the motion in the model, this simulation of magnetospheric shielding is sufficient as a first approximation. An improved mechanism has been suggested by *Erickson* [1992].

3.4.2 Time Parameterisation

Time is parameterised by the value of the total vector potential at the magnetopause through equation 3.15. For a given electric field at the magnetopause, $E = E_{mp}$, and a specified value for A_{mp}, 3.15 may be integrated [*Erickson*, 1984]:

$$\int_0^t E_{mp}(t')\, dt' = -A_{mp} \tag{3.24}$$

This holds for $A_{mp} = 0$ at $t = 0$, as is the case in the initial configuration. More generally [*Voigt and Wolf*, 1988],

$$\int_{t_i}^{t_{i+1}} E_{mp}(t')\, dt' = A_{mp}(t_i) - A_{mp}(t_{i+1})$$

A negative increment in A_{mp} thus corresponds to an increment in time for a constant electric field at the magnetopause. For the numerical calculation of the elapsed time refer to section 3.5.1.

3.4.3 Adiabatic Constraint

After decreasing A_{mp}, a new solution to 3.16 is sought under the added requirement that it have the same $PV^{\gamma}(A)$ as the initial solution. All subsequent solutions must thus satisfy the condition

$$PV_{t_i}^{\gamma}(A) = G(A) \tag{3.25}$$

where

$$G(A) \equiv PV_{t_0}^{\gamma}(A)$$

The magnetic field lines may be traced by constructing contours of constant vector potential. The volume of these lines may then be calculated according to the relation 3.13 and values for the above functions obtained. This is done for all field lines crossing the equatorial plane between the shielding distance and the far-tail boundary. The adiabatic condition is not enforced earthward of the shielding distance or on the day-side of the earth.

The ratio of specific heats, γ, is 5/3 for a monatomic plasma in three dimensions. Even though the model is two-dimensional, the individual particles are assumed to gyrate in three dimensions.

As the flux in the tail increases, field lines that previously intersected the far-tail boundary now cross the equatorial plane. In order to conserve PV^{γ} for these field lines, it is necessary to know the required value for this function as defined by the initial configuration. To do this, the t_0 solution is solved for a magnetotail that extends to $x = -97.2$ R_E. All subsequent configurations have a far-tail boundary at $x = -60.3$ R_E.

By decreasing the value of A at both interior and boundary points, an initial approximation to the solution is made while the boundary conditions are changed at the same time. Subtracting $|\Delta A|$ from a solution $A(x,z)$ does not change the structural appearance of the magnetic field. The volume of the field lines as a function of radial distance, $V(x_e)$, remains the same, as does $PV^\gamma(x_e)$, since the equatorial pressure is not changed. The values of $A(x_e)$, however, have decreased, so that the value of PV^γ at that point will be too low. The equatorial pressure values thus need to be modified.

3.4.4 Updating Boundary Conditions

The equatorial pressure is adjusted according to the algorithm described by *Erickson* [1992]. This involves evaluating the ratio

$$R = \frac{PV^\gamma(J)}{G(J)}$$

where $G(J)$ is the required value of PV^γ corresponding to the value of A at that point. Let the previous pressure at an equatorial point, J, be denoted $P(J)$, and the updated pressure, $P'(J)$. Then

- *for* $R = 1$: $P'(J) = P(J)$
- *for* $R < 1$: $P'(J) = P(J) + \omega(R-1)[P(J) - P'(J-1)]$
- *for* $R > 1$: $P'(J) = P(J) - \omega(\frac{1}{R} - 1)[P(J) - P'(J-1)]$

This routine reflects the fact that, since the pressure is only allowed to increase to the maximum value defined by the pressure inside the shielding distance, P remains constant or decreases with x_e. The variable ω is a weighting factor [*Erickson*, 1992] that speeds up or slows down the updating procedure.

The first pressure value to be altered is that at the grid point immediately tailward of the shielding distance. At the far-tail boundary, the value of the pressure at

the equatorial plane is found by extrapolation of the updated values earthward of this point.

Since the equatorial pressure at the far-tail boundary has changed, the boundary values $A(z)$ and dP/dA here need to be adjusted accordingly.

With these new boundary conditions, the iteration procedure is once again performed to find a solution to 3.16. PV^{γ} for this equilibrium configuration is calculated, with the updating of boundary conditions as before. This continues until a solution is found for which condition 3.25 holds.

3.4.5 Quasi-static, time-dependent convection

To summarise, quasi-static, time-dependent magnetospheric magnetic field configurations are obtained by

1. Subtracting $|\Delta A|$ from the t_{i-1} solution for all $A(x,z)$ (thus changing A_{mp} and generating an initial approximation).
2. Calculating $PV^{\gamma}(A)$ for this configuration.
3. Updating the pressure boundary values at the equatorial plane.
4. Updating the far-tail boundary conditions.
5. Solving 3.16 for the new boundary conditions.
6. Repeating steps 2 to 5 until PV^{γ} for each point lies within 1% of the required value, G.

This generates an equilibrium solution for time t_i. Steps 1 to 5 are repeated to extend the convection sequence for a longer period of time. Each quasi-static, equilibrium configuration represents the progressive convection of plasma sheet flux tubes in the original solution.

Physical Quantity	Symbol	Model Units	SI Units
distance	x,z	R_E	m
magnetic field	**B**	nT	T
vector potential	**A**	$nT.R_E$	T. m
pressure	P	$nT.A.R_E^{-1}$	$N.m^{-2}$
current density	dP/dA	$A.R_E^{-2}$	$A.m^{-2}$
volume of unit magnetic flux tube	$\int ds/B$	$R_E.nT^{-1}$	$m^3.Wb^{-1}$
permeability of free space	μ_0	$nT.R_E.A^{-1}$	$Wb.A^{-1}.m^{-1}$
scale factor	k	R_E^{-1}	m^{-1}

Table 3.1: Model and SI units for the physical quantities used in the computational analysis.

3.5 Model Units

The modelling units and corresponding MKS units for the various quantities used in the computation are given in table 3.1. The unit of distance is the earth radius, R_E, where

$$1\ R_E = 6.38 \times 10^6\ m$$

All quantities may be converted to MKS units using the above relation and noting that $1\ nT = 1 \times 10^{-9}$ T. For example, the permeability of free space is

$$\mu_0 = 4\pi \times 10^{-7}\ Wb.A^{-1}.m^{-1}$$

in SI units, where $Wb \equiv T.m^2$. This corresponds to

$$\begin{aligned} \mu_0 &= 4\pi \times 10^{-7} \times 6.38 \times 10^6 \times 10^9\ nT.R_E.A^{-1} \\ &= 1.97 \times 10^{-4}\ nT.R_E.A^{-1} \end{aligned}$$

3.5.1 Evaluating t_i

As noted in section 3.4.2, time is parameterised through the value of the vector potential at the magnetopause, A_{mp}. Performing the integration in equation 3.24 gives

$$E_{mp}\, t = -A_{mp} \tag{3.26}$$

For A_{mp} in nT.R_E and E_{mp} in V.m^{-1}, the time, in seconds, is obtained from

$$t = -\frac{A_{mp}}{E_{mp}} \times 6.38 \times 10^{-3}\ \text{s} \tag{3.27}$$

The elapsed time is thus dependent on the value of the electric field at the magnetopause. *Erickson* [1992] has taken $E_{mp} = 2.2 \times 10^{-4}$ V.m^{-1}. Substitution into equation 3.27 shows that, for this value of the electric field and $\Delta A_{mp} = -10$, $\Delta t = 290\ \text{s} \simeq 4.83$ min.

For the modelling procedure described, time steps of $\Delta t = 4.83$ min ($\Delta A_{mp} = -10$) were used to convect the equilibrium configurations in time.

Changing the value of E_{mp} changes the timescale of the convection through equation 3.26. The equilibrium configurations remain the same.

Chapter 4

Results

The programs described in Chapter 3 were used to model the time-development of an average quiet magnetospheric magnetic field under growth phase conditions. The resulting configurations are seen to have characteristic equatorial magnetic field and pressure profiles. These are tested for stability against the ballooning mode using the condition derived in Chapter 2.

4.1 Initial configuration

The initial self-consistent solution to the Grad-Shafranov equation for the prescribed boundary conditions is shown in figure 4.1. The earth is not depicted, but lies at the origin of the coordinate system. The magnetic flux, Φ, in an interval of x or z is proportional to A by the relations

$$\Phi \propto \int B_x \, dz = A$$

and

$$\Phi \propto \int B_z \, dx = A$$

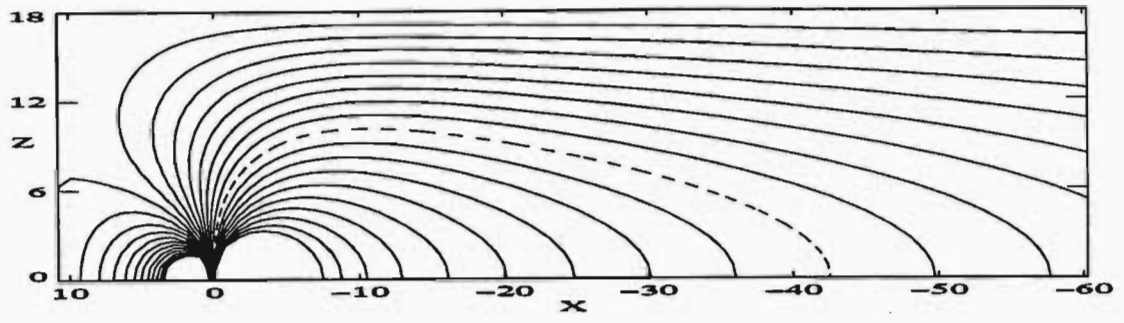

Figure 4.1: The initial self-consistent magnetospheric magnetic field configuration. The distances along each axis are in units of earth radii (R_E).

The field lines in figure 4.1 have been traced at intervals of constant $|\Delta A|$ so that equal amounts of magnetic flux are contained between each line. The shielding distance is taken as $x = -4.5\ R_E$.

The equatorial pressure corresponding to this configuration is shown in figure 4.2. This graph reflects the fact that the pressure within the shielding distance is assumed constant. The pressure tailward of this position declines exponentially down the tail as expected.

The equatorial magnetic field for this solution is depicted in figure 4.3. The tailward variation is also exponential, with the magnetic field decreasing monotonically anti-sunwards. This field is due to dipole and plasma current contributions. The strength of the dipole field may be modified by changing the value of the dipole moment until the total field is in agreement with the average observed magnetic field. The tail lobe field is, in general, larger than the equatorial field in the mid-tail region.

The equatorial current density, $J \equiv dP/dA$, is plotted as a function of radial distance in figure 4.4. The inner edge of the current sheet is very sharp as a result of the constant pressure requirement within the shielding distance. Tailward of $-4.5\ R_E$ the current flows westward (from dawn-to-dusk) in the equatorial plane

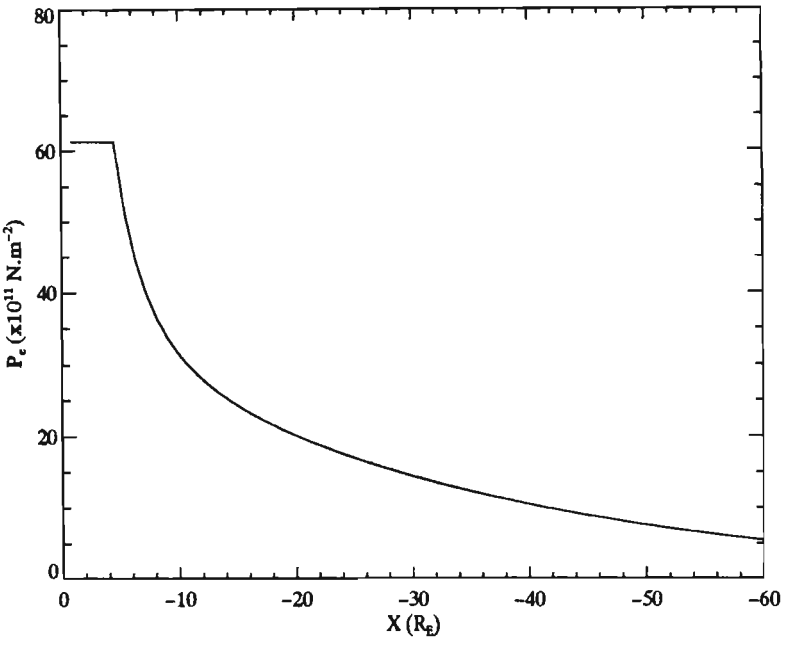

Figure 4.2: The equatorial pressure variation for the initial solution.

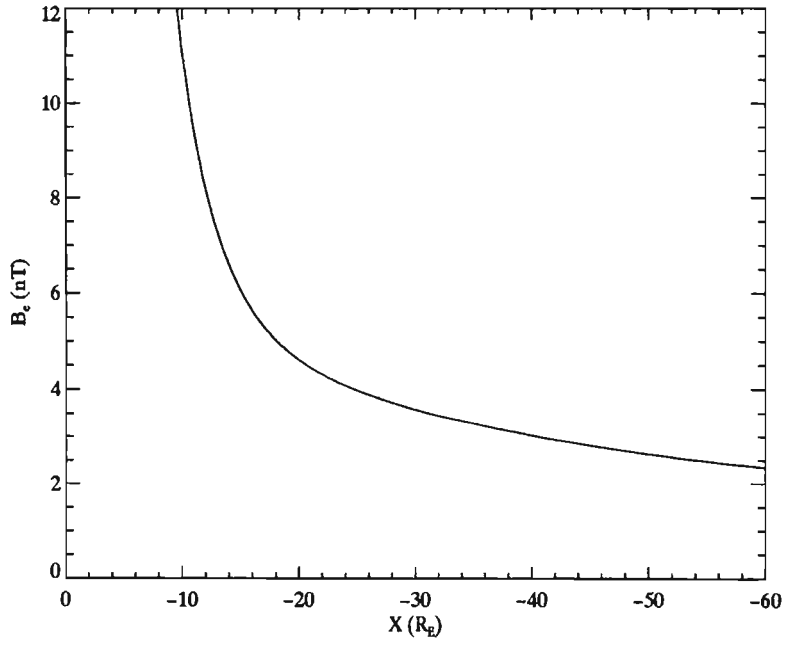

Figure 4.3: The equatorial magnetic field variation for the initial configuration.

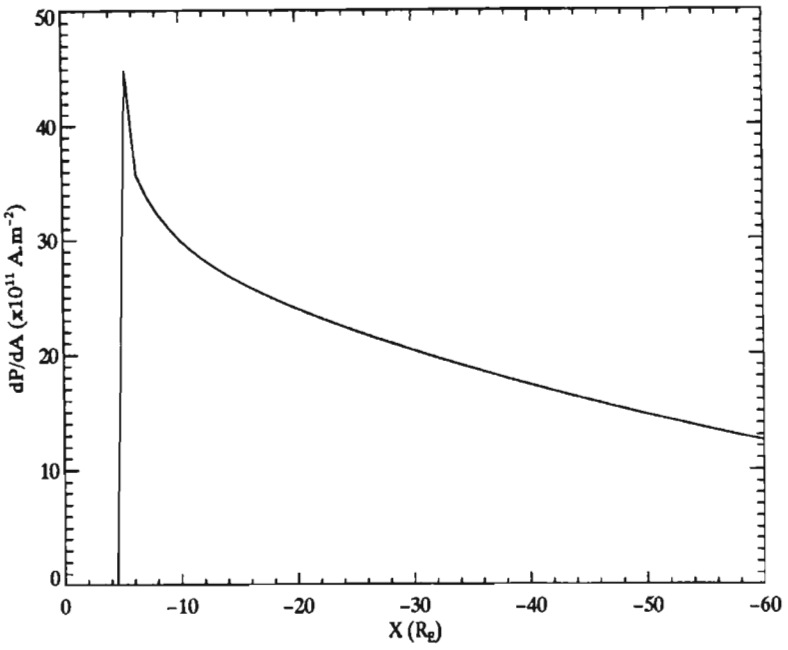

Figure 4.4: The initial equatorial current density as a function of radial distance from the earth.

as indicated by the positive values for dP/dA.

The variation of PV^γ with x is shown in figure 4.5. In order to match PV^γ values for those field lines which enter the modelling region at the tailward boundary during convection, the initial model is solved for a tail boundary at $x = -97.2$ R_E. $PV^\gamma(x)$ is seen to increase with distance down the tail and then start to decrease tailward of $x = -63$ R_E as the pressure begins to fall off faster than the flux tube volume increases. Figure 4.6 shows the variation of the vector potential with x for the initial solution.

The adiabatic condition requires that $PV^\gamma(A)$ be constant in time. The values of $PV_{t_0}^\gamma \equiv G$ are plotted against the total vector potential in figure 4.7. Since A is constant for a field line, the earthward motion of the magnetic field lines which is achieved by subtracting $|\Delta A|$ from a previous solution results in the values for PV^γ on each field line being too low. This applies for A greater than approximately 130 nT.R_E. If A is less than 130 nT.R_E, the values for PV^γ are

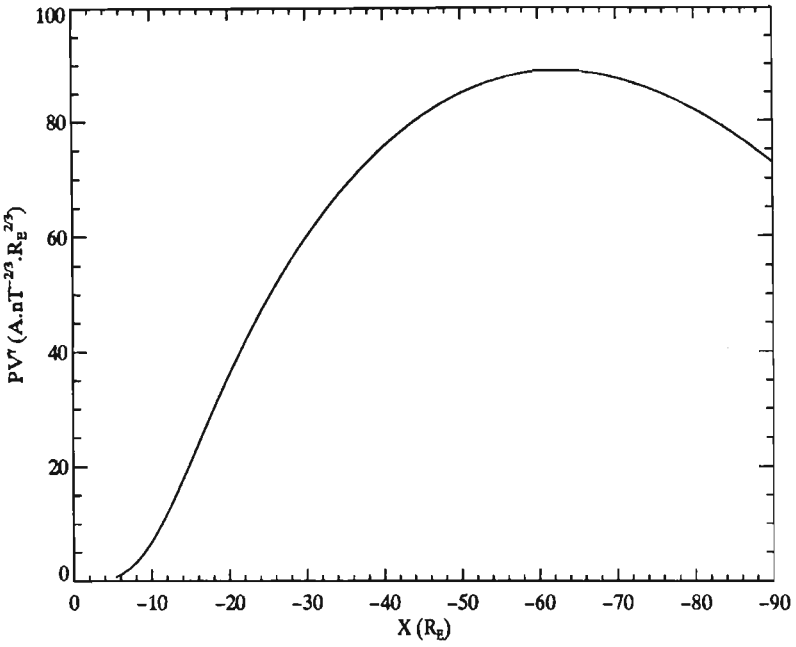

Figure 4.5: Values of PV^{γ} plotted as a function of x for the initial solution.

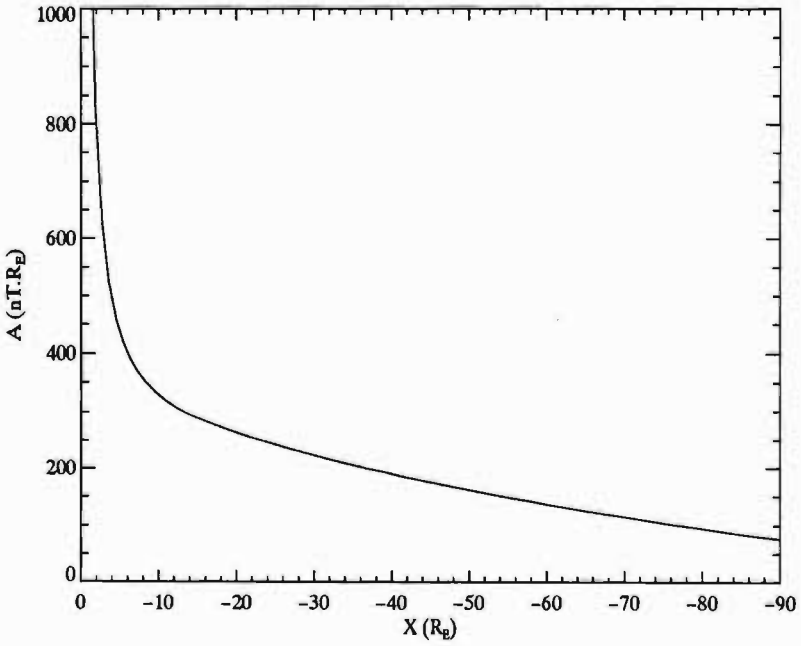

Figure 4.6: Values of A plotted as a function of x for the initial solution.

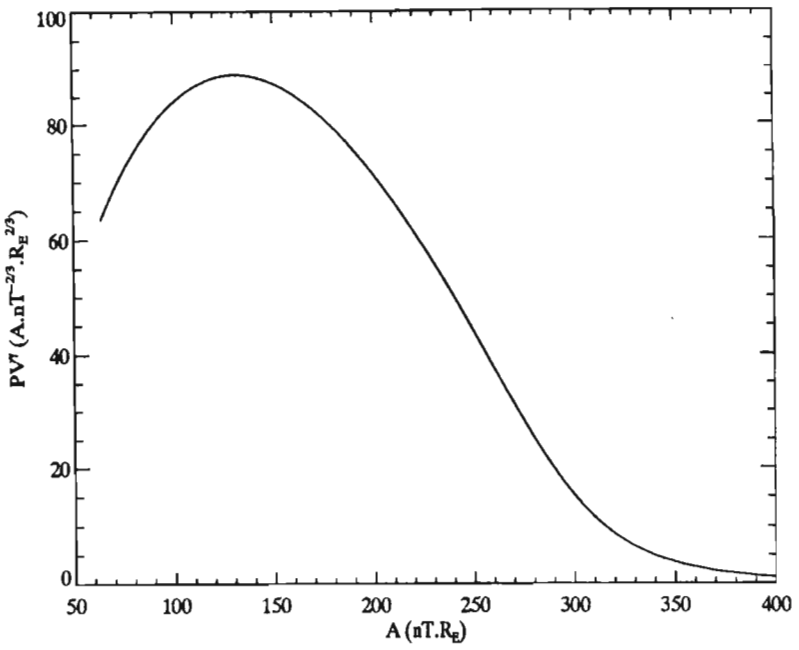

Figure 4.7: Values of PV^{γ} plotted as a function of the total vector potential. This curve is the same for all solutions as a consequence of the adiabatic restriction.

too high. This is adjusted by successive approximation to attain the quasi-static configuration for each time step.

4.2 Convection Sequences

Convecting the initial configuration in time results in the sequence of configurations depicted in figure 4.8. The initial configuration is included for comparison. In each of the convected solutions, a particular field line is indicated for reference. It is clear that the tail field becomes more stretched as the flux contained in the tail increases. The boundary between the dipole-like and tail-like field lines anti-sunward of the earth becomes more pronounced. This is particularly noticeable in the latest configuration shown in figure 4.8 ($t = 74.9$ min).

The development of the equatorial pressure is shown in figure 4.9. The shielding

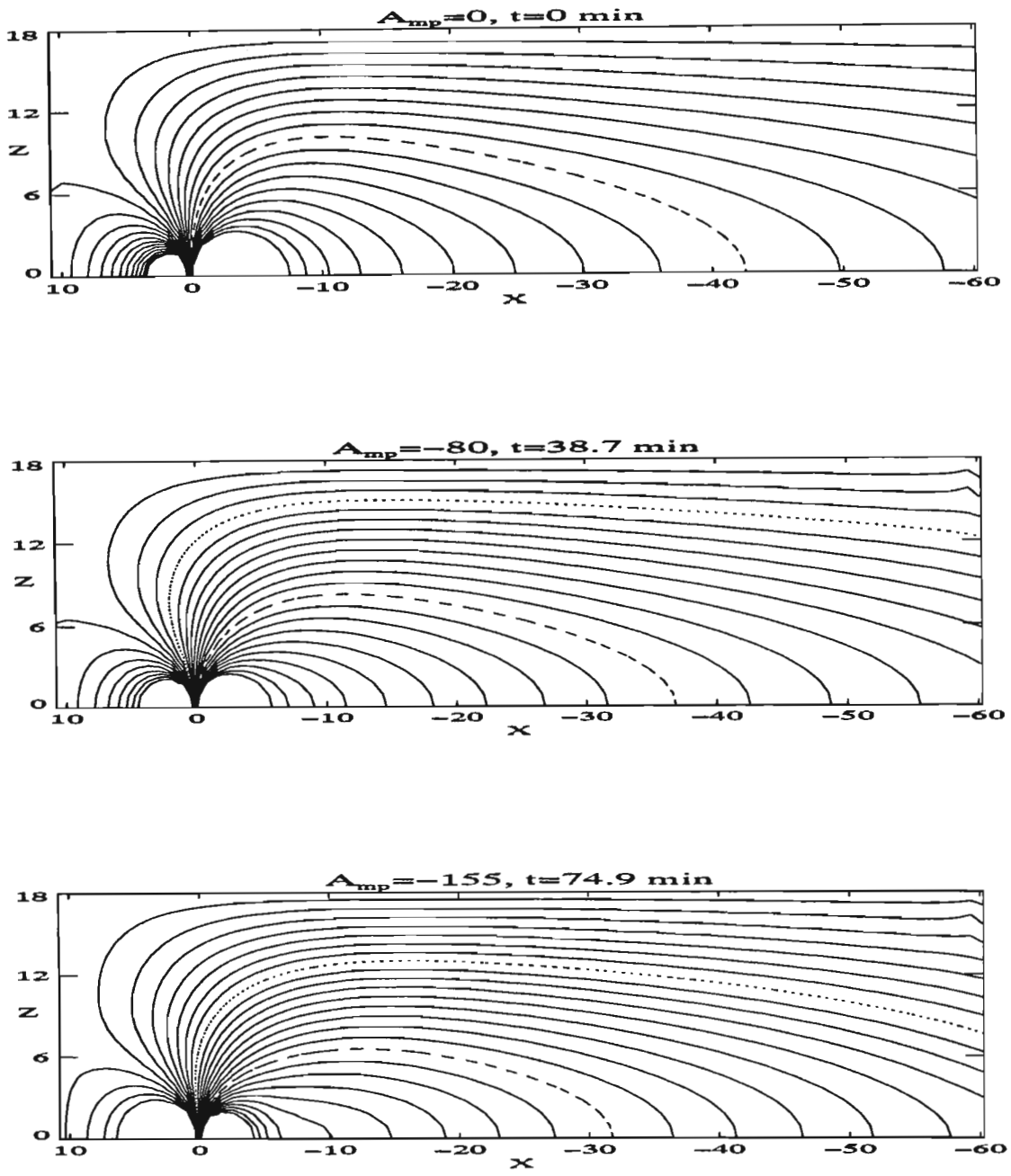

Figure 4.8: This shows the sequence of magnetic field configurations obtained when the initial solution is convected under the adiabatic constraint. The initial configuration is included for reference. The $A = 0$ field line is dotted. The dashed field line is $A = 180$. A is in units of $\mathrm{nT.R_E}$ throughout. The distances along each axis are in units of earth radii ($\mathrm{R_E}$).

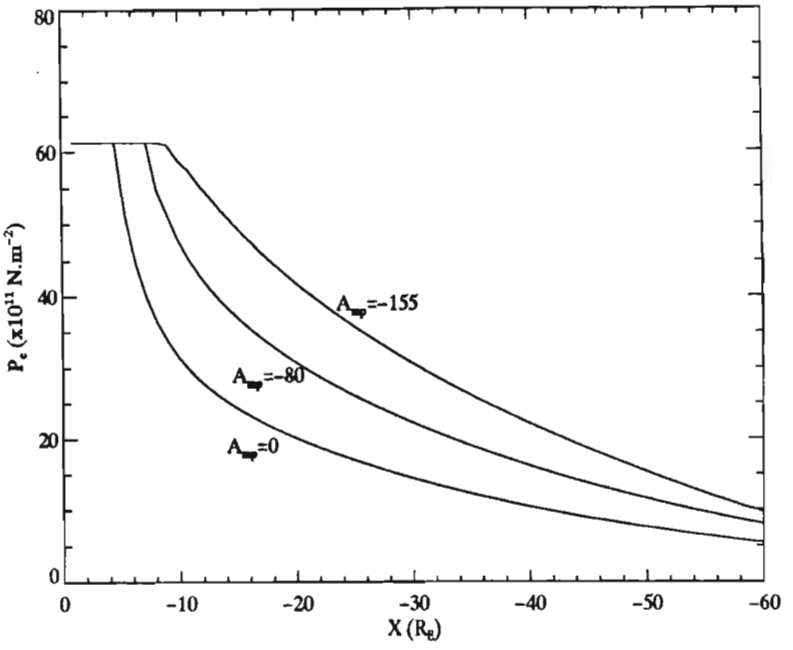

Figure 4.9: The development of the equatorial pressure during convection. Each curve corresponds to a configuration in the convection sequence as indicated by the value of A_{mp} (in units of nT.R_E).

distance is seen to have moved tailward to -9 R_E for $A_{mp} = -155$ nT.R_E. This is a consequence of the artificial shielding mechanism that has been used. The thermodynamic constraint enforced through the modification of the equatorial pressure has resulted in the radial pressure gradient becoming smaller in the near-earth regions and slightly larger near the tail boundary. The pressure in all regions has increased with time.

Figure 4.10 demonstrates that the equatorial current density at the inner edge of the plasma sheet has increased for $t > 0$ with a peak which moves tailward with the shielding distance. By excluding any pressure build-up, the current is prevented from reversing direction and flowing eastward near the inner edge. The negative values for dP/dA earthward of the shielding distance in figure 4.10 for $A_{mp} < 0$ are not real, but are the result of the five point fit that has been used to calculate dP/dA in the equatorial plane. This becomes evident when two

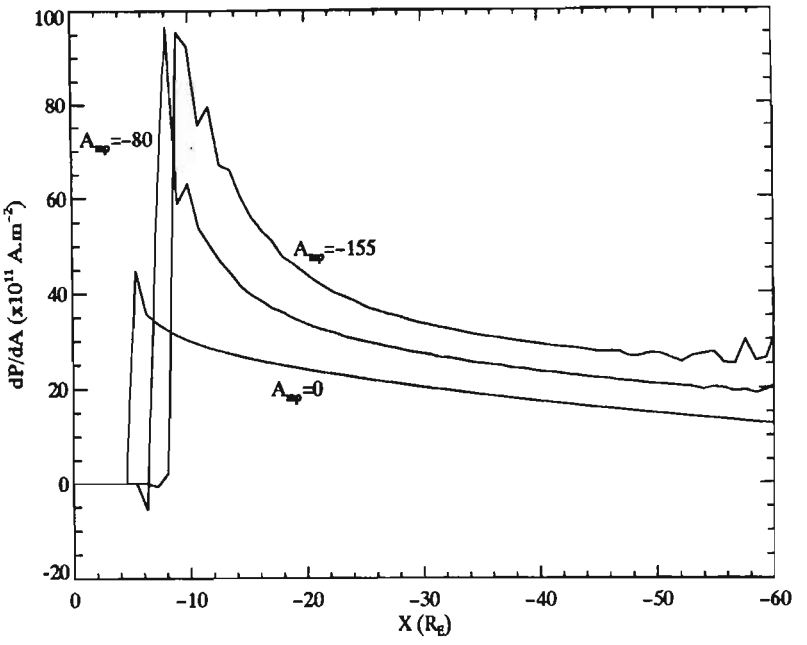

Figure 4.10: The development of the current density in the equatorial plane. Here a five point fit for dP/dA has been used.

point numerical differentiation is used. Figure 4.11 shows the development of the equatorial current density for the two point approximation, $\Delta P/\Delta A$. Here the current density is never negative.

The oscillations in dP/dA just tailward of the inner edge and at the far-tail boundary are also a result of the errors introduced by the numerical differentiation used in the model. These errors become larger as the pressure increases towards the end of the convection sequence and are evident for both the five and two point current density approximations.

The equatorial magnetic field corresponding to each configuration in figure 4.8 is plotted in figure 4.12. As convection proceeds, a local minimum in B_e forms at $L \simeq 10$. This is related to the stretching of the field lines in this region and is a direct consequence of the adiabatic restriction. Altering the pressure gradient, dP_e/dx, to conserve PV^γ effectively changes the current density, dP/dA, the magnetic field, $B(x)$, and the flux tube volume, V. This minimum in B_e is first

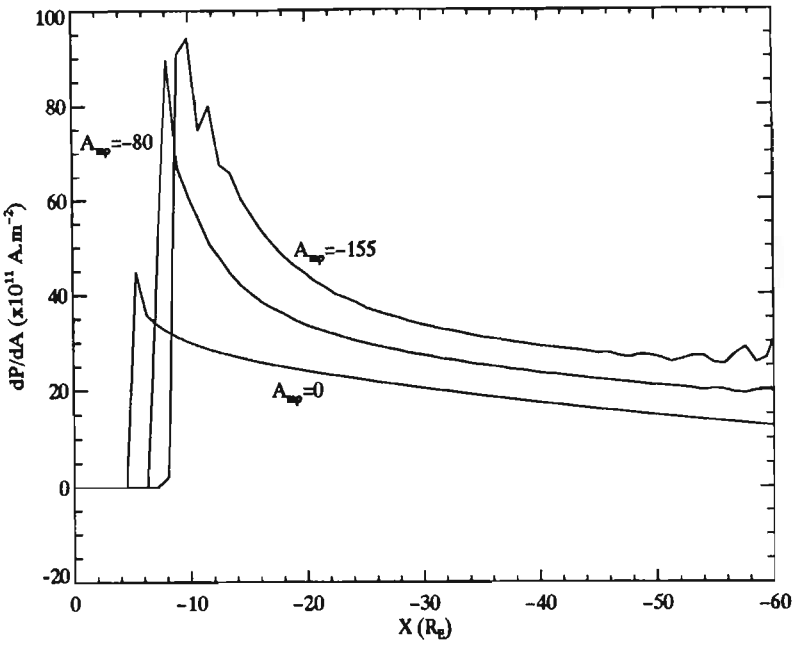

Figure 4.11: The development of the current density in the equatorial plane when a two point fit is used.

apparent at approximately $t = 48.33$ min and becomes deeper with time.

The development of the magnetic field in the equatorial plane due to magnetopause and plasma currents, $B_{p,e}$, is shown in figure 4.13. This component of the magnetic field becomes more largely negative (southward) near the inner edge as convection proceeds. Since the dipole field remains constant, it is the southward development of this component which contributes to the formation of the minimum in the equatorial magnetic field. The equatorial variation of the dipole component of the magnetic field is demonstrated in figure 4.14.

As the field lines become more tail-like with the increasing flux in the magnetotail, a time is reached in the convection sequence for which the code will no longer converge. *Erickson* [1992] has reported that this may be due to a "bifurcation of the static solution", or may even be related to some real physical effect in which an instability has caused a reconfiguration of the field. The last solution in the convection sequence in figure 4.8 represents the latest equilibrium configuration

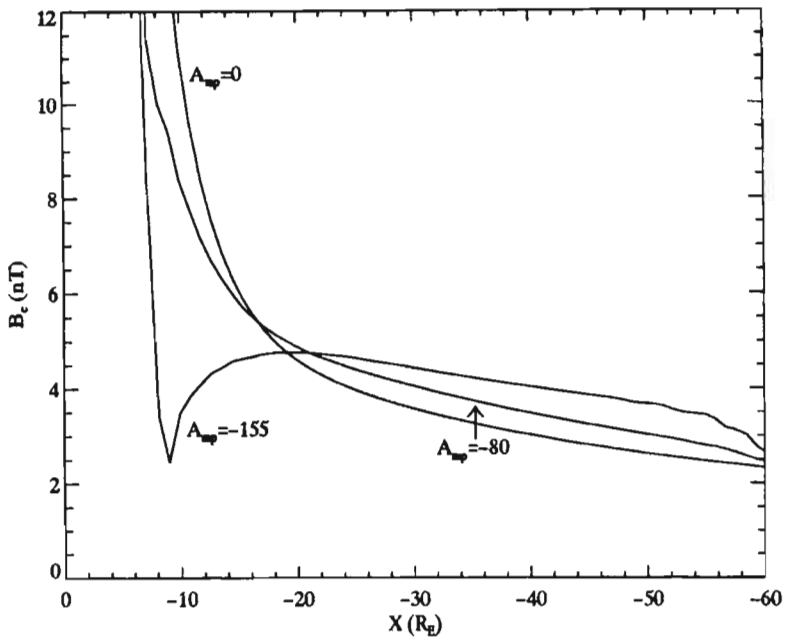

Figure 4.12: The development of the equatorial magnetic field.

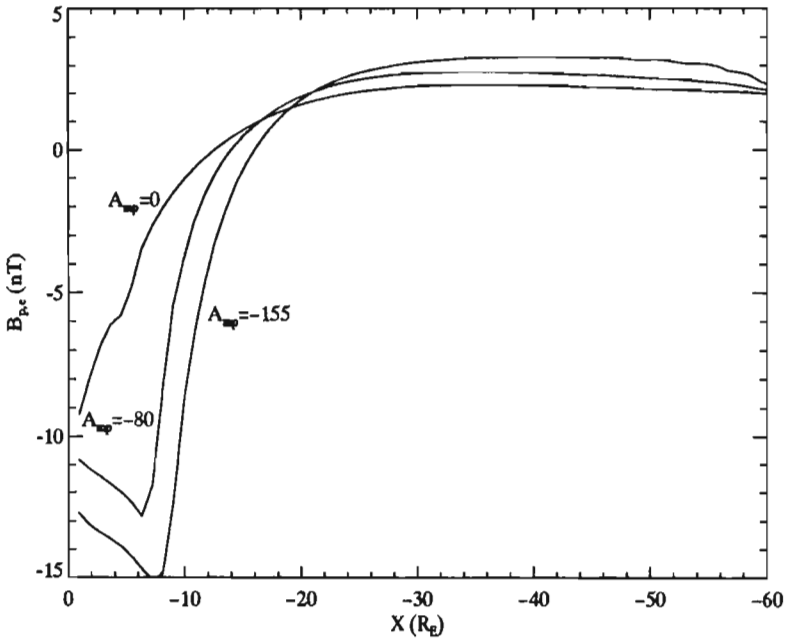

Figure 4.13: The development of the plasma current component of the equatorial magnetic field.

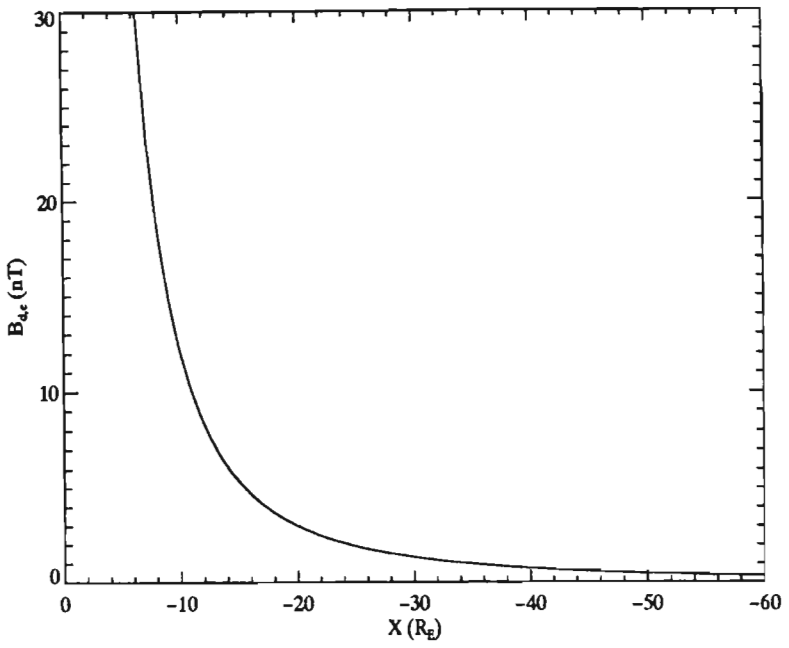

Figure 4.14: The dipole magnetic field component in the equatorial plane.

for which the code would converge.

4.3 Ballooning Instability

For the tail to be unstable to ballooning, the condition (refer to equation 2.80)

$$\kappa\left(\gamma P - \frac{B^2}{\mu_0}\right) - \kappa_\nu\left(\gamma P + \frac{B^2}{\mu_0}\right) < 0 \tag{4.1}$$

derived in Chapter 2 must be satisfied. Now pressure and magnetic field values are known at each point on the modelling grid. In the above equation, the curvature, κ, may be expressed in terms of κ_p and κ_ν by using the relation (refer to equation 2.36)

$$\kappa = -\left(\kappa_\nu + \frac{1}{2}\beta\kappa_p\right) \tag{4.2}$$

Here

$$\frac{1}{2}\beta = \frac{P}{B^2/\mu_0}$$

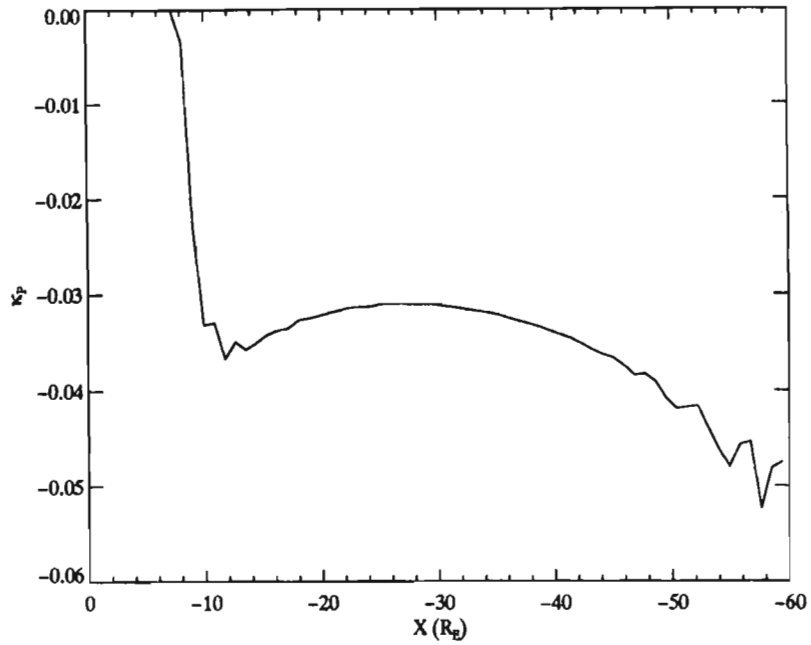

Figure 4.15: The inverse scale length for the pressure gradient, κ_p, for $A_{mp} = -155$ nT.R_E.

The left-hand side of equation 4.1 was evaluated for all x tailward of the shielding distance in the equatorial plane each time an equilibrium solution was obtained.

The shielding mechanism which has been used forces κ_p to be zero inside the shielding distance and negative tailward of this position, as demonstrated in figure 4.15. The oscillations in κ_p are again a result of error introduced by the use of numerical differentiation.

For a magnetic field which decreases with increasing radial distance from the earth, κ_ν is also negative. With the development of a minimum in B_e, κ_ν may be positive for a limited range of x. This does not necessarily result in instability — the relative sizes of the pressure and magnetic field are also important. For the model which has been used, κ remained at least eight times as large as κ_ν for the region in which κ_ν was positive (figure 4.16). At the same time, the minimum in

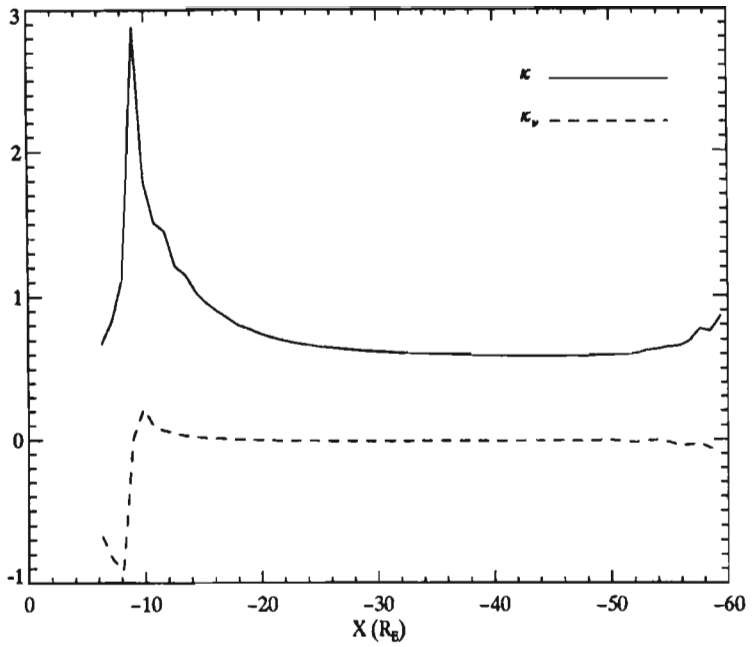

Figure 4.16: The curvature, κ, and the inverse scale length, κ_ν, for $A_{mp} = -155$ nT.R_E. The magnetic field increases from -9 R_E to -19.8 R_E (refer to figure 4.12).

the equatorial magnetic field means that the difference

$$\gamma P - \frac{B^2}{\mu_0}$$

is a maximum while

$$\gamma P + \frac{B^2}{\mu_0}$$

is a minimum for a given P. The result is that the instability condition was not satisfied for any of the configurations in the convection sequence. Indeed, the increase in field line curvature in the near-earth region appears to have a stabilising effect on the plasma sheet. This is in agreement with the results of *Ohtani and Tamao* [1993].

Chapter 5

Discussion

5.1 Synopsis

The magnetospheric substorm is a complex and dynamic phenomenon. Over the past thirty years, efforts to describe the physical processes responsible for substorm development have greatly increased. The result is a wealth of substorm models, with each model having both merit and fault. These contrasting scenarios have demonstrated that many possible physical mechanisms may be invoked to account for similar sequences of events. Synthesis models such as those proposed by *Lui* [1991a, 1991b] and *Kan* [1993] have come closer to providing a model which can describe all of the phases of substorm evolution.

Walker and Samson [1994] have demonstrated yet another approach to the substorm mechanism. Their magnetohydrodynamic model is attractive in its simplicity and flexibility. It can account for substorms both with and without a growth phase and in conditions of both northward and southward IMF. The ballooning instability is but one of the substorm triggering mechanisms suggested in the MHD model. It is therefore useful to determine how viable a candidate the ballooning mode is for substorm initiation.

A threshold condition for the instability, which applies near the equatorial plane, was derived using the simplified model outlined in Chapter 2. This model assumes cylindrical symmetry as well as symmetry about the equatorial plane. The tilt of the dipole axis and the torsion of the magnetic field are thus neglected.

Numerical results for the instability condition were obtained by adopting a two-dimensional, self-consistent, quasi-static equilibrium model for the magnetospheric magnetic field. The thermodynamic constraint in the model forces time-dependent magnetic field configurations which describe the earthward convection of plasma sheet flux tubes during growth phase conditions. As the magnetic field becomes more stressed, the curvature of the field in the near-earth regions increases while the flux tube volume is forced to increase as a result of the imposed adiabatic condition. This results in a minimum in the equatorial magnetic field which grows deeper with time.

The radial plasma pressure and magnetic field gradients from the model were used to compute the numerical values of the appropriate scale lengths and the curvature of the magnetic field. The Alfvén and sound speeds were also calculated. Using these quantities, it was deduced that the magnetotail was stable against the ballooning mode.

5.2 B_e minimum formation

In the equatorial plane, the contribution to B_z from the dipole component of the magnetic field is positive. The presence of the current sheet results in a southward contribution to B_z earthward of the inner edge. With the mechanism that has been employed to account for inner magnetospheric shielding, the inner edge of the current sheet moved tailwards as convection proceeded. This makes the formation of a minimum in the equatorial magnetic field more probable as the two-dimensional dipole field drops off as r^2, where r is the radial distance

from the earth.

Using a more realistic shielding mechanism, *Erickson* [1992] has demonstrated that the B_e minimum formation is not a consequence of the tailward motion of the current sheet inner edge. The improved mechanism allows the shielding distance to move earthward as the growth phase evolves. The B_e minimum which forms can then be seen to be a consequence of the intensification of the current at the inner edge and not any unrealistic motion of the current sheet.

5.3 Improved modelling

Erickson [1992] introduced a new approach to including the effects of inner magnetospheric shielding. He considered the plasma in the magnetotail to convect toward the earth within a "channel" which becomes wider as the Alfvén layer is approached. This is achieved by defining a new flux function which depends on the original flux function (the vector potential) as well as the radial distance from the earth and the position of the shielding distance (which is allowed to vary). This channel becomes wide enough to halt the flow of plasma at the shielding distance. Plasma is effectively "lost" from the flux tubes which reach this point. Although this mechanism is also artificial, it allows the model magnetotail to exhibit characteristics which are observed to be common to the real magnetotail. Most notably, the shielding distance in this model moves earthward as the growth phase proceeds. The plasma pressure is also free to vary and may build-up as a consequence of the thermodynamic restriction.

The models presented by *Erickson* [1992] also include a more realistic magnetopause shape which is rounded at the dayside and allowed to flare at the tail boundary. The minimum in the equatorial magnetic field still develops, regardless of magnetopause geometry.

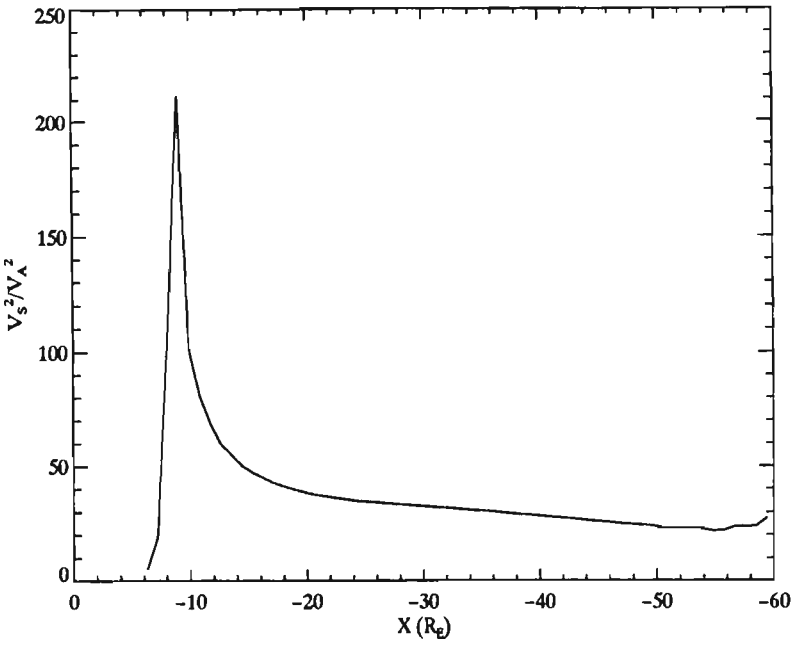

Figure 5.1: The ratio V_S^2/V_A^2 for $A_{mp} = -155$ nT.R_E.

5.4 Instability condition

The values for the pressure and magnetic field obtained in the previous chapter indicate that, for this model, the condition

$$V_S^2 >> V_A^2$$

holds at all equatorial points tailward of the shielding distance. For those points where κ_ν is positive, V_S^2 is at least (approximately) forty times greater than V_A^2 (figure 5.1). At equatorial points where κ_ν is negative, the ratio of V_S^2 to V_A^2 decreases, but always remains greater than twenty. The instability condition

$$\kappa(V_S^2 - V_A^2) - \kappa_\nu(V_S^2 + V_A^2) < 0$$

may thus be simplified to

$$\kappa - \kappa_\nu < 0 \tag{5.1}$$

for these regions.

Within the shielding distance, there are a few points for which V_A^2 is not negligible. Here, though, κ_ν is negative so that the instability condition cannot be satisfied. The same holds for all equatorial points tailward of the shielding distance where κ_ν is negative.

5.4.1 Stability considerations

If the plasma and magnetic field pressure gradients in the magnetotail are both directed earthward, the configuration of the tail is potentially unstable. The forces due to these gradients are directed tailward, and are balanced by the earthward directed force due to the field line curvature. For a configuration in which one of the pressure gradients is directed tailward and the other earthward, the situation may still be potentially unstable if the earthward directed gradient is large enough. For the case presented in Chapter 4, the pressure gradient was not sufficient to cause the onset of instability.

The question that must now be addressed is whether the formation of a peak in the equatorial pressure at the inner edge of the plasma sheet can alter the stability of a configuration which has a minimum in the equatorial magnetic field. This may be investigated using the results presented by *Erickson and Heinemann* [1992].

5.4.2 Deduced results

Figures 2 and 3 from *Erickson and Heinemann* [1992] (reproduced in figure 5.2 and figure 5.3) show the development of a plasma pressure peak near the inner edge and a minimum in the equatorial magnetic field, respectively. In this model, the shielding distance moved from 8 R_E (the initial position) to approximately 7 R_E. The simplified condition 5.1 will be used to determine the stability of this configuration. Where the curvature, κ, is positive, 5.1 implies that instability may

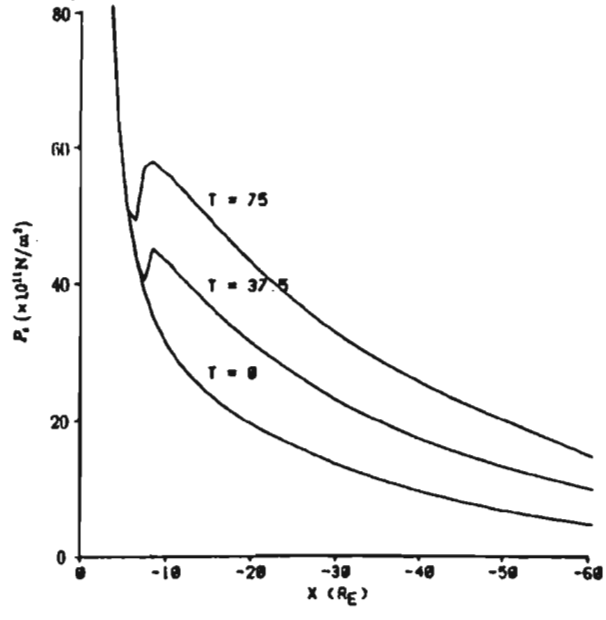

Figure 5.2: The evolution of the equatorial plasma pressure for the convection sequence in *Erickson and Heinemann* [1992]. From *Erickson and Heinemann* [1992].

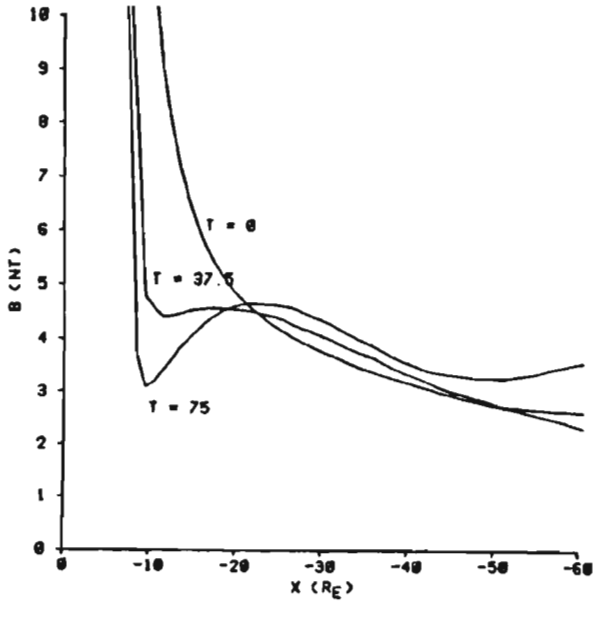

Figure 5.3: The evolution of the equatorial magnetic field for the convection sequence in *Erickson and Heinemann* [1992]. From *Erickson and Heinemann* [1992].

only be expected for those regions where the equatorial magnetic field increases with increasing radial distance from the earth ($\kappa_\nu > 0$). In the equatorial plane, the exclusion of neutral lines means that the curvature here is always positive.

In the model presented by *Erickson and Heinemann* [1992], the pressure peak is formed where $\kappa_\nu < 0$. This may be concluded from figures 5.2 and 5.3. The region for which κ_ν is positive is also the region for which the pressure is decreasing tailward of the pressure peak. This situation is therefore analogous to the results presented in Chapter 4. Qualitatively, numerical estimates deduced from figures 5.2 and 5.3 demonstrate that, for $\kappa_\nu > 0$, the curvature is approximately two orders of magnitude larger than κ_ν. Equation 5.1 then implies that the configuration is stable.

5.5 The pressure balance inconsistency

Erickson and Wolf [1980] have argued that steady state convection is not possible in the earth's magnetotail where isotropic pressure is assumed. As a flux tube convects earthwards, its volume decreases. If PV^γ is conserved, the plasma pressure for the flux tube must increase. *Erickson and Wolf* [1980] have demonstrated that the required increase in plasma pressure is too large to be balanced by the tail lobe magnetic pressure. This discrepancy, known as the "pressure-balance inconsistency", becomes larger the closer a flux tube comes to the earth.

Erickson and Wolf [1980] speculated that the inconsistency could be resolved if flux tubes close to the earth were allowed to become more stretched, or tail-like. This would increase the volume of the flux tube, allowing the magnitude of the plasma pressure necessary to conserve PV^γ to be smaller. The stretching of flux tubes outside the Alfvén layer is consistent with the formation of a minimum in the equatorial magnetic field.

Hau et al. [1989] obtained magnetospheric magnetic field configurations consistent with steady state convection only if an extreme B_e minimum was allowed. These solutions are possible representations of the development of the field late in the growth phase at times for which no solutions were obtained with the model used by *Erickson* [1984, 1992]. The lack of observation of deep minima in the equatorial magnetic field seems to indicate that such a situation is unstable and results in a reconfiguration of the field.

Kivelson and Spence [1988] have also investigated steady convection in the magnetotail. They have reported that, for intervals of low geomagnetic activity, the pressure of an earthward convecting flux tube between -30 and -60 R_E would not increase enough to give rise to any inconsistency. This arises from three-dimensional considerations. For disturbed conditions, however, the plasma pressure may become very large earthward of -30 R_E.

While the existence or non-existence of steady state convection in the earth's magnetotail poses an interesting problem, it is sufficient to note that, since the model under investigation represents the development of the growth phase in disturbed conditions, formation of a B_e minimum may be expected.

5.6 Conclusions

Although the results obtained in this investigation indicate that the magnetotail is stable against ballooning, it must be recognised that the models that have been used contain simplifications and approximations which, while making the analysis easier, may have been misleading.

In deriving the dispersion relation in Chapter 2 it was assumed that variation both tangential and normal to the magnetic field in the meridian plane was slow enough to be described by eikonal functions. In a more accurate description, these

variations in the x_μ and x_ν directions could be obtained by integrating along a field line. A more realistic model of the magnetospheric magnetic field would also be desirable for deducing numerical results for instability, although the intricate and dynamic nature of the three-dimensional magnetotail makes this a difficult task. The results obtained in this analysis are nevertheless in agreement with similar investigations by *Ohtani and Tamao* [1993] and *Lee and Wolf* [1992].

The triggering of the magnetospheric substorm remains the most controversial aspect of substorm research. The various instabilities — both microscopic and macroscopic — suggested to be responsible for initiating the substorm expansion phase need to be quantitatively assessed before this debate is decided.

Appendix A

Description of Program Routines

This appendix describes the procedures and algorithms in the programs Mag.f and Timestep.f. These programs are written in Sun FORTRAN 1.4. The first section describes Mag.f while the second discusses Timestep.f.

A.1 Mag.f

The program *Mag* is used to generate the initial ($t = 0$) solution to equation 3.16 for specific boundary conditions, as described in Chapter 3. The source code listing for the program may be found on the accompanying diskette.

Step 1: Generating the vector potential dipole component

The dipole component of the vector potential is generated using the expression in 3.18:

$$A_d = m_d \frac{x}{x^2 + z^2} \tag{A.1}$$

The factor μ_0 is incorporated in the constant m_d.

Step 2: Generating an initial approximation

An initial approximation to the solution is calculated using the Fuchs-Voigt model (section 3.3.3). The analytical solution for $k = 1.54$ is computed first using *Subroutine Fvk154*. This involves evaluating the expression

$$A(x,z) = -\frac{m}{2}\sum_{n=0}^{\infty}\left[e^{-|\lambda_n x|}\text{sign}(x) + e^{-|\lambda_n(x+2b)|}\text{sign}(x+2b)\right].\cos(\alpha_n z)$$

The upper limit of the summation in the above equation is reached when the expression being summed contributes less than 1×10^{-10} to the total summation. The variable α_n is calculated from the relation

$$\alpha_n = \frac{\pi}{2}(2n+1)$$

and the variable λ_n through

$$\lambda_n = \sqrt{\alpha_n^2 - k^2}$$

The factor b is the radial distance of the magnetopause from the earth. For this model, $b = 10.8$ R_E. The *sign* function is defined by *Function sig(p)*. It is a function which has a value of -1, $+1$ or 0 depending on whether its argument is negative, positive or zero, respectively. The unit of distance in the Fuchs-Voigt model is normalised in terms of the distance from the equatorial plane to the magnetopause (18 R_E).

For *Subroutine Fvk0*, $k = 0$. This means that $\alpha_n = \lambda_n$. Aside from this, the routines *Fvk154* and *Fvk0* are the same.

To obtain an initial approximation to the plasma current vector potential, A_p, at each point on the grid, the values generated by *Fvk0* are subtracted from those generated by *Fvk154* by *Subroutine Subtract*.

Step 3: Generating boundary conditions

At each boundary the values of A and P, and thus dP/dA, must be specified.

Magnetopause boundary

In the initial configuration, the value of the vector potential at the magnetopause boundary is zero. From the values of A_d generated in Step 1, A_p is generated by the condition

$$A = A_d + A_p = 0$$

Since the pressure at the magnetopause is zero for $t = 0$, the current density, dP/dA, is also zero.

Far-tail boundary

The asymptotic approximation and form of $P(A)$ given in section 3.3.1 lead to

$$\frac{d^2A}{dz^2} = -k^2A \tag{A.2}$$

The general solution to this equation is

$$A(z) = C_1 \cos(kz) + C_2 \cos(kz) \tag{A.3}$$

In the initial configuration, $B_x(z = 0) = 0$, and $A(0) = A_e$ where A_e is the value of the vector potential at the intersection of the far-tail boundary with the equatorial plane. This implies that

$$A(z) = A_e \cos(kz) \tag{A.4}$$

The component A_p is then generated by subtracting the vector potential dipole component. The pressure at this boundary is given by

$$P = \frac{1}{2\mu_0} k^2 A^2 \tag{A.5}$$

Equatorial boundary

The equatorial boundary is initialised by Fuchs-Voigt model values for A_p and P. The current density A dependence has thus the same form as that at the tail boundary

$$\frac{dP}{dA} = \frac{1}{\mu_0} k^2 A \tag{A.6}$$

The equatorial pressure is also described by the dependence A.5.

As the analytical form for the equatorial pressure in the initial approximation is known, A.6 may be used to generate initial values for the rest of the modelling grid.

Step 4: Gauss-Seidel iteration

Subroutine Iterate computes the solution to 3.16 using the Gauss-Seidel method. Values for A_p and thus A, corresponding to an equilibrium solution, are obtained for each point on the grid.

The boundary values for A and dP/dA are constantly updated during the iteration procedure to enforce the symmetry condition described in section 3.3.1. This requires keeping the vector potential at one grid point above the equatorial plane equal to the vector potential one grid spacing below the plane. Strictly speaking, then, the "equatorial boundary" lies at $z = -0.9$ R_E although these points are never depicted or plotted.

To find the new values for dP/dA, the updated values of A are used to evaluate

$P(x_e)$ according to A.5. Since magnetic field lines are surfaces of constant A, P and $J = dP/dA$, the current density need only be computed in the equatorial plane. These values are then mapped along the field lines.

For improved accuracy, a five point central difference is used to evaluate dP/dx. This numerical differentiation has the form

$$f'(x_j) = \frac{1}{12\Delta}[8f(x_{j+1}) - 8f(x_{j-1}) - f(x_{j+2}) + f(x_{j-2})]$$

Now $B_x = 0$ at the equatorial plane. B_z is evaluated using a two point central difference for $\partial A_p/\partial x$ and adding the dipole contribution m_d/x^2. The relation

$$\begin{aligned} \mu_0 \frac{dP}{dA} &= \mu_0 \frac{dP}{dx} / \frac{dA}{dx} \\ &= \mu_0 \frac{dP}{dx} / B_z \end{aligned}$$

is then used to calculate the current density.

To map A onto the equatorial plane, it is assumed that field lines do not intersect at any point and that the vector potential increases monotonically toward the earth. Neutral lines are thus excluded. Once the corresponding A at the equatorial plane has been found, the appropriate dP/dA value is assigned. The iteration procedure is then repeated until the convergence criterion

$$|A_p^n - A_p^{n+1}| < \epsilon$$

is satisfied at each grid point.

Output files are generated after the conversion from model to SI units has been made. To calculate the values of the function $PV^\gamma(A)$, the equatorial pressure and vector potential values are written as separate arrays.

Step 5: Tracing magnetic field lines

The magnetic field lines are traced with the aid of an Interactive Graphics Language (IDL) contouring routine. A system call to IDL is made, with the data

input read from FORTRAN generated files and not passed directly to IDL. The IDL source code may be found on the accompanying floppy disk.

Contours of constant A are traced for all values of the equatorial vector potential from the shielding distance to the tail boundary. IDL uses a "contour following" method which follows each contour line until it closes or reaches a boundary. The output is in the form of a file containing the normalised coordinates which define the contour position. Each contour record is preceded by a "header structure" describing various properties of the contour.

Step 6: Conversion of coordinates

The IDL output is now converted to model coordinates using *Subroutine Coord.* It is also desirable to know the coordinates at constant arc distances along the field line. This will make the calculation of the field line volume more accurate. These adjusted coordinates are also generated by *Subroutine Coord* using the converted IDL output.

The algorithm takes two points, (x_1, z_1) and (x_2, z_2), and calculates the gradient between them. The arc length between the two points is approximated by a straight line so that

$$ds = \sqrt{(x_1 - x_2)^2 + (z_1 - z_2)^2}$$

Let the specified arc length be ds_r. Then

$$ds_r = \sqrt{(x_r - x_2)^2 + (z_r - z_2)^2} \tag{A.7}$$

where x_r and z_r define the required coordinate point. Now the gradient, m, is given by

$$m = \frac{z_2 - z_1}{x_2 - x_1} = \frac{z_r - z_1}{x_r - x_1}$$

therefore

$$(z_r - z_2)^2 = m^2(x_r - x_2)^2 \tag{A.8}$$

Substituting A.8 into A.7,

$$ds_r^2 = (x_r + x_1)^2(1 + m^2)$$

which gives

$$x_r = \frac{ds_r}{\sqrt{1 + m^2}} + x_1$$

From A.8,

$$z_r = m(x_r - x_1) + z_1$$

The last two equations are used to modify the coordinates given by IDL into coordinates at constant arc intervals of 0.9 R_E along the field line. The signs are changed according to the curvature of the field.

Step 7: Evaluating plasma current magnetic field

Before the volume of the field lines can be calculated, the magnetic field at each point must be evaluated. Now B_d, the dipole component, may be computed directly from the expression

$$B_d^2 = \left(\frac{\partial A_d}{\partial x}\right)^2 + \left(\frac{\partial A_d}{\partial z}\right)^2$$

With A_d given by equation A.1,

$$B_d^2 = \left[-\frac{2m_d xz}{(x^2 + z^2)^2}\right] + \left[\frac{m_d(x^2 - z^2)}{(x^2 + z^2)^2}\right] \tag{A.9}$$

The plasma current component is evaluated using two point central differences in x (for B_z) and z (for B_x) for interior grid points, and three point forward or backward differences for boundary points. The numerical differentiation formulae are given by

$$f'(x_j) = \frac{1}{2\Delta}[f(x_{j+1}) - f(x_{j-1})]$$

for a two point central difference,

$$f'(x_j) = \frac{1}{2\Delta}[-3f(x_j) + 4f(x_{j+1}) - f(x_{j+2})]$$

for a three point forward difference, and

$$f'(x_j) = \frac{1}{2\Delta}[3f(x_j) - 4f(x_{j-1}) + f(x_{j-2})]$$

for a three point backward difference.

Step 8: Calculating PV^γ

Subroutine PV calculates the values of $PV^\gamma(A)$. To do so, the volume of each field line traced by IDL needs to be computed. The integral

$$V = \int \frac{ds}{B(s)}$$

is evaluated by summing the contributions of the line segments between the coordinates generated by *Coord.* For each segment, then, $ds = 0.9$ R_E. The value of $B(s)$ is taken as the average value of the magnetic field on the arc segment.

The plasma current component of the magnetic field is only known at a grid point. If a coordinate point lies on a grid line, the value is linearly interpolated from the two nearest grid points. If the point lies arbitrarily between grid points, the value is interpolated from the four nearest grid points. This is done by finding the value of B_z and B_x at the two nearest points on grid lines at the same x value as the coordinate, and at the two points at the same z value. These are in turn interpolated and averaged to find the required values at the coordinate point. The dipole x and z components are found using equation A.9. The total magnetic field is then evaluated by adding, component-wise, the dipole and plasma current contributions.

Since the coordinates of the field line are only known for the one hemisphere, the volume integral extends from the equatorial plane to the northern ionosphere. To obtain the total volume, this value must be doubled. The values of PV^γ follow using the appropriate pressure value for each field line.

An initial magnetic field configuration has now been generated, with the values of $PV^{\gamma}(x)$ calculated by the above routine. By noting the variation of the vector potential in the equatorial plane, $A_{eq}(x)$, $PV^{\gamma}(A)$ is obtained. This function will be common to all subsequent solutions.

A.2 Timestep.f

The program *Timestep* is used to generate convected forms of the initial configuration which satisfy the adiabatic constraint 3.25. The source code listing may also be found on the accompanying diskette.

Step 1: Generate A_d

The dipole component of the vector potential is generated as in *Mag*.

Step 2: Subtracting $|\Delta A|$

The previous solution is read into an array. Ten units of A are subtracted from this solution at each grid point. This generates new boundary conditions, as well as an initial approximation to the equilibrium solution. Values of A_p are found by subtracting the dipole component from the total vector potential.

Step 3: Tracing magnetic field lines

The magnetic field lines are traced by performing a system call to IDL. This procedure is as described in Step 5 of program *Mag*.

Step 4: Conversion of coordinates

This is identical to Step 6 of program *Mag*, using *Subroutine Coord.*

Step 5: Calculating PV^{γ}

The values of the plasma current magnetic field are calculated before calling *Subroutine PV* by the procedure described in Step 7 of program *Mag*. *Subroutine PV* is the same as the subroutine of the same name described in Step 8 of program *Mag*.

Step 6: Adjust equatorial pressure boundary condition

The equatorial pressure values are now adjusted according to the value of the ratio of PV^{γ} to G (the required value of PV^{γ}). This algorithm was described in section 3.4.4. The array `tcheck(J)` keeps track of which field lines satisfy the adiabatic condition.

Step 7: Calculate new tail boundary condition

The value of the vector potential at the magnetopause is now negative, so that dP/dA here is zero. Below the field line $A = 0$ A.2, and therefore A.3 hold. The first step in *Subroutine Tail* is thus to locate the position of the $A = 0$ field line. This point is defined by z_0 and is found by linear interpolation if necessary. For z greater than z_0

$$\frac{d^2A}{dz^2} = 0$$

therefore

$$A(z) = \frac{A_{mp}}{z_{mp} - z_0}(z - z_0)$$

where $z_{mp} = 18\ R_E$. For z less than z_0, the pressure varies parabolically with A as before. Equation A.4 with the condition $A(z_0) = 0$ implies that

$$kz_0 = \frac{\pi}{2}$$

Now the pressure at the equatorial point which intersects the tail boundary, P_e, is given by the equatorial pressure modification algorithm. The vector potential at this corner is then calculated using equation A.5. The values for $A(z)$ and dP/dA may now be computed.

Step 8: Find new plasma current magnetic field

These values are calculated as in Step 7 of *Mag*.

Step 9: Compute new dP/dA

Since the equatorial pressure values have changed, the values of dP/dA must be recalculated. *Subroutine Newdp* uses the same updating algorithm that is used in *Subroutine Iterate* (see Step 4 of program *Mag*).

Step 10: Gauss-Seidel iteration

This calls *Subroutine Iterate*, as in *Mag*.

Step 11: Instability condition

The instability condition derived in Chapter 2 is applied to equatorial grid points tailward of the original shielding distance. This involves evaluating each of the terms in equation 2.80. The known values at each grid point are the pressure and

the magnetic field. Two point central differences are used to find κ_p and κ_ν. The curvature is then computed using the expression

$$\kappa = -\left(\kappa_\nu + \frac{1}{2}\beta\kappa_p\right)$$

Appendix B

Source Code Listing

Please see the accompanying diskette for the source code listing of programs Mag.f and Timestep.f.

REFERENCES

Akasofu, S.-I., The development of the auroral substorm, *Planet. Space Sci., 12*, 273–282, 1964.

Akasofu, S.-I., *Physics of magnetospheric substorms*, D. Reidel, Dordrecht, Holland, 1977.

Akasofu, S.-I., What is a magnetospheric substorm?, in *Dynamics of the Magnetosphere*, ed. S.-I. Akasofu, D. Reidel, Dordrecht, Holland, 1979a.

S.-I. Akasofu (ed.), *Dynamics of the Magnetosphere*, D. Reidel, Dordrecht, Holland, 1979b.

Akasofu, S.-I., Development of magnetospheric physics, in *Magnetospheric Substorms, Geophysical Monograph 64*, American Geophysical Union, Washington D.C., 1991.

Akasofu, S.-I. and S. Chapman, The ring current, geomagnetic disturbance, and the Van Allen belts, *J. Geophys. Res., 66*, 1321–1350, 1961.

Akasofu, S.-I. and S. Chapman, The development of the main phase of magnetic storms, *J. Geophys. Res., 68*, 125–129, 1963a.

Akasofu, S.-I. and S. Chapman, Magnetic storms: the simultaneous development of the main phase (DR) and of polar magnetic substorms (DP), *J. Geophys. Res., 68*, 3155–3158, 1963b.

Allan, W., S.P. White and E.M. Poulter, Impulse-excited hydromagnetic cavity and field-line resonances in the magnetosphere, *Planet. Space Sci., 34*, 371–385, 1986.

Axford, W.I. and C.O. Hines, A unifying theory of high-latitude geophysical

phenomena and geomagnetic storms, *Can. J. Phys., 39*, 1433–1464, 1961.

Axford, W.I., H.E. Petschek and G.L. Siscoe, Tail of the magnetosphere, *J. Geophys. Res., 70*, 1231–1236, 1965.

Axford, W.I., Magnetic field reconnection, in *Magnetic Reconnection in Space and Laboratory Plasmas*, ed. E.W. Hones Jr., pp. 1–8, American Geophysical Union, Washington D.C., 1984.

Baumjohann, W., The plasma sheet boundary layer and magnetospheric substorms, *J. Geomag. Geoelectr., 40*, 157–175, 1988.

Birn, J. and K. Schindler, Self-consistent theory of three-dimensional convection in the geomagnetic tail, *J. Geophys. Res., 88*, 6969–6980, 1983.

Burch, J.L., Terrestrial and planetary magnetospheres, in *Solar System Plasma Physics*, ed. J.H. Waite Jr., J.L. Burch and R.L. Moore, pp.9–15, American Geophysical Union, Washington D.C., 1989.

Chao, J.K., J.R. Kan, A.T.Y. Lui and S.-I. Akasofu, A model for thinning of the plasma sheet, *Planet. Space Sci., 25*, 703–710, 1977.

Chapman, S., Earth storms: retrospect and prospect, *J. Phys. Soc. Jpn., 17*, 6, 1962.

Chapman, S., *Solar Plasma, Geomagnetism and Aurora*, Gordon and Breach, New York, 1964.

Chapman, S. and V.C.A. Ferraro, A new theory of magnetic storms, *Terrest. Magnetism and Atmospheric Elec., 36*, 77–97; 171 – 186, 1931.

Chapman, S. and V.C.A. Ferraro, A new theory of magnetic storms, II; The main phase, *Terrest. Magnetism and Atmospheric Elec., 38*, 79–96, 1933.

Chapman, S. and V.C.A. Ferraro, The theory of the first phase of a geomagnetic storm, *Terrest. Magnetism and Atmospheric Elec., 45*, 245–268, 1940.

Chen, L. and A. Hasegawa, A theory of long-period magnetic pulsations 1. Steady state excitation of field line resonance, *J. Geophys. Res., 79*, 1024–1037, 1974.

Coroniti, F.V. and C.F. Kennel, Can the ionosphere regulate magnetospheric convection?, *J. Geophys. Res., 78*, 2837–2851, 1973.

Cowling, T.G., *Magnetohydrodynamics*, Adam Hilger, Bristol, England, 1976.

Davis, N.T. and M. Sugiura, Auroral electrojet activity index AE and its universal time variations, *J. Geophys. Res., 71*, 785–801, 1966.

Dungey, J.W., Interplanetary magnetic field and the auroral zones, *Phys. Rev. Lett., 6*, 47–48, 1961.

Egeland, A., Ø. Holter and A. Omholt, Cosmical geophysics; historical preamble, in *Cosmical Geophysics*, ed. A. Egeland, Ø. Holter, A. Omholt, pp.11 – 17, Universiteitsforlaget, Norway, 1973.

Erickson, G.M., On the cause of X-line formation in the near-earth plasma sheet: results of adiabatic convection of plasma sheet plasma, in *Magnetic Reconnection in Space and Laboratory Plasmas*, ed. E.W. Hones Jr., pp.296–302, American Geophysical Union, Washington D.C., 1984.

Erickson, G.M., A quasi-static magnetospheric convection model in two dimensions, *J. Geophys. Res., 97*, 6505–6522, 1992.

Erickson, G.M. and R.A. Wolf, Is steady convection possible in the earth's magnetotail, *Geophys. Res. Lett., 7*, 897–900, 1980.

Erickson, G.M. and M. Heinemann, A mechanism for magnetospheric substorms,

in *Substorms 1, Proceedings of the International Conference on Substorms (ICS-1), Kiruna, Sweden, 23–27 March 1992* , ESA SP-335, pp.587–592, European Space Agency, Noordwijk, 1992.

Fairfield, D.H. and N.F. Ness, Configuration of the geomagnetic tail during substorms, *J. Geophys. Res., 75*, 7032–7046, 1970.

Fuchs, K. and G.-H. Voigt, Self-consistent theory of a magnetospheric B-field model, in *Quantitative Modeling of Magnetospheric Processes*, ed. W.P. Olson, pp.86–95, American Geophysical Union, Washington D.C., 1979.

Goertz, C.K. and R.A. Smith, The thermal catastrophe model of substorms, *J. Geophys. Res., 94*, 6581–6596, 1989.

Hargreaves, J.K., *The Upper Atmosphere and Solar-Terrestrial Relations*, Van Nostrand Reinhold, New York, 1979.

Hau, L.-N., R.A. Wolf, G.-H. Voigt and C.C. Wu, Steady state magnetic field configurations for the earth's magnetotail, *J. Geophys. Res., 94*, 1303–1316, 1989.

Hones, E.W. Jr, Transient phenomena in the magnetotail and their relation to substorms, *Space Sci. Rev., 23*, 393–410, 1979.

Hones, E.W. Jr, J.R. Asbridge, S.J. Bame and S. Singer, Substorm variations of the magnetotail plasma sheet from $X_{SM} \approx -6\,R_E$ to $X_{SM} \approx -60\,R_E$, *J. Geophys. Res., 78*, 109–132, 1973.

Hones, E.W. Jr, Plasma sheet behaviour during substorms, in *Magnetic Reconnection in Space and Laboratory Plasmas*, ed. E.W. Hones Jr., pp. 178–184, American Geophysical Union, Washington D.C., 1984.

Jacobs, J.A., *Geomagnetic Micropulsations*, Springer-Verlag, Germany, 1970.

Kan, J.R., Developing a global model of magnetospheric substorms, *EOS, Trans AGU, 71*, 1083; 1086–1087, Sept. 18, 1990.

Kan, J.R., A global magnetosphere-ionosphere coupling model of substorms, *J. Geophys. Res., 98*, 17263–17275, 1993.

Kan, J.R., L. Zhu and S.-I. Akasofu, A theory of substorms: onset and subsidence, *J. Geophys. Res., 93*, 5624–5640, 1988.

King, J.W. and W.S. Newman (ed.), *Solar-Terrestrial Physics*, Academic Press, London, 1967

Kivelson, M.G. and D.J. Southwood, Resonant ULF waves: a new interpretation, *Geophys. Res. Lett., 12*, 49–52, 1985.

Kivelson, M.G. and D.J. Southwood, Coupling of global magnetospheric MHD eigenmodes to field line resonances, *J. Geophys. Res., 91*, 4345–4351, 1986.

Kivelson, M.G. and H.E. Spence, On the possibility of quai-static convection in the quiet magnetotail, *Geophys. Res. Lett., 15*, 1541–1544, 1988.

Lee, D.-Y. and R.A. Wolf, Is the earth's magnetotail balloon unstable?, *J. Geophys. Res., 97*, 19251–19257, 1992.

Lui, A.T.Y., Observations of plasma sheet dynamics during magnetospheric substorms, in *Dynamics of the Magnetosphere*, ed. S.-I. Akasofu, D. Reidel, Dordrecht, Holland, 1979.

Lui, A.T.Y. (ed.), *Magnetotail Physics*, Johns Hopkins University Press, Baltimore, Maryland, 1987.

Lui, A.T.Y., Road map to magnetotail domains, in *Magnetotail Physics*, ed. A.T.Y. Lui, Johns Hopkins University Press, Baltimore, Maryland, 1987.

Lui, A.T.Y., A synthesis of magnetospheric substorm models, *J. Geophys. Res.*, *96*, 1849–1856, 1991a.

Lui, A.T.Y., Extended consideration of a synthesis model for magnetospheric substorms, in *Magnetospheric Substorms, Geophysical Monograph 64*, American Geophysical Union, Washington D.C., 1991b.

Lyons, L.R. and D.J.Williams, *Quantitative Aspects of Magnetospheric Physics*, D.Reidel, Dordrecht, Holland, 1984.

Lyons, L.R. and A. Nishida, Description of substorms in the tail incorporating boundary layer and neutral line effects, *Geophys. Res. Lett.*, *15*, 1337–1340, 1988.

Matsushita, S. and W. H. Campbell (ed.), *Physics of geomagnetic phenomenon, Volumes I and II*, Academic Press, New York, 1967

McPherron, R.L., Growth phase of magnetospheric substorms, *J. Geophys. Res.*, *75*, 5592–5599, 1970.

McPherron, R.L., C.T. Russell and M.P. Aubry, Satellite studies of magnetospheric substorms on August 15, 1968: 9. Phenomenological model for substorms, *J. Geophys. Res.*, *78*, 3131–3149, 1973.

Mitchell, A.R. and D.F. Griffiths, *The Finite Difference Method in Partial Differential Equations*, John Wiley & Sons, 1980.

Moos, N.A.F., *Colaba Magnetic Data; Part 2: The Phenomenon and its Discussion*, Bombay, 1910.

Morse, P.M. and H. Feshbach, *Methods of Theoretical Physics, Part I*, pp.678–706, McGraw-Hill, New York, 1953.

Nishida, A., S.J. Bame, D.N. Baker, G. Gloeckler, M. Scholer, E.J. Smith, T. Terasawa and B. Tsurutani, Assessment of the boundary layer model of the magnetospheric substorm, *J. Geophys. Res., 93*, 5579–5588, 1988.

Ohtani, S.-I., and T. Tamao, Does the ballooning instability trigger substorms in the near-earth magnetotail?, *J. Geophys. Res., 98*, 19369–19379, 1993.

Parks, G.K., G. Laval and R. Pellat, Behaviour of the outer radiation zone and a new model of magnetospheric substorm, *Planet. Space Sci., 20*, 1391–1408, 1972.

Piddington, J.H., Geomagnetic storm theory, *J. Geophys. Res., 65*, 93–106, 1960.

Press, W.H., B.P Flannery, S.A. Teukolsky and W.T. Vetterling, *Numerical Recipes (FORTRAN version)*, Cambridge University Press, New York, 1989.

Rostoker, G., Macrostructure of geomagnetic bays, *J. Geophys. Res., 73*, 4217–4229, 1968.

Rostoker, G., Some observational constraints for substorm models, in *Magnetospheric Substorms, Geophysical Monograph 64*, American Geophysical Union, Washington D.C., 1991.

Rostoker, G., S.-I. Akasofu, J. Foster, R.A. Greenwald, Y. Kamide, K. Kawasaki, A.T.Y. Lui, R.L. McPherron and C.T. Russell, Magnetospheric substorms — definition and signatures, *J. Geophys. Res., 85*, 1663–1668, 1980.

Rostoker, G. and T. Eastman, A boundary layer model for magnetospheric substorms, *J. Geophys. Res., 92*, 12187–12201, 1987.

Roux, A., S. Perraut, A. Morane, P. Robert, A. Korth, G. Kremser, A. Pederson, R. Pellinen and Z.Y. Pu, Role of the near-earth plasmasheet at substorms, in *Magnetospheric Substorms, Geophysical Monograph 64*, American Geophysical Union, Washington D.C., 1991a.

Roux, A., S. Perraut, P. Robert, A. Morane, A. Pederson, A. Korth, G. Kremser, B. Aparicio, D. Rodgers and R. Pellinen, Plasma sheet instability related to the westward traveling surge, *J. Geophys. Res., 96*, 17697–17714, 1991b.

Ruohoniemi, J.M., R.A. Greenwald, K.B. Baker and J.C. Samson, HF radar observations of Pc5 field line resonances in the midnight/early morning MLT sector, *J. Geophys. Res., 96*, 15967–15710, 1991.

Rutherford, D.E., *Vector Methods, 9th edition*, Oliver & Boyd, Edinburgh, 1957.

Samson, J.C., J.A. Jacobs and G. Rostoker, Latitude-dependent characteristics of long-period geomagnetic micropulsations, *J. Geophys. Res., 76*, 3675–3683, 1971.

Samson, J.C., R.A. Greenwald, J.M. Ruohoniemi, T.J. Hughes and D.D. Wallis, Magnetometer and radar observations of magnetohydrodynamic cavity modes in the earth's magnetosphere, *Can. J. Phys., 69*, 929–937, 1991.

Schield, M.A., J.W. Freeman and A.J. Dessler, A source for field-aligned currents at auroral latitudes, *J. Geophys. Res., 74*, 247–256, 1969.

Schindler, K. and J. Birn, Self-consistent theory of time-dependent convection in the earth's magnetotail, *J. Geophys. Res., 87*, 2263–2275, 1982.

Siscoe, G.L. and W.D. Cummings, On the cause of geomagnetic bays, *Planet. Space Sci., 17*, 1795–1802, 1969.

Smith, R.A., C.K. Goertz and W. Grossmann, Thermal catastrophe in the plasma sheet boundary layer, *Geophys. Res. Lett., 13*, 1380–1383, 1986.

Southwood, D.J., Some features of field line resonances in the magnetosphere, *Planet. Space Sci., 22*, 483–491, 1974.

Stern, D.P., The beginning of substorm research, in *Magnetospheric Substorms, Geophysical Monograph 64*, American Geophysical Union, Washington D.C., 1991.

Van Allen, J.A., *Origins of Magnetospheric Physics*, Smithsonian Institution Press, Washington D.C., 1983.

Voigt, G.-H., Magnetospheric equilibrium configurations and slow adiabatic convection, in *Solar Wind - Magnetosphere Coupling*, ed. Y. Kamide and J.A.Slavin, pp.233–273, Terra Scientific, Tokyo, 1986.

Voigt, G.-H. and R.A. Wolf, Quasi-static magnetospheric MHD processes and the "ground state" of the magnetosphere, *Rev. Geophys., 26*, 823–843, 1988.

Walker, A.D.M., The Kelvin-Helmholtz instability in the low-latitude boundary layer, *Planet. Space Sci., 29*, 1119–1133, 1981.

Walker, A.D.M., Space Physics Research Institute, University of Natal, Durban, Personal communication, 1994.

Walker, A.D.M., J.M. Ruohoniemi, K.B. Baker and R.A. Greenwald, Spatial and temporal behaviour of ULF pulsations observed by the Goose Bay HF radar, *J. Geophys. Res., 97*, 12187–12202, 1992.

Walker, A.D.M. and J.C. Samson, A magnetohydrodynamic model of substorm intensifications, *in preparation for submission to J. Geophys. Res.*, 1994.

Walker, R.J. and D.J. Southwood, Momentum balance and flux conservation in model magnetospheric magnetic fields, *J. Geophys. Res., 87*, 7460–7466, 1982.

Woods, L.C., *Principles of Magnetoplasma Dynamics*, Oxford University Press, Oxford, 1987.